Aalborg Universitet

Synchronization for the uplink of OFDMA-based System

Nguyen, Huan Cong

Publication date:
2008

Document Version
Publisher's PDF, also known as Version of record

[Link to publication from Aalborg University](#)

Citation for published version (APA):
Nguyen, H. C. (2008). *Synchronization for the uplink of OFDMA-based System*.

Synchronization for the uplink of OFDMA-based systems

by

Huan Cong Nguyen

A Dissertation for the Degree of Doctor of Philosophy

defended on 2008

at Aalborg University

Aalborg, Denmark

Supervisors:

Prof. Dr. Ramjee Prasad, Aalborg University, Denmark

Assoc. Prof. Dr. Elisabeth de Carvalho

The Assessment Committee:

Prof. Dr. Enrico Del Re, Department of Electronic and Telecommunications (DET), University of Florence, Italy

Dr. Werner Mohr, Nokia Siemens Networks GmbH & Co. KG, Munich, Germany

Prof. Dr. Preben Mogensen, Department of Electronic Systems, Aalborg University, Denmark

Committee Chairman:

Prof. Dr. Preben Mogensen, Department of Electronic Systems, Aalborg University, Denmark

Moderator:

Prof.

Abstract

The Orthogonal Frequency Division Multiple Access (OFDMA) has recently emerged as one of the prime multiple access schemes for the future broadband wireless networks. In OFDMA, available subcarriers are grouped into subchannels, which are assigned to different users operating simultaneously. Preserving the orthogonality among these subchannels is essential, as it prevents the inter-carrier interference (ICI), which consequently eliminates multi-user interference (MUI).

While the orthogonality among subchannels can be maintained relatively easily in the downlink, keeping the orthogonality in the uplink is much more difficult. In the uplink, the received signal is the sum of multiple signals coming from different users, each experiences a independent carrier frequency offset (CFO) due to oscillator instability and / or Doppler shift. Conventional CFO correction method used in the downlink are designed for single-user system, and therefore are not able to correct multiple CFOs in the uplink.

The aim of this thesis is to provide practical solutions for the synchronization issues occurring in the uplink of the OFDMA-based broadband wireless systems. Several data-aided CFO estimation algorithms are proposed to achieve accurate measurements of the multiple CFOs in different scenarios. Once the estimates are available, novel MUI cancellation schemes are introduced to mitigate the self- and cross-interference occurring due to multiple CFOs. Evaluation results show that the proposed schemes outperform the existing techniques in literature with comparable or even lower additional complexity.

ABSTRACT

Dansk Resumé

En af tidens vigtigste protokoller for kanaladgang i fremtidens trådløse bred-
båndsnetværk er orthogonal frequency division multiplexing (OFDMA). I
OFDMA grupperes de til rådighed værende kanaler i såkaldte sub-kanaler
som tildeles samtidige brugere. Det er essentielt at bibeholde orthogonalite-
ten af disse sub-kanaler med henblik på at undgå interferens imellem sub-
kanalerne (ICI) og som følge heraf undgå interferens imellem brugerne (MUI).

Orthogonaliteten imellem sub-kanalerne er relativt let at opretholde i
retningen mod brugeren (downlink), hvorimod det er væsentligt sværere i
retningen fra brugeren (uplink). I uplink er det modtagne signal en sum af
signalerne fra de forskellige brugere, hver med et individuel offset fra den no-
minelle bærefrekvens (CFO) som følge af oscillator ustabilitet og/eller Dop-
plerforskydning. Konventionelle metoder til korrektion for CFO i downlink'en
er designet til enkeltbrugersystemer og er derfor ikke i stand til at korrigere
multiple CFO'er i uplink'en.

Målet for denne afhandling er at give praktiske løsninger til synkro-
niseringsproblemerne som opstår i uplink'en af OFDMA-baserede trådløse
bredbåndssystemer. Adskillige data-assisterede CFO estimeringsalgoritmer
foreslås til at opnå nøjagtige estimater af de multiple CFO'er i forskellige
scenarier. Derudover introduceres nye metoder som på baggrund af CFO
estimaterne afhjælper den selv- og krydsinterferens som skyldes multiple C-
FO'er, dvs. MUI. Resultaterne af evalueringer viser at de foreslåede metoder
fungerer bedre end eksisterende metoder i litteraturen ved sammenlignelig
eller endda lavere kompleksitet.

Acknowledgements

First of all, I would like to thank my supervisors, Professor Ramsee Prasad and Associate Professor Elisabeth de Carvalho, for their guidance and confidence in me throughout my Ph.D program. Their insight comments have sharpened my thoughts and helped to improve the quality of this work.

I would like to thank the members of the JADE research group for their friendship and helpful discussions: Petar Popovski, Hiroyuki Yomo, Mohamed Imardur Rahman, Suvra S. Das, Daniel Vaz Pato Figueiredo, Nicola Marchetti, Ragnar Vidir Reynisson, Basak Can, Sren Skovgaard Christensen, Frank Fitzek, Simone Frattasi and Megumi Kaneko. Many of the ideas discussed in this thesis come from the collaborations within the group.

I am thankful to the members of the Antenna, Propagation and Networking (APNet) Section for their assistance and comments. And I appreciate the efforts of the administrative staffs at the Department of Electronic Systems, Aalborg University, including Dorthe Sparre, Inga Hauge and Kirsten Jensen, who have helped me with many formality procedures and paper works.

I woe a great deal to my Vietnamese friends in Denmark and back in Vietnam, who have provided me with companionship throughout my years staying abroad.

Last but not least, I would like to thank my family for their love and encouragement. I am indebted to my parents, parents in-law, my brother and sister in-law, who have been watching closely and supporting every steps of my life. And special thank go to my wife, Tran My Lan, and my lovely daughter, Nguyen Lan Huong, who are truely "the wind beneath my wings". Without their constant affections and inspirations, surely I cannot come this far.

ACKNOWLEDGMENTS

Contents

ACRONYMS

1G 1st Generation

2G 2nd Generation

3G 3rd Generation

3GPP The Third Generation Partnership Project

4G 4th Generation

AWGN Additive White Gaussian Noise

B3G Beyond 3G

BER Bit Error Rate

BPSK Binary Phase Shift Keying

BS Base Station

CDMA Code Division Multiple Access

CFO Carrier Frequency Offset

CINR Carrier to Interference-plus-Noise Ratio

CIR Channel Impulse Response

CLJL Choi-Lee-Jung-Lee

CNR Carrier to Noise Ratio

CP Cyclic Prefix

CSA Contiguous Subcarrier Assignment

CSI Channel State Information

CSOD Correlation-based Shortened Observation Distance

CRB Cramer-Rao Bound

CTF Channel Transfer Function

CTYH Cao-Tureli-Yao-Honan

DFT Discrete Fourier Transform

DSL Digital Subcriber Line

DTDR Direct Time-Domain Ranging

DVB-RCT Digital Video Broadcasting - Return Channel Terrestrial

FDM Frequency Division Multiplexing

FDMA Frequency Division Multiple Access

FDR Frequency-Domain Ranging

FEC Forward Error Correction

FFT Fast Fourier Transform

GSM Global System for Mobile communication

IA Interference Avoidance

IC Interference Cancellation

ICI Inter-Carrier Interference

IDFT Inverse Discrete Fourier Transform

IEA Iterative Estimation and Adjustment

IEEE Institute of Electrical and Electronics Engineers

IFFT Inverse Fast Fourier Transform

ISI Inter-Symbol Interference

ITDR Indirect Time-Domain Ranging

ITU International Telecommunication Union

LP-OFDMA Linearly Precoded-Orthogonal Frequency Division Multiple Access

LTE Long-Term Evolution

MAC Medium Access Control

MC-CDMA Multicarrier Code Division Multiple Access

ML Maximum Likelihood

MMSE Minimum Mean Square Error

MS Mobile Station

MSE Mean Square Error

MSOD Moose-based Shortened Observation Distance

MUI Multi-User Interference

MUSIC Multiple Signal Classification

TD-MUIC Time-Domain Multi-User Interference Cancellation

SI-MUIC Simple Time-Domain Multi-User Interference Cancellation Scheme

CA-MUIC Code-Aided Time-Domain Multi-User Interference Cancellation Scheme

FD-MUIC Frequency-Domain Multi-User Interference Cancellation

NCSA Non-Contiguous Subcarrier Assignment

OFDM Orthogonal Frequency Division Multiplexing

OFDM-TDMA Orthogonal Frequency Division Multiplexing - Time Division Multiple Access

OFDMA Orthogonal Frequency Division Multiple Access

PAPR Peak to Average Power Ratio

PDP Power Delay Profile

PHY Physical Layer

PIC Parallel Interference Cancellation

P/S Parallel to Serial

PSK Phase Shift Keying

QAM Quadrature Amplitude Modulation

QPSK Quadrature Phase Shift Keying

RF Radio Frequency

rms root mean square

RSS Received Signal Strength

SAGE Space-Alternating Generalized Expectation-Maximization

SC-FDMA Single Carrier-Frequency Division Multiple Access

SDMA Space Division Multiple Access

SIC Successive Interference Cancellation

S/P Serial to Parallel

STD Standard Deviation

TDMA Time Division Multiple Access

TO Timing Offset

UMTS Universal Mobile Telecommunications System

WLAN Wireless Local Area Network

Chapter 1

Introduction

1.1 Objective

In this PhD project, we address the synchronization aspect of the Orthogonal
Frequency Division Multiple Access (OFDMA) technique in the context of
the future broadband wireless systems. The goal of the project is to provide
practical solutions to mitigate the negative effects of timing- and carrier
frequency offset misalignments, so that OFDMA technique can be applied in
the uplink without severe performance degradation. Throughout the thesis,
the following topics shall be discussed:

- The sensitivity of OFDMA technique to synchronization mis-match,
  especially in the uplink. The effects of multiple independent Carrier
  Frequency Offsets (CFOs) to the system performance shall be studied,
  which serves as problem definition for all the works in this thesis.

- We provide solution for the CFO estimation problem in the initial rang-
  ing scenario, where users are allowed to overlap on the same time-
  frequency block. Various factors that affect the estimator's perfor-
  mance shall be discussed and evaluated.

- We introduce methods to shorten the preamble used for synchronization
  in the data transmission phase of a OFDMA-based packet-oriented
  wireless system. The aim is to reduce the system's overhead, with a
  reasonable degradation in performance.

- We propose simple, but effective, multi-user interference cancellation
  schemes to alleviate the effect of multiple CFOs in the uplink, once
  the CFO estimations are available. The performance of the proposed

schemes is evaluated analytically and numerically in comparison with the existing methods.

The scientific methodology applied throughout the project is deterministic and statistical analysis of the transmitted and received OFDMA signals and the relations between different signal's parts. The performance of the discussed schemes are verified by mean of Monte Carlo simulation in Matlab environment.

Although the scope of this thesis is infrastructure-based wireless systems, its outcome can also be applied for ad-hoc network, if the conditions of an infrastructure-based uplink system are satisfied.

1.2 Thesis Outline

The thesis is organized as following. Chapter 2 begins with the introduction of OFDMA technique, together with its advantages and drawbacks. The effects of Timing Offset (TO) and CFO on the uplink of OFDMA-based systems are mentioned in this chapter, along with several other useful definitions, which serves as the background for understanding the rest of the thesis.

In Chapter 3, we discuss the initial ranging scenario in the Institute of Electrical and Electronics Engineers (IEEE) 802.16 standard. Two existing schemes for code detection and TO estimation are analyzed, and their implementations are enhanced and evaluated. We also propose a CFO estimation technique that can be applied for both schemes. The findings in this chapter are taken from the following publications:

P1) Huan Cong Nguyen, Elisabeth de Carvalho and Ramjee Prasad, "*Joint estimation of the timing and frequency offset for uplink OFDMA*", to be appeared on the special issue of Springer's Wireless Personal Communications Journal.

P2) Huan Cong Nguyen, Elisabeth de Carvalho, Jin-Kyu Koo, Su-Ryong Jeong, Young-Kwon Cho, Jae Weon Cho, Dong-Seek Cho and Hokyu Choi, "*Timing and frequency offset estimation in the uplink OFDMA*", Patent Number: KR2006-0033844. 2007-04-14.

P3) Huan Cong Nguyen, Elisabeth de Carvalho and Ramjee Prasad, "*Timing and frequency offset estimation in the uplink OFDMA*", Wireless Personal Multimedia Communications Symposium (WPMC) 2006, USA.

Chapter 4 focuses on the CFO estimation issue during data transmission phase, where Mobile Stations (MSs) have been assigned independent resources for uplink transmission. We propose two estimators based on the phase difference between two observation vectors, whose distance is less than the length of an OFDMA symbol. The aim is to shorten the preamble required for synchronization, so as to reduce the overhead in packet-based wireless communications. A part of this chapter is published in the following paper:

P4) Huan Cong Nguyen, Elisabeth de Carvalho and Ramjee Prasad, "*A generalized carrier frequency offset estimator of uplink OFDMA*", accepted to IEEE International Symposium on Personal, Indoor and Mobile Radio Communications (PIMRC) 2008, France.

In Chapter 5, novel Multi-User Interference (MUI) cancellation schemes are proposed to mitigate the self- and cross-interference occurring in the OFDMA uplink due to multiple CFOs. The proposed schemes are analyzed and numerically evaluated in comparison with the existing techniques in literature. The results indicate that the proposed schemes outperform the other reference techniques: in particular scenario, CFO-free performance can be achieved with CFO values as high as 38% of subcarrier spacing. The content of this chapter is taken from these publications:

P5) Huan Cong Nguyen, Elisabeth de Carvalho and Ramjee Prasad, "*Multi-user interference cancellation schemes for carrier frequency offset compensation in uplink OFDMA*", to be appeared on the IEEE Transaction on Wireless Communications.

P6) Huan Cong Nguyen, Petar Popovski, Elisabeth de Carvalho, Hiroyuki Yomo, Jin-Kyu Koo, Eun-Taek Lim, Tae-Young Lim, Dong-Seek Park and Young-Kwon Cho, "*Asynchronous reception for uplink OFDMA*", Patent Number: KR2006-0014707. 2006-02-15.

P7) Huan Cong Nguyen, Elisabeth de Carvalho and Ramjee Prasad, "*Multi-user interference cancellation scheme(s) for multiple carrier frequency offset compensation uplink*", IEEE International Symposium on Personal, Indoor and Mobile Radio Communications (PIMRC) 2006, Finland.

Finally, Chapter 6 is for conclusions and remarks. Major results and findings of the thesis are summarized in this chapter. Some discussion and directions for future works are also included.

Chapter 2

Background

Just before the twentieth century came to an end, the world experienced
the explosion of information and telecommunication technologies, fueled par-
tially by the increased popularity and affordability of personal computing de-
vices. The most obvious evidence is the Internet phenomenon, which evolved
from a small network that links several universities and research centers to a
global medium for information dissemination, collaboration and interaction
between individuals without regard for geographic location. The Internet
had attracted around 400 million users worldwide by the year 2000, which is
ten times growth comparing to 1996 [1], and continues to expand to nearly
1.5 billion users today [2]. To meet the demand for Internet services, the
telephone line, which was traditionally used for voice service, has gradually
turned into a data carrier. From the first generation dial-up modem, which
had a limited speed of few kbps, the Digital Subcriber Line (DSL) modem
today can achieve a data rate up to 24Mbps [3] over the telephone line.
Such a broadband connection removes the restriction of text-based services
on the Internet, and opens up the opportunity for multimedia contents and
applications, from exchanging high quality graphics and fancy documents,
downloading music and movies to real-time video conferencing and collabo-
rating over the Internet. These new services have provided more values, thus
attracted even more people to the Internet and created greater demand for
the broadband connections.

Another trend in communications in the last few decades of the twentieth
century is the shift from the wired connection to wireless one. Since the
early 80's, after the Global System for Mobile communication (GSM) was
developed, digital mobile communications have succeeded in replacing the
fixed telephone lines: in many countries, such as US, China, Japan or in
Europe, the mobile phone penetrations grew past fixed landline penetration
levels, and few countries like Luxembourg even have the number of mobile

phones exceeds the population [4]. The fact that people can communicate at any place and any time, even if they are in motion, has given the mobile communications a huge advantages over the wired connections. However, the services provided by the mobile operators were mostly voice and transmission of short text-based messages, due to the limitation of low-speed wireless connection.

The twenty-first century begins with the convergence of the trends started in the end of the last century. They are in short: higher data rate, more multimedia services and greater mobility [5, 6, 7, 8, 9, 10, 11]. Due to the abundance of more and more intelligent and portable computing devices, many new wireless standards are developed to enhance the data transfer rate in the existing 2nd Generation (2G) wireless systems, as shown in Figure 2.1. If the move from the 1st Generation (1G) to the 2G mobile systems is characterized by the conversion from analog to digital, then the shift from 2G to 3rd Generation (3G) is from circuit-switch to packet-switch for bandwidth-on-demand packet-data services [12] and the support of minimum data-rate of up to 2Mbps for indoor/small-cell-outdoor environments and 384kbps for wide-area coverage [9]. While the 3G mobile operators are trying to conquer the global market, the research on the 4th Generation (4G) wireless systems, which is also known as Beyond 3G (B3G), have already started. Its vision is to provide fully IP-based packet services, with very high data rate, between 100Mbps and 1Gbps, for both indoor and outdoor by 2010 [13]. Such a broadband capacity aims at replacing the landline DSL service and providing high quality of service for the next generation multimedia applications (real-time audio and high-definition video, high speed data, mobile TV...) ubiquitously, i.e. at any time and any place.

The broadband nature of the next generation wireless systems creates a requirement a simple-to-implement, highly-spectral efficiency and flexible multiple access scheme for its air-interface. The OFDMA technique is one of the most prominent candidates [14], which has been adopted in several industrial standards, such as the Digital Video Broadcasting - Return Channel Terrestrial (DVB-RCT), the IEEE 802.16 standard (also known as WiMax) and the Universal Mobile Telecommunications System (UMTS). In this chapter, we will give a short introduction to OFDMA and its predecessor, the Orthogonal Frequency Division Multiplexing (OFDM) technique. Their basic advantages and trade-offs are reviewed. And the remainder of the chapter discusses the challenges that must be solved for the OFDMA technique to be applied in the uplink of the 4G wireless systems.
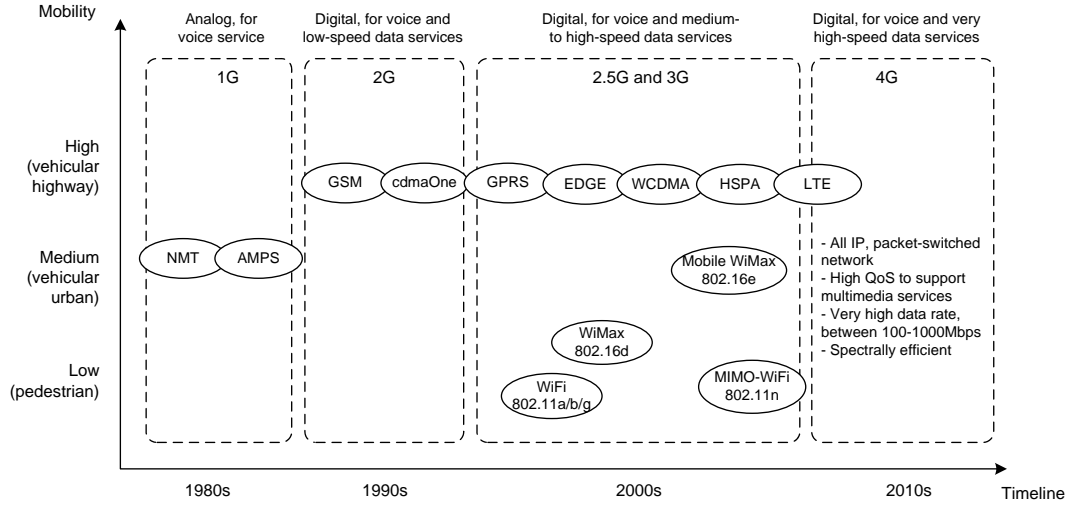
Figure 2.1: The evolution of wireless systems

2.1 The Orthogonal Frequency Division Multiplexing

The most challenging obstacle for broadband wireless communications is the hostile wireless channel. There are different propagation phenomena making reliable mobile communications more difficult to achieve, among which the multipath fading is the toughest one to deal with [15, 16, 17, 18, 19].

The multipath fading occurs when a transmitted signal takes different paths to propagate from a transmitter, for example a MS, to a receiver, for example a Base Station (BS). One portion of the signal may go directly to the destination, but other parts will bound off walls, cars, trees, human bodies or any other objects that get in the way and arrive at the receiver at different delays, phases and attenuations. These different signal paths add up incoherently at the receiver, which causes fading and distortion of the received signal [15, 18].

If the channel's delay spread, which is a measure of the level of delay in a channel, is much smaller than the symbol period of the transmitted signal, then the received signal is said to undergo "flat fading" [16]. The term "flat" indicates that all frequencies of the transmitted signal experience the same level of channel attenuation, and therefore the transmitted spectrum is preserved at the receiver. On the other hand, if the symbol period is much shorter than the channel's delay spread, we have "frequency-selective fading". In this case, the channel gain is not only fluctuating in time, but also

is different for different frequency components of the transmitted signal. This type of fading channel is more severe than the flat fading one, as it induces Inter-Symbol Interference (ISI) [16]. The higher the data-rate, the higher the probability that a wireless system experiences frequency-selective fading. In that case, complex and costly filtering techniques are often required to equalize the effect of the channel, so as to remove the ISI.

The frequency-selective fading channel occurs when the bandwidth of the transmitted signal, which is reciprocal of the symbol period, is larger than the channel's coherence bandwidth, which is inversely proportional to the channel's root mean square (rms) delay spread [19]. Thus, if we can divide the total bandwidth of transmitted signal into several fractions, each of which is less than the coherence bandwidth of the channel, then those sub-channels only experience flat fading condition. In other words, we can apply the well-known Frequency Division Multiplexing (FDM) technique to turn the frequency-selective fading channel into a flat fading one, improving the performance of the transmission link, and also removing the need for the complex channel equalizer.

In classical FDM transmitter, the high-speed data stream is first divided into N parallel streams, which are running only at $1/N$ the rate of original one. These streams are then modulated onto N non-overlapping frequency subcarriers. Figure 2.2 shows the spectrum of the FDM system. Typically, in FDM system, there is a need for guard bands between different subcarriers to prevent Inter-Carrier Interference (ICI). This leads to inefficient use of available spectrum in FDM technique.

The OFDM technique can be seen as an enhanced version of FDM, where its subcarriers are allowed to overlap. Figure 2.2 illustrates the difference between conventional FDM and OFDM techniques, and it is clear that a large portion of the frequency spectrum can be saved by using the overlapping subcarriers. Overlapping is possible in OFDM system, because its subcarriers are orthogonal with each other, which is explained in details later. The information is modulated onto a subcarrier by adjusting the subcarrier's phase, amplitude or both.

An OFDM signal consists of a sum of subcarriers that are modulated using Phase Shift Keying (PSK) or Quadrature Amplitude Modulation (QAM). If $\tilde{X}[k]$ is the complex PSK or QAM symbol at the kth subcarrier, N is the number of subcarriers, T_o is the OFDM symbol duration and f_c is the carrier frequency, then one OFDM symbol starting at $t = t_s$ can be expressed as [20]:

$$\tilde{x}(t) = \begin{cases} \sum_{k=0}^{N-1} \tilde{X}[k] \exp\left[j2\pi \frac{k}{T_o}(t - t_s)\right] & t_s \leq t \leq t_s + T_o \\ 0 & \text{otherwise} \end{cases} \tag{2.1}$$

Channel 1   Channel 2   Channel 3   Channel 4

(a)

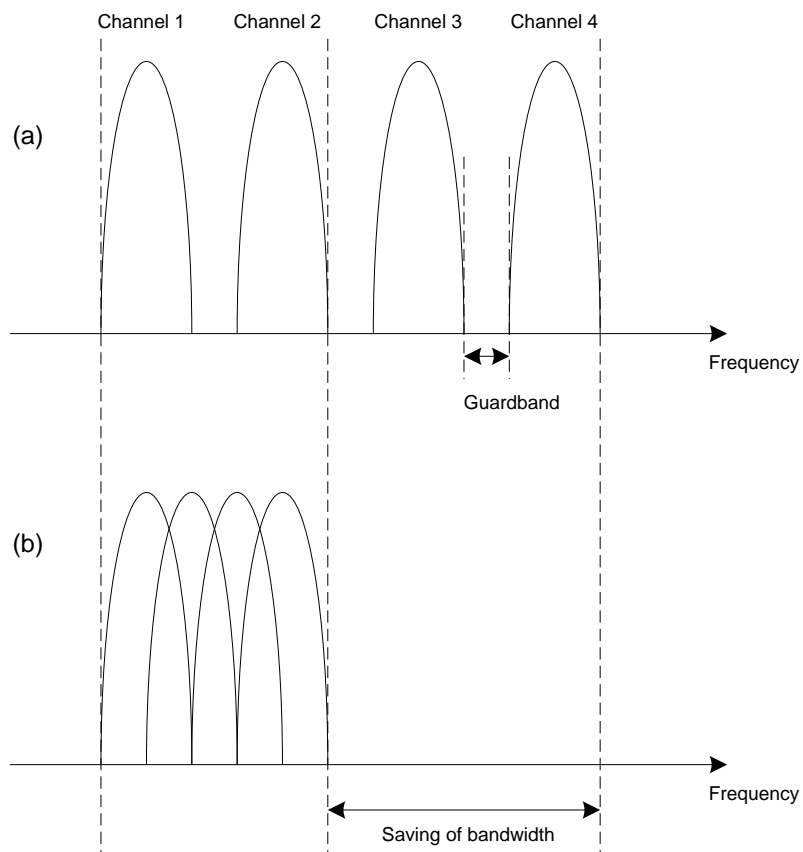Frequency

Guardband

(b)

Frequency

Saving of bandwidth

Figure 2.2: The spectrums of (a) conventional FDM and (b) OFDM technique

where $\tilde{x}(t)$ is the complex baseband OFDM symbol, and $\Psi_k(t) = e^{j2\pi\frac{k}{T_o}(t-t_s)}$ is the kth subcarrier of the OFDM symbol, where $k = 0, 1, \ldots, N-1$. Note that each subcarrier has exactly an integer number of cycles in the interval T_o, and the number of cycles between adjacent subcarriers differs by exactly one. Due to this property, the subcarriers are 'orthogonal' with each other, i.e. they pass the following orthogonality test:

$$
\int_{t_s}^{t_s+T_o} \Psi_k(t)\Psi_{k'}^*(t)dt = \int_{t_s}^{t_s+T_o} e^{j2\pi\frac{k-k'}{T_o}(t-t_s)}dt
$$
$$
= \begin{cases} T_o & k = k' \\ 0 & k \neq k' \end{cases} \tag{2.2}
$$

The orthogonal property of subcarriers enables us to obtain the modulated data from each subcarrier individually, even though they are overlapping. For example, to demodulate the kth subcarrier from Eq. (2.1), we first down-convert the signal with a frequency of k/T_o and then integrate the signal over T_o seconds. The result of these operations is the desired output $\tilde{X}_{k+\frac{N}{2}}$ (multiplied by a constant factor T_o), as shown in Eq. (2.3).

$$
\int_{t_s}^{t_s+T_o} e^{-j2\pi\frac{k}{T_o}(t-t_s)} \sum_{k'=0}^{N} \tilde{X}[k'] e^{j2\pi\frac{k'}{T_o}(t-t_s)} dt = \sum_{k'=0}^{N-1} \tilde{X}[k'] \int_{t_s}^{t_s+T_o} e^{j2\pi\frac{k'-k}{T_o}(t-t_s)}
$$
$$
= T_o \tilde{X}[k] \tag{2.3}
$$

2.1.1 The implementation of OFDM transceiver

Back in the 1960s, a large array of sinusoidal generators is used to implement the OFDM transmitter, while the receiver consists of a large bank of coherent demodulator with very high frequency accuracy [21, 22, 23, 24]. Such direct implementation is unreasonably complex and expensive, making the OFDM technology unattractive for commercial applications. Thus, it initially was deployed only for military communications.

Fortunately, Weinstein and Ebert [25] has derived another form for implementing the OFDM system in 1971. The complex baseband OFDM signal as defined by Eq. (2.1) is in fact nothing more than the inverse Fourier transform of N PSK or QAM symbols, where the time variable t is replaced by a sampling index n [20]:

$$
\tilde{x}[n] = \frac{1}{N}\sum_{k=0}^{N-1} [k] e^{j2\pi\frac{nk}{N}} \tag{2.4}
$$

| Information source | → | Error correction encoder | → | Interleaver | → | Symbol mapping | → | Serial to parallel | → | Inverse FFT | → | Parallel to serial | → | Cyclic prefix extension | → |

(a) OFDM transmitter

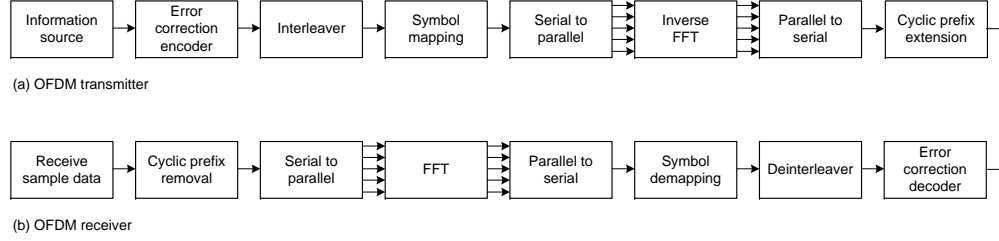| Receive sample data | → | Cyclic prefix removal | → | Serial to parallel | → | FFT | → | Parallel to serial | → | Symbol demapping | → | Deinterleaver | → | Error correction decoder | → |

(b) OFDM receiver

Figure 2.3: Block diagrams of OFDM system based on IFFT/FFT technique

In practice, the Discrete Fourier Transform (DFT) can be implemented very efficiently by the Fast Fourier Transform (FFT) algorithm. The only requirement is that the number of subcarriers, N, must be in the power of 2. The banks of sinusoidal generators and coherent demodulators in Figure **??** are now replaced by Inverse Fast Fourier Transform (IFFT) and FFT operators, respectively. Today, the availability of fast and cheap IFFT/FFT processors has made OFDM technique a favorable choice for both wired and wireless applications, from the high-speed DSL modems, digital television broadcasting, Wireless Local Area Network (WLAN) to the future 4G wireless systems.

A typical implementation of an OFDM system is presented in Figure 2.3. As mentioned earlier, the high-rate bit stream is first mapped into PSK or QAM symbols via the mapping module. The symbol stream is then divided into N parallel sub-streams by the Serial to Parallel (S/P) converter, and transformed into time-domain by IFFT operation. The Parallel to Serial (P/S) converter combines the parallel signals into OFDM symbols.

A sufficient guard interval between two symbols is essential for operation of the OFDM technique. Due to the multipath delay, adjacent OFDM symbols interfere with each other, which causes degradation of the system performance [20]. This problem can be avoided by inserting a guard interval, which is larger than the expected delay spread of the channel, between two OFDM symbols. The guard interval, T_g, could consist of no signal at all, which is referred to as "zero-padding". However, the zero-padding guard interval causes ICI, i.e. subcarriers are no longer orthogonal and crosstalk between different subcarriers occurs [20]. In order to eliminate ICI, the OFDM symbol is cyclically extended in the guard interval. This ensures that delayed replicas of the OFDM symbols always have an integer number of cycles within the FFT interval, as long as the delay is smaller than the guard interval, so as to maintain the orthogonality between subcarriers [20]. This whole process is referred to as "cyclic prefix insertion" in the block diagram.
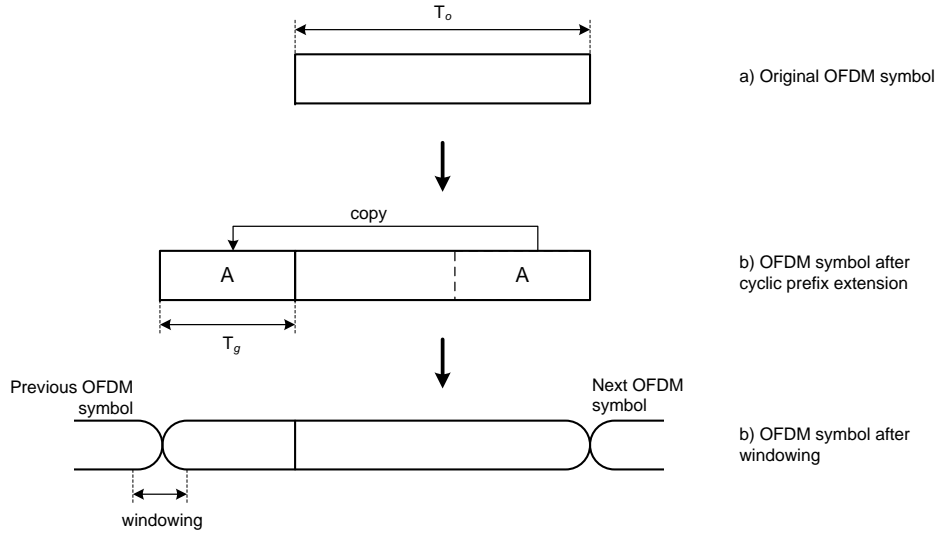
Figure 2.4: The cyclic prefix insertion and windowing processes

To further optimize the spectrum of the transmitted signal, windowing can be applied to the individual OFDM symbols. Windowing an OFDM symbol makes the amplitude go smoothly to zero at the symbol boundaries (see Figure 2.4). This procedure helps to greatly reduce the spectrum side-lopes of transmitted signal [20].

At the receiver, reverse operations are performed to achieve the transmitted binary data. First, the cyclic prefix is removed from received signal. The FFT operation is applied on the received OFDM stream. Finally, demapping block converts the obtained PSK or QAM symbols back to binary stream.

2.2 Advantages and disadvantages of OFDM

The OFDM technique has several advantages compared to the single-carrier modulation. As we have discussed earlier, the key reasons to use OFDM are its spectrum efficiency and the ability to deal with frequency-selective fading channel with a reasonable implementation complexity. In a single-carrier system, the implementation complexity is dominated by the channel equalization, which is necessary when the channel delay spread is larger than about ten percent of the symbol duration. The OFDM system does not required equalization, and therefore the complexity is greatly reduced. For example, in IEEE 802.11a WLAN application, the usage of OFDM technique

reduces the system complexity to 1/10 compared to the equivalent single-carrier system [20].

In single-carrier system, the equalization hardware is often built into the system and is unalterable. If the delay spread exceeds the value for which the equalizer is designed to work with, the system performance degrades abruptly. Due to error propagation in equalizer, the raw bit error probability increases so quickly that introducing lower rate coding or a lower constellation size does not significantly improve the situation. For OFDM, however, there are no such nonlinear effects as error propagation, and lower rate coding and/or lower constellation sizes can be employed to provide fall-back rates that are significantly more robust against large delay spread. This feature is desirable, as it enhances the coverage area and avoids the situation that users in bad spots (e.g. having very large delay spread) cannot get any connection at all [20].

The OFDM technique is also more robust to timing offset than the single-carrier system. In fact, the symbol timing offset may vary over an interval equal to the guard time without causing ICI or ISI. Hence, OFDM is quite insensitive to timing offsets. Nevertheless, any deviation from the optimum timing instant means that the sensitivity to delay spread increases, or the system can handle less delay spread than the value it was designed for. To minimize this loss of robustness, the OFDM system should be designed such that the timing error is small compared with the guard interval [20].

Since the data stream is transmitted over the wireless channel using the parallel subcarriers, the quality of reception on individual subcarrier is not very important, compared to the single-carrier system. If one of the subcarriers is in error due to deep fade or narrowband interference, the whole data stream can still be recovered with sufficient channel error coding and interleaving [26]. This is an inherent advantage of the spread spectrum communication.

On the other hand, two main drawbacks of the OFDM technique are the high Peak to Average Power Ratio (PAPR) and sensitivity to phase noise and frequency offset. An OFDM signal consists of N subcarriers, which are independently modulated. If all of those signal are in-phase, they add up coherently to produce a peak power that is N times the average power. This high PAPR brings several disadvantages to implementation of OFDM system, such as an increased complexity of the analog-to-digital and digital-to-analog converters, and a requirement of Radio Frequency (RF) power amplifier with high dynamic range [20]. However, there are several techniques to reduce the PAPR in OFDM system. For example, a special Forward Error Correction (FEC) code set that excludes OFDM symbols with large PAPR can be applied, so that the high PAPR situation can be avoided.

Another solution involves pre-coding linearly the OFDM's subcarriers prior to the IFFT operation, so as to minimize the PAPR of the output. A well-known version of this solution is the Single Carrier-Frequency Division Multiple Access (SC-FDMA) or Linearly Precoded-Orthogonal Frequency Division Multiple Access (LP-OFDMA), which is selected as uplink's multiple access scheme for The Third Generation Partnership Project (3GPP) Long-Term Evolution (LTE) standard [27].

All OFDM subcarriers are orthogonal if they all have a different integer number of cycles within the FFT interval. If there is a frequency offset between the transmitter and the receiver, then the number of cycles in the FFT interval is not an integer anymore, with the result that ICI occurs after the FFT. Another related problem is phase noise [28]. A practical oscillator does not produce a carrier at exactly on frequency, but rather a carrier that phase modulated by random phase jitter. As a result, the frequency, which is the time derivative of the phase, is never perfectly constant and therefore causing ICI in the OFDM receiver. For single-carrier system, phase noise and frequency offsets only give a degradation in the received Carrier to Noise Ratio (CNR), rather than introducing interference. This is the reason that the sensitivity to phase noise and frequency offset is mentioned as disadvantages of OFDM system [20].

2.3 The Orthogonal Frequency Division Multiple Access

The OFDM itself is just a modulation technique, and it is up to system designers to choose a multiple access technique which allows users to share the resources. In wireless cellular communications, the resources can be time, frequency, power and space, and therefore the choice of multiple access technique can be Time Division Multiple Access (TDMA), Frequency Division Multiple Access (FDMA), Code Division Multiple Access (CDMA), Space Division Multiple Access (SDMA) or any combination of those. The Time Division Multiple Access (TDMA) can be applied on OFDM by assigning each user one or more independent OFDM symbols for transmission. This technique is simplest, but it is also less flexible due to the fact that all subcarriers must be given to one user at any given time, even if that particular user does not require that much resource. The combination of Code Division Multiple Access (CDMA) and OFDM is often referred to as Multicarrier Code Division Multiple Access (MC-CDMA), where each input data bit is multiplied with a given spreading code and then modulated in the baseband

by IFFT for transmission [29, 30, 31, 32]. The spreading can be done in frequency, i.e. the spreaded bits are transmitted via parallel subcarriers, or in time, where the spreaded bits are transmitted over several OFDM symbols, or a combination of both frequency and time [30]. MC-CDMA inherits the OFDM's sensitivity to synchronization error and PAPR issue, and in addition, it is more complex than the Orthogonal Frequency Division Multiplexing - Time Division Multiple Access (OFDM-TDMA) scheme, since the spreading and despreading operations are involved. SDMA employes multiple antennas to allow multiple users to transmit in the same time-frequency block. It makes use of the fact that users are seldom at exactly the same spatial location, and if we can find spatial multipath that only talk to the user being address but not the others, then users are said to be separable in space domain. Combination of SDMA and OFDM is attractive because OFDM effectively turns the frequency-selective fading channel into flat fading one, and allows for simple SDMA algorithm to be implemented. However, the number of separable users in SDMA is restricted by the number of antennas in the system, which is often limited due to complexity and physical constrains.

If the FDMA is adopted in OFDM system, it is referred to as Orthogonal Frequency Division Multiple Access (OFDMA) technique. In this multiple access scheme, each user is given an independent time-frequency block, which spans one or several OFDM symbols and consists of a number of subcarriers. The main different between the canonical OFDM and OFDMA is that multiple users are allowed to share the same OFDM symbol(s), but using different sets of subcarriers. This allows for an increment in the level of bit-granularity and straightforward dynamic subchannel assignment for multi-user diversity [33]. These, combining with the advantages inherited from OFDM, make OFDMA a promising candidate for multiple access technique of the future broadband wireless systems.

If one looks at the downlink of OFDMA-based systems, there are no different between OFDMA and OFDM-TDMA, except that an user can now only access a smaller and pre-defined set of subcarriers. Since the same BS generates all users' data, and transmits the sum via the same channel to a particular user, the timing and frequency-offset related to the received signal is unique, and therefore that user can applied traditional synchronization techniques designed for OFDM at the downlink of the OFDMA-based systems. In the uplink, however, the received signal is the sum of transmitted signals from different sources, each of which may experience an independent timing and frequency-offset, which make the situation more complicated. In the following section, we will present the system model for the uplink of the OFDMA-based wireless communications, which incorporates the timing and frequency misalignment between multiple transmitters and the receiver so

that the effect of such misalignment can be analyzed.

2.3.1 System model for the uplink of OFDMA-based systems

Consider an OFDMA system using the FFT of size N. We define the set $\Delta_{u,s}$ is the subcarrier indices for the uth user at the sth symbol, which is independent from the other users, i.e. $\Delta_{u,s} \cap \Delta_{u'=\emptyset,s}, \forall u \neq u'$. The size of the set $\Delta_{u,s}$ is denoted as $|\Delta_{u,s}|$, which is equivalent to the number of subcarriers allocated to the uth user in the sth symbol. There are different methods for selecting the set $\Delta_{u,s}$, which are referred to as subcarrier allocation schemes. In the generalized subcarrier allocation schemes, subcarriers can be assigned in different order to users, following specific resource allocation rules, to achieve a specific goal, such as maximizing the system efficiency. Since it is impossible to evaluate infinite number of generalized subcarrier allocation schemes, we focus on two special allocation schemes throughout this thesis. The Contiguous Subcarrier Assignment (CSA) assigns a block of adjacent subcarriers to a user, while in the Non-Contiguous Subcarrier Assignment (NCSA) scheme, available subcarriers are uniformly interleaved across all the users, therefore it is also called interleaved subcarrier allocation scheme. Users are assumed to have equal number of subcarriers. Each of these subcarrier allocation schemes has advantages and trade-offs of its own [34], which we will discuss in more details in the evaluation of our proposals.

The transmitted symbol of the uth user at the kth subcarrier, $k = 0, 1, \ldots, N-1$, of an OFDMA-based system can be expressed as:

$$\tilde{X}_u[k] = \begin{cases} \tilde{d}_{u,s,k} & k \in \Delta_{u,s} \\ 0 & \text{otherwise} \end{cases} \tag{2.5}$$

where $\tilde{d}_{u,s,k}$ is the data symbol belong to the uth user at the kth subcarrier of the sth symbol. The OFDM modulation is performed via IFFT operation, and then the Cyclic Prefix (CP) is inserted. The transmitted complex baseband signal of the sth OFDM symbol from the uth user in Figure 2.5 can be described as [35]:

$$\tilde{x}_{u,s}(t) = \frac{1}{N} \sum_{k \in \Delta_{u,s}} \tilde{X}_{u,s}[k] e^{j2\pi \frac{k}{T_o}(t - T_g - sT_s)} \Xi_{T_s}(t - sT_s)$$
$$sT_s \leq t \leq (s+1)T_s \tag{2.6}$$

where T_o is OFDM symbol duration without guard interval, T_g is the CP duration, and $\Xi_{T_s}(t)$ is the unity amplitude gate pulse of length $T_s = T_o + T_g$, i.e:
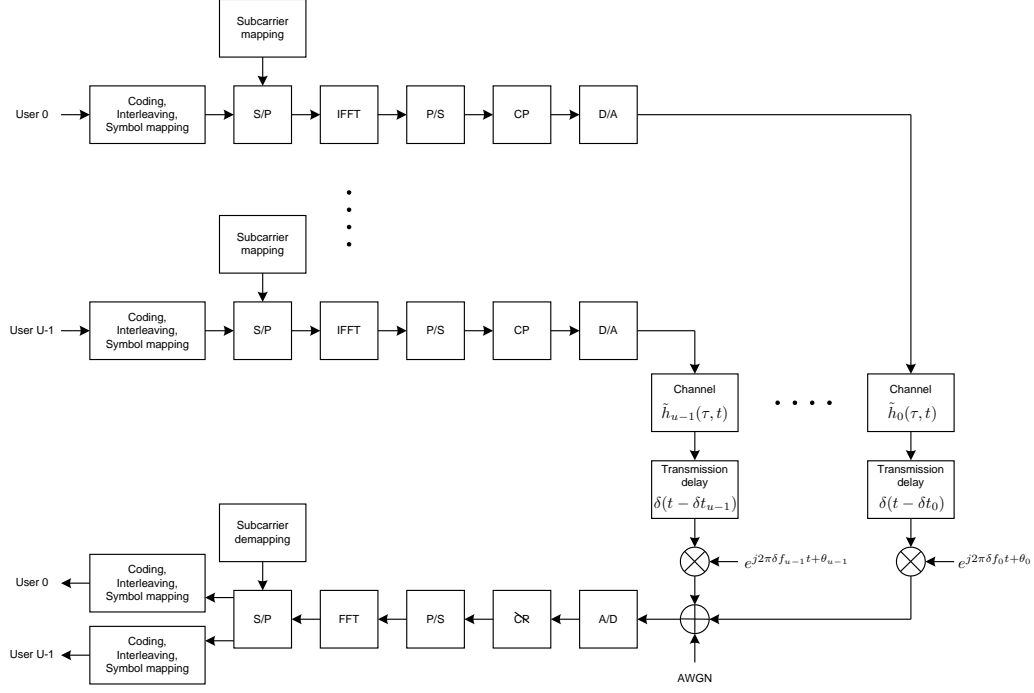
Figure 2.5: The simplified diagram of system model for uplink OFDMA

$$\Xi_{T_s}(t) = \begin{cases} 1 & 0 \leq t \leq T_s \\ 0 & \text{otherwise} \end{cases} \tag{2.7}$$

Assume that the uth user transmission experiences independent frequency-selective fading channel, with the following complex baseband Channel Impulse Response (CIR):

$$\tilde{h}_u(\tau, t) = \sum_{l=0}^{L-1} \tilde{h}_{u,l}(t)\delta(\tau - \tau_{u,l}) \tag{2.8}$$

where L is the number of multipath components, and $\tilde{h}_{u,l}(t)$ and $\tau_{u,l}$ are the complex gain and the time delay of the lth multipath component experienced by the uth user at time t, respectively. We assume that the channel gain is static for the duration of one OFDM symbol, i.e. $\tilde{h}_{u,l}(t) = h_{u,s,l}$, $\forall sT_s \leq t \leq (s+1)T_s$, and the path gain coefficients for each path contribution are

17

assumed to be uncorrelated. As a result, the Eq. (2.8) can be redefined as:

$$\tilde{h}_{u,s}(t) = \sum_{l=0}^{L-1} \tilde{h}_{u,s,l} \delta(\tau - \tau_{u,l}) \tag{2.9}$$

The corresponding Channel Transfer Function (CTF) at the kth subcarrier is given by:

$$\tilde{H}_{u,s}[k] = \sum_{l=0}^{L-1} \tilde{h}_{u,s,l} e^{-j2\pi \frac{k}{T_o} \tau_l} \tag{2.10}$$

We also assume that each user observes different timing-offset δt_u and frequency-offset δf_u. The timing- and frequency-offset are considered to be constant during observation period. As illustrated in Figure 2.5, the complex baseband received signal, therefore, is given by:

$$\tilde{r}(t) = \sum_{u=0}^{U-1} \sum_{s=-\infty}^{+\infty} \sum_{l=0}^{L-1} \tilde{h}_{u,s,l} \tilde{x}_{u,s}(t - \delta t_u - \tau_{l,s}) e^{j2\pi \delta f_u t + \theta_u} + \tilde{n}(t) \tag{2.11}$$

where $\tilde{n}(t)$ is the complex baseband Additive White Gaussian Noise (AWGN) at the input of the OFDMA receiver.

At the receiver, the continuous-time signal is sampled before further processing. In practice, the sampling clock at the receiver could be different with the one at the transmitter. However, the performance degradation due to sampling clock mismatch is often negligible compared that of timing- and frequency-offset [35, 36]. Therefore, we assume that the sampling clocks of the MSs and the BS are identical, so that we can focus on analyzing the effects of timing- and frequency-offset. After sampling and removing the CP, the sth received OFDM symbol is represented by a vector of length N:

$$\mathbf{r}_s = \{\tilde{r}_s[0], \tilde{r}_s[1], \dots, \tilde{r}_s[N-1]\} \tag{2.12}$$

in which $\tilde{r}_s[n] = \tilde{r}([sN + N_g + n]\Delta t) = \tilde{r}(sT_s + T_g + n\Delta t)$ and N_g is number of samples in the guard interval. Using IFFT to demodulate the received OFDM vector, we obtain:

$$\tilde{z}_{u,s}[k] = \sum_{n=0}^{N-1} \tilde{r}_s[n] e^{-j2\pi \frac{n}{N} k} = \tilde{p}_{u,s}[k] + \tilde{v}_{u,s}[k] \qquad \forall k \in \Delta_{u,s} \tag{2.13}$$

where:

$$\tilde{p}_{u,s}[k] = \frac{1}{N} \sum_{n=0}^{N-1} \sum_{u=0}^{U-1} \sum_{s'=-\infty}^{+\infty} \sum_{l=0}^{L-1} \sum_{k' \in \Delta_{u,s'}} \tilde{h}_{u,s',l} \tilde{X}_{u,s'}[k'] e^{j2\pi \frac{k'}{T_o} \left[n\Delta t - \delta t_u - \tau_{u,l} - (s'-s)T_s \right]}$$

$$\times \Xi_{T_s} \left[n\Delta t + T_g - \delta t_u - \tau_l - (s'-s)T_s \right] e^{j2\pi \delta f_u (n\Delta t + T_g + sT_s) + \theta_u} e^{-j2\pi \frac{n}{N} k}$$

$$\tilde{v}_{u,s}[k] = \sum_{n=0}^{N-1} \tilde{n}(sT_s + T_g + n\Delta t) e^{-j2\pi \frac{n}{N} k} \tag{2.14}$$

are the useful signal plus interference and the AWGN contribution at the kth subcarrier of the output of OFDM demodulator, respectively.

We assume that the total delay, $D_{max} = \delta t_{\max} + \tau_{\max}$, where $\delta t_{\max}$ is the maximum transmission delay of all users and $\tau_{\max}$ is the maximum delay spread of the multipath channel, is smaller than the guard interval, so that there is no influence of the adjacent OFDM symbols transmitted. This is referred to as "quasi-synchronous" scenario, and if it is true, the useful signal plus interference part can be re-written as:

$$\tilde{p}_{u,s}[k] = \tilde{H}_{u,s}[k] \tilde{X}_{u,s}[k] e^{-j2\pi \frac{k}{N} \epsilon t_u} e^{j2\pi \epsilon f_u \frac{(sN_s + N_g)}{N} + \theta_u} \tilde{\mathcal{C}}(\epsilon f_u)$$

$$+ \text{ICI}_{u,s,\text{self}}[k] + \text{ICI}_{u,s,\text{cross}}[k] \tag{2.15}$$

where:

$$\text{ICI}_{u,s,\text{self}}[k] = \sum_{k'' \in \Delta_{u,s}; k'' \neq k} \tilde{H}_{u,s}[k''] \tilde{X}_{u,s}[k''] e^{-j2\pi \frac{k''}{N} \epsilon t_u} e^{j2\pi \epsilon f_u \frac{(sN_s + N_g)}{N} + \theta_u}$$

$$\times \tilde{\mathcal{C}}(k'' - k + \epsilon f_u) \tag{2.16}$$

$$\text{ICI}_{u,s,\text{cross}}[k] = \sum_{u'=0; u' \neq u}^{U-1} \sum_{k' \in \Delta_{u',s}} \tilde{H}_{u',s}[k'] \tilde{X}_{u',s}[k'] e^{-j2\pi \frac{k'}{N} \epsilon t_{u'}} e^{j2\pi \epsilon f_{u'} \frac{(sN_s + N_g)}{N} + \theta_{u'}}$$

$$\times \tilde{\mathcal{C}}(k' - k + \epsilon f_{u'}) \tag{2.17}$$

The first term in Eq. (2.15) indicates the useful signal, while the second and the third represent the self- and cross-interference terms, i.e. ICI due to other subcarriers of the same user and the MUI due to subcarriers of the other active users in the system, respectively. The $\epsilon t_u = \delta t_u / \Delta t$ and $\epsilon f_u = \delta f_u / \Delta f$ are the normalized timing- and frequency-offset, and $\tilde{\mathcal{C}}(\phi) = \frac{\sin \pi \phi}{N \sin \pi \phi / N} e^{j\pi \phi (N-1)/N}$ is the periodic sinc-function [37].
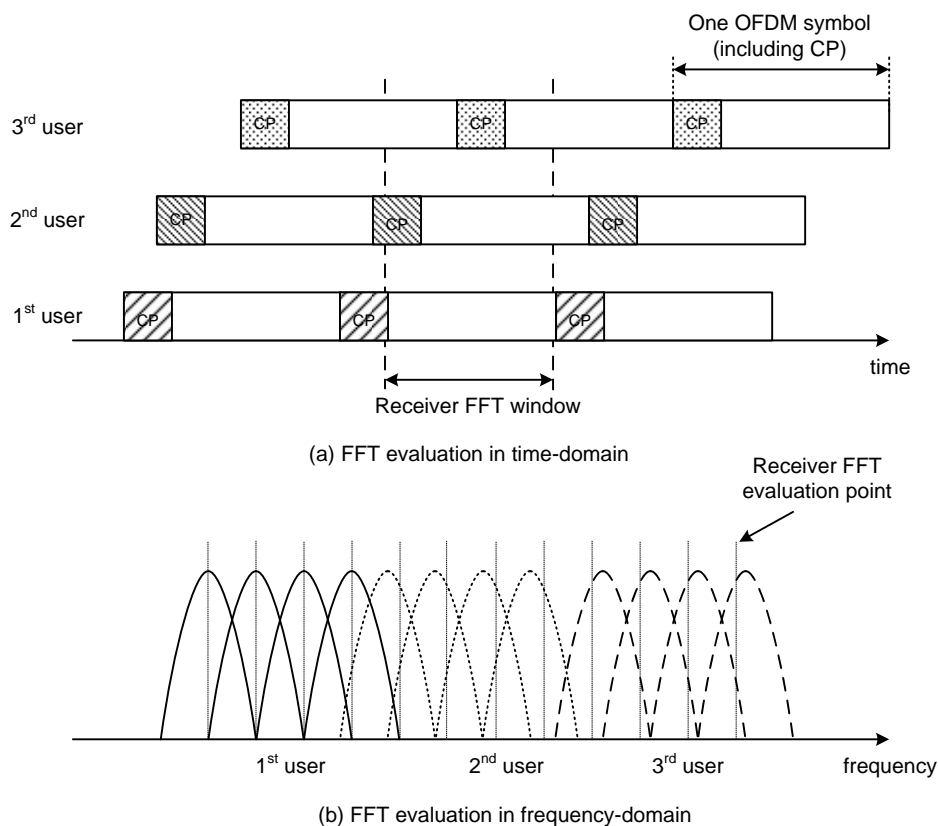
Figure 2.6: The effects of timing- and frequency-offset in the uplink OFDMA: (a) Time-domain, and (b) Frequency-domain

2.3.2 Problem identification

From Eq. (2.13) and (2.15), we can observe the effects of multiple timing- and frequency-offsets on the output of the OFDMA demodulator. These effects can be viewed in both time- and frequency-domain, as illustrated in Figure 2.6. In this section, we will look into details of these problems.

Timing offset

In single-user or downlink multiple-user scenarios, the timing offset is caused by incorrect symbol timing synchronization. In [35], it is shown that the orthogonality of the OFDM system is preserved if the timing offset is within

the allowable range:

$$0 \leq \epsilon t \leq N_g - \left\lfloor \frac{\tau \mathrm{max}}{\Delta t} \right\rfloor \tag{2.18}$$

where $\lfloor . \rfloor$ is floor function, τ_{max} is the maximum delay spread of the channel, and ϵt is the timing offset of single-user system expressed in terms of number of samples.

In uplink multi-user scenario, the performance degradation is not only introduced by incorrect symbol timing estimation, but also by the relative delays between users. Consider a scenario where three MSs are transmitting to the BS, as illustrated in Figure 2.6. Due to different transmission delays, their signals arrive at the BS at different times. Without loss of generality, we can assume that the BS's FFT window is aligned to the first user. Clearly, when the other users are misaligned, their timing offsets are equal to the relative delays to the first user. In cellular scenario, when the cell size is large, the range of relative delay between users can be considerable long, and therefore the effects of timing offset becomes much more significant than those in case of single-user scenario.

In Figure 2.6, if the FFT operation is performed, there will be ISI and ICI for the third user, as the FFT duration is extended over symbol boundary [38]. Although the OFDMA symbol from the second user lies within the FFT window of the BS, it is now less robust to delay spread of the channel, and thus might also experience ISI and ICI. This is due to the fact that its effective guard interval is now shortened by the timing offset. The ISI and ICI from the second and third users not only cause performance degradation to themselves, but also to the first user who is in synchronization.

In general, the multiple timing-offsets issue in the OFDMA uplink can be solved by increasing the CP duration, so that it covers both the longest transmission delay and the channel's maximum delay spread. This technique, however, increases system's overhead, and therefore reduces the system's throughput [38, 39]. Another method to alleviate the multiple timing-offsets is called "timing advance" in GSM world, where the BS periodically measures the transmission delay of each user, and sends a message in the downlink control channel to request the user to transmit earlier by a *timing-advance* value so that its signal reaches the BS at the same time as the others. The OFDMA system with sufficient CP can handle small timing offset misalignment, and such timing offset only introduces a phase rotation at the output of the OFDMA modulator. This phase is linear in terms of frequency, i.e. time-invariant and frequency-dependent, and will be removed in the channel estimation/correction process [40].

Carrier frequency offset

The frequency offset is resulted from the misalignment of the carrier-frequency oscillator at the receiver with the one at the transmitter, and also from the Doppler shift of the wireless medium [39]. From Eq. (2.15), one can see that the CFO causes the following effects:

1) The attenuation of received signal, since the amplitude of the periodic-sinc function, $|\tilde{\mathcal{C}}(\epsilon f_u)|$, is always less than unity if ϵf_u is non-zero. This attenuation reduces the effective Carrier to Interference-plus-Noise Ratio (CINR), and thus degrades the system performance.

2) Two phase shifts: (a) A starting phase, $e^{j2\pi \frac{\epsilon f_u N_g}{N}}$, which is constant over all OFDM symbols, and (b) a linear phase in terms of time, $e^{j2\pi \frac{\epsilon f_u s N_s}{N}}$, which is time-variant and frequency-independent phase shift. The first phase shift will be removed in the channel estimation/correction process [40]. On the other hand, the second phase shift, which is time-variant, required the use of pilots to remove. Coherent demodulation is only possible if the accumulation of this phase shift are small and negligible [41, 35]. The second phase shift is very important, since its property is exploited for CFO estimation in various estimators, including the ones proposed in this thesis.

3) The ICI between subcarriers of the same user (i.e. the "self-interference"), as shown in Eq. (5.16).

4) Finally, the MUI from subcarriers of the other active users in the OFDMA system (referred to as the "cross-interference"). which is indicated in Eq. (2.17).

It is worth to note that both of the ICI terms can be expressed as deterministic function, which depend on a number of parameters, namely the channel gain, modulated data symbol, and the distance (in terms of frequency) between interfering subcarrier and interfered one. If the distance between interfering subcarrier and interfered one is an integer number of subcarrier spacing, then the ICI is evaluated to zero, or the orthogonality between subcarriers are preserved. In this case, there is no interference occurring. If the distance is non-integer, the value of the periodic-sinc function will be non-zero. The characteristic of the periodic-sinc function, $\tilde{\mathcal{C}}(k' - k + \epsilon f_u)$, is plotted in Figure 2.7. One can observe that the ICI level decreases quickly as the distance between the two subcarriers k and k' increases [42], and it reaches local maximum when the CFO value ϵf_u approaches half of the subcarrier spacing.
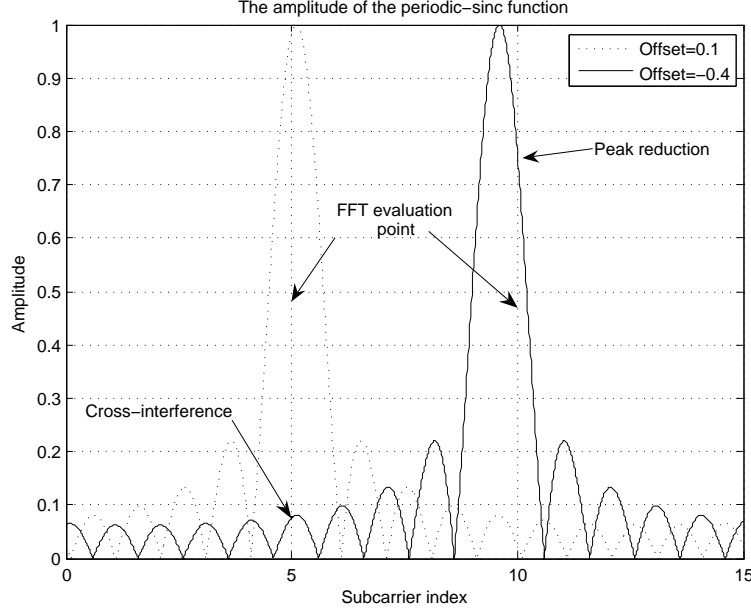
Figure 2.7: The peak reduction and cross-interference due to CFO

Figure 2.8 shows the performance degradation due to CFO in several scenarios. The applied wideband channel model is 7-tap exponential decay Rayleigh [43], with rms delay spread of 1 micro-second (us), and the CNR is 40dB. The CFO value of user(s), which indicates the frequency misalignment between the transmitter and the receiver, is selected randomly between $[-\epsilon f_{max}, +\epsilon f_{max}]$, where ϵf_{max} is the maximum normalized CFO. The FFT size is $N = 1024$, and the modulation scheme used in evaluation is Quadrature Phase Shift Keying (QPSK). In the single-user without CFO correction scenario, where there is only one user in the system and the receiver does not compensate for the user's CFO, one can observe that the performance degrades quickly with the increase of CFO value. This is expected result, as the OFDM technique is known to be very sensitive to frequency offset: To achieve negligible degradation of about 0.1 dB, the frequency offset must be kept to be less than 1% of the subcarrier spacing [38]. Therefore, it is strictly required that any frequency offset in the received signal be estimated and corrected before arriving to the OFDM demodulator.

In the second scenario, there are 5 users in the system, which are assigned equal number of subcarriers using either CSA or NCSA scheme. In this scenario, the receiver also does not try to compensate for the users' CFO. We can see that the CSA scheme performs very close to the single-user case, while the NCSA experiences significantly higher degradation. This
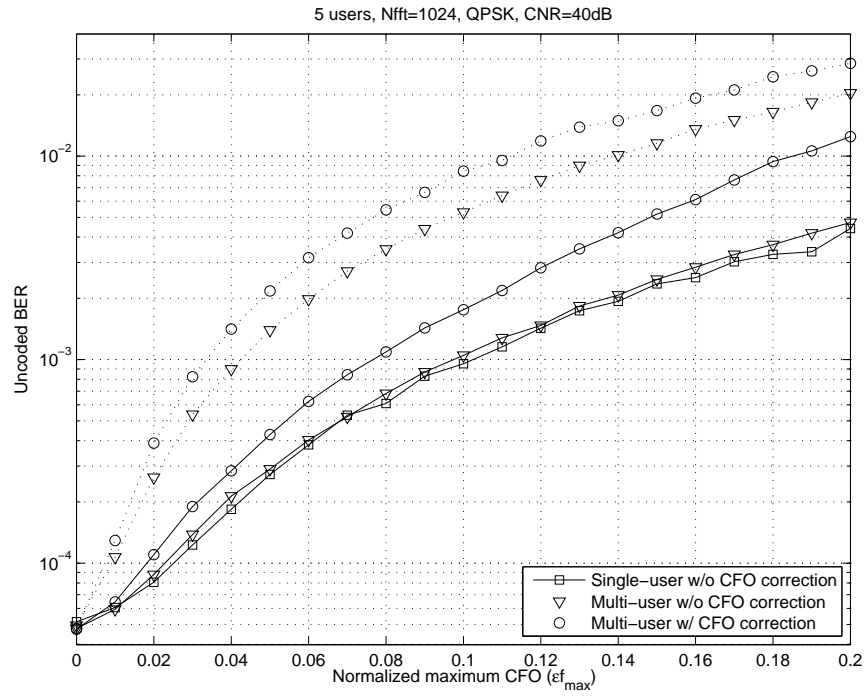
Figure 2.8: The performance degradation due to multiple CFOs in the OFDMA uplink. Dotted lines indicate non-contiguous subcarrier allocation, while solid lines represent contiguous subcarrier allocation.

indicates that the cross-interference has much greater impact on the performance than the self-interference. In CSA, due to the fact that each user is assigned block of adjacent subcarriers, most of their subcarriers only experience self-interference, except for those at the edge of the block. In contrast, the subcarriers in NCSA are interleaved, thus they have higher level of cross-interference, but lower self-interference. In general, for any subcarrier allocation scheme, the performance of the OFDMA uplink is more sensitive to carrier frequency misalignment than that of the OFDM or OFDMA downlink.

For the uplink OFDMA scenario, as illustrated in Figure 2.6, the OFDM demodulator can only be adapted to one user at a time, i.e. correction to one user's frequency offset would misalign the others [36]. In fact, correction to one user's frequency offset could cause bigger problem: Assume that users are allowed to have CFO between $[-0.1, 0.1]$ of the subcarrier spacing. If the first user has CFO value of 0.1 and the second has CFO value of -0.1, then by correcting to the first user's CFO could increase the CFO value of the second user to 0.2. The third scenario in Figure 2.8, multi-user with CFO correction, illustrates such situation: The receiver now try to adjust its carrier frequency base to one of the users. As we can see, the uncoded Bit Error Rate (BER) performance in this scenario drops significantly comparing to that of the second scenario, for both subcarrier allocation schemes.

The above-mentioned analysis motivates us to produce this work. The goal of this thesis is to solve the synchronization problem occurring in the uplink of the OFDMA-based system. We shall investigate and propose practical techniques to estimate the multiple CFOs in different scenario. Once the estimations of multiple CFOs are available, we shall introduce MUI cancellation techniques that enabling the receiver to remove the negative effects of both self- and cross-interference due to CFO. It is important to mention that our analysis does not make special assumptions about the input of the subcarriers in our OFDMA model, and therefore linearly-precoded algorithms can be applied on the input. It means that the techniques discussed in this thesis can also be extended to the attractive SC-FDMA technique, which has been selected as the uplink multiple access scheme for 3GPP LTE standard [27].

2.4 Conclusions

In this chapter, we introduce the background that are necessary to understand the rest of the thesis. The OFDMA technique is currently considered as the preferred solution for the physical layer of the next generation broadband

wireless networks. This success comes from the fact that OFDMA combines the multiuser ability of FDMA with the advantages of the famous OFDM technique, thus creating a flexible and highly efficient multiple access scheme. Similar to OFDM, OFDMA is capable of simplifying the equalization task at the receiver in a multipath fading environment, increasing the robustness to narrowband interference and offer high spectra efficiency. In addition, by letting users share available subcarriers simultaneously, OFDMA offers an increment in the level of bit-granularity and a possibility to apply dynamic subcarrier allocation scheme to achieve multiuser diversity.

However, one of the major drawbacks of OFDMA is its sensitivity to the TO and CFO, especially in the uplink. While the TO can be overcome by using sufficiently long CP, the CFO problem is more difficult to deal with. Due to oscillator inaccuracy and Doppler shift, each user in the uplink of the OFDMA-based system experiences an independent CFO, which destroys the orthogonality among subcarriers and consequently produces ICI and MUI. These CFOs must be estimated and accounted for before decoding data at the receiver, or severe performance degradation will occur. The goal of this thesis is to provide practical solutions to alleviate the synchronization issues in the uplink of the OFDMA-based system.

Chapter 3

Synchronization in initial ranging scenario

In this chapter, our focus is the synchronization procedure for MSs entering OFDMA-based wireless network for the first time or after a signal loss. We consider the OFDMA Physical Layer (PHY) layer, defined in the IEEE 802.16e-2005 standard [44], as illustrative model for our study. Nevertheless, the principles discussed hereafter can be applied for any OFDMA-based system in general. They shall allow MSs to synchronize in time and in frequency with a BS without prior information exchange with the BS.

Our contributions in this chapter includes:

- Analysis and performance comparison between two time-domain correlation-based techniques for code detection and TO estimation, namely the Direct Time-Domain Ranging (DTDR) and the Indirect Time-Domain Ranging (ITDR).

- Propose a CFO estimation scheme that can be applied in both DTDR and ITDR.

- Numerical evaluation of different implementations for DTDR and ITDR.

3.1   The initial ranging scenario

The IEEE 802.16e-2005 [44] is an amendment to the existing IEEE 802.16-2004 standard, which aims at standardizing a Medium Access Control (MAC) and several PHY layers for combined fixed and mobile broadband wireless access in licensed bands [44]. After its approval in 2005, the most well-received PHY layer's multiple access scheme is the OFDMA, which has been

adopted for Mobile WiMAX. The Mobile WiMAX is a broadband wireless technology for fixed, nomadic, portable and mobile services promoted by WiMAX Forum, which is an industry-led, non-profit organization consisting of more than 500 companies, the majority of which are operators, component and equipment companies in the communication ecosystem [45]. Recently, in October 2007, Mobile WiMAX was admitted to the family of the IMT-2000 radio interface specifications by the International Telecommunication Union (ITU) Radio Section [45], which gives the OFDMA interface the chance of competing with existing 3G technologies, such as TDMA and CDMA.

In the IEEE 802.16e-2005, when a MS enters the system for the first time or after a signal loss, it must send to BS a request for contention of the shared resources, and go through a synchronization process so that its transmission parameters fall within a tolerable range. Such procedure is referred to as "initial ranging", or hereafter "ranging" for short. The term "ranging" was migrated into wireless communications from the radar world, in which it is used to describe the process of acquiring distance to a remote object, from a known observation or reference point. In the IEEE 802.16e-2005 standard, however, the goal of the ranging procedure is slightly different, namely to identify contention requests, to acquire TOs and CFOs, and also to adjust the transmit powers of MSs [44].

A MS starts an initial ranging process by listening to the downlink broadcast channel to synchronize itself to the BS, and to obtain uplink transmission parameters. It then chooses randomly a ranging slot (with the use of a binary truncated exponent algorithm to avoid possible re-collisions) to transmit a random ranging code. A ranging slot consists of 144 adjacent subcarriers, and occupies two or four consecutive OFDMA symbols [44]. Since users are allowed to collide on this ranging slot, CDMA technique is applied: each user shall select a random code from a set of specified binary codes for ranging transmission. The code is Binary Phase Shift Keying (BPSK) modulated onto the subcarriers in the ranging slot, one bit per subcarrier. After an IFFT operation, the OFDMA ranging symbol is extended to two or four symbols, in a way that there is no phase discontinuity between them [44]. Figure 3.1 illustrates the construction of a initial ranging signal that is two-symbol length.

Upon receiving successfully a ranging code, the BS's main tasks are to determine the power, TO and CFO associated with that particular code, and then to request the MS that sent the code to adjust its transmission parameters. In order to address the correct user, the BS must include the code as well as the ranging slot information, such as OFDMA symbol number, subchannel etc, in the ranging response broadcast. The ranging response message shall contain all the necessary adjustments, namely power, TO and
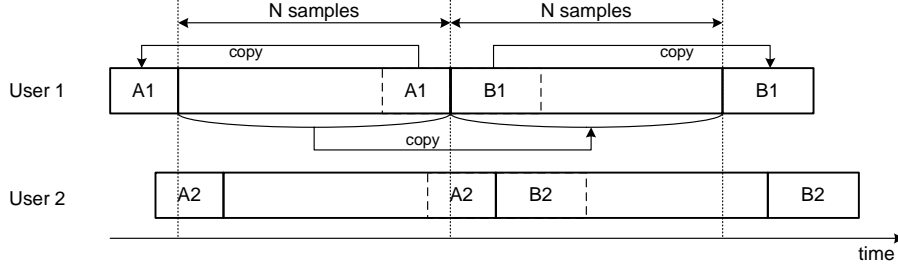
Figure 3.1: Construction of the ranging code extending two OFDMA symbols [44]

CFO. The MS uses these information to correct its transmission parameters, and after that it transmits another random ranging code to the BS. From this point, the MS enters the "periodic ranging" loop, which the key purpose is to make sure the transmission parameters of the MS is always under a tolerable range [44].

The IEEE 802.16e-2005 requires that the TO of all uplink OFDMA symbols do not exceed 25% of the minimum guard-interval or better, and the CFO be less than 2% of the subcarrier spacing [44]. The closed-loop periodic ranging is necessary to obtain synchronization satisfying the above-mentioned requirements, since the TO cannot be measured at the MS's side due to the lack of a common reference, and the CFO experienced by the MS is different from that experienced by the BS. A MS moving at speed v relatively to BS experiences a frequency offset of $f_m = v f_c / c$ due to Doppler shift, where f_c is the carrier frequency and $c = 3 \times 10^8$ (m/s) is the speed of electromagnetic waves traveling in vacuum. If the MS synchronizes itself to the downlink transmission, it actually shifts its carrier frequency by a value of f_m due to the fact that the carrier frequency of the downlink is now $f_c + f_m$. The uplink transmission is also affected by the Doppler phenomenon, and shifted by another f_m. In another words, the received signal at the BS now has an offset of $2 \times f_m$, unless a closed-loop periodic synchronization procedure is used [34]. For example, if a MS operates at $f_c = 5$ GHz, moving at $v = 60$ km/h, the experienced frequency offset at the BS is approximately $2 \times f_m = 556$ Hz. Since the subcarrier spacing is fixed at 9.76 kHz in the IEEE 802.16e-2005 scalable OFDMA PHY, this frequency offset due to Doppler shift is as high as 5.7% of the subcarrier spacing, which is more than double of the 2% required by the standard. Therefore, a CFO estimation technique is necessary at the BS during the ranging period, so that the BS can request the MS to adjust its carrier frequency base to remove CFO in the uplink. This is our motivation to look for an efficient CFO

estimation scheme for the initial ranging scenario in this chapter.

3.2 The state of the art

The choice of synchronization techniques in the ranging scenario depends on
the applied multiple access method. If the ranging procedure is designed
based on TDMA and / or FDMA principle, so as each ranging request occu-
pies one separate time - frequency block, then various estimation techniques
for OFDM- and OFDMA-based systems, for example in [46, 47, 48, 36, 49,
50], can be used. These techniques are all based on the assumption that there
is only one user in the system, or users are separable either in time-domain or
in frequency-domain. In [51], a new set of ranging codes using the orthogonal
principle is proposed, which allows more than one MS to transmit in one time
- frequency block without MUI. This technique assumes perfect frequency
synchronization, or very small residual frequency offset, so as to maintain
the orthogonality of the codes. The advantage of using TDMA or FDMA or
orthogonal principle is that the ranging requests are interference-free, which
can result in better performance than CDMA-based ranging under certain
conditions. Nevertheless, these techniques can offer only a limited number
of ranging codes, because each code is a unique time-frequency block, or
orthogonal code, which cannot be arbitrarily large. The limited number of
ranging code increases the probability of code collision, and thus reduces the
system efficiency.

In IEEE 802.16e-2005, the ranging procedure is defined based on the
CDMA principle, and ranging requests are allowed to overlap. This causes
interference among ranging requests, but also offers a larger code set, which
lowers the code collision's probability. Several estimation techniques have
been proposed for CDMA-based ranging in IEEE 802.16e-2005. In [52, 53,
54, 55], a bank of correlators is used after the FFT, hence it is referred to as
Frequency-Domain Ranging (FDR) technique, to scan the received signal for
known CDMA codes over a 'sliding' phase, which acts as a compensation for
the experienced timing offset. The peak of the correlator output, which must
be greater than a pre-defined threshold, marks a hit (i.e. a code is detected),
and the value of the sliding phase gives the timing offset of that particular
user. This method offers very poor performance under realistic multiuser,
multipath environment, because (i) the CDMA sequence is designed to pro-
vide good auto- and cross-correlation properties when it is shifted in time,
but not when its bits are phase-rotated, (ii) the multipath channel intro-
duces a different complex scaling on every bit of the CDMA code, which
causes the reduction of correlation peak [53, 56]. In [57], a bank of corre-

lators is used before the FFT to directly correlate the received signal with the known time-domain version of the ranging codes, hence it is referred to as Direct Time-Domain Ranging (DTDR) technique. The correlation peak, which must be greater than a pre-set threshold, indicates a hit and the corresponding correlation lag gives the timing offset. [57] assumes there is no CFO in the system, and therefore does not provide a method to estimate the CFO. On the other hand, the Indirect Time-Domain Ranging (ITDR) technique is introduced in [56, 58], where the bank of correlators is replaced by FFT blocks. While the analysis in [56] does not consider CFO at all, [58] provides a frequency-domain CFO estimator. A bank of correlators is used after the FFT to correlate the received signal with known CDMA codes, and the CFO estimate is calculated from the differential phase between two correlations at one OFDMA symbol apart. In order to obtain accurate CFO measurement, [58] requires two ranging transmission: one for coarse TO adjustment, and another for fine TO and CFO estimation. This increasing overhead will reduce the efficiency of the system. In the following sections, we are going to propose simple and efficient method to allow the CFOs to be estimated in only one transmission in both DTDR and ITDR schemes.

3.3   The system model

Let's consider an OFDMA system using a FFT of size N. There are G active ranging channels allocated for ranging MSs. The set of subcarrier indices given to the gth ranging channel is denoted as Δ_g, which can be shared by more than one user in the system. To facilitate TO and CFO estimation, CDMA principle is applied, where the uth user shall pick a random code from a set of M available ranging codes, and transmit over one of the active ranging channels, for instance the gth ranging channel. Note that the BS knows *a prior* this set of available ranging codes, as well as the active ranging channels. Since users are allowed to transmit using any code over any channel, the number of possible combinations, which is also the searching space of the BS, is $G \times M$. The larger this number, the less the probability of code collision, i.e. situation when two or more MSs select the same ranging code and transmit in the same ranging channel simultaneously. But this number cannot be arbitrary large, it is limited by the computational capacity of the BS. The transmitted information of the uth user on the kth subcarrier is given by:

$$\tilde{X}_u[k] = \begin{cases} c_m\big[\mathcal{M}_{k \to i}^g(k)\big] & k \in \Delta_g \\ 0 & \text{otherwise} \end{cases} \tag{3.1}$$

where $k = 0, 1, \ldots, N-1$ is the subcarrier index, $c_m[i]$ is the ith subcarrier symbol belonging to the mth ranging code, and $\mathcal{M}^g_{k \to i}(.)$ is a function that maps k to i depending on the gth ranging channel. This information is modulated by the IFFT operation to form the corresponding time-domain representation of the ranging code:

$$\tilde{x}_u(t) = \frac{1}{N} \sum_{k=0}^{N-1} \tilde{X}_u[k] e^{j2\pi \frac{k}{T_o}(t)} \Xi_{T_o}(t) \tag{3.2}$$

where T_o is the OFDMA symbol duration without guard interval and $\Xi_{T_o}(t)$ is the unity amplitude gate pulse of length T_o. Next, the obtained signal is transmitted consecutively on two OFDMA symbols with CP and cyclic postfix, as described in Figure 3.1. The complex baseband preamble from the uth user now can be described as [35]:

$$\tilde{y}_u(t) = \frac{1}{N} \sum_{k=0}^{N-1} \tilde{X}_u[k] e^{j2\pi \frac{k}{T_o}(t-T_g^A)} \Xi_{T_s}(t) \tag{3.3}$$

where $\Xi_{T_s}(t)$ is the unity amplitude gate pulse of length $T_s = T_g^A + 2T_o + T_g^B$, and T_g^A and T_g^B are the two guard intervals, respectively. Let's consider that the uth user transmission experiences independent frequency-selective block fading channel, with the following CIR:

$$\tilde{h}_u(\tau) = \sum_{l=0}^{L-1} \tilde{h}_{u,l} \delta(\tau - \tau_{u,l}) \tag{3.4}$$

where L is the total number of multipath components, $\tilde{h}_{u,l}$ and $\tau_{u,l}$ are the complex gain and time delay of the lth multipath component of the uth user, respectively. The channel is assumed to be static for the ranging duration, and the gain coefficients for each path contribution are assumed to be uncorrelated. If each user observes independent TO and CFO, denoted respectively as δt_u and δf_u, which are assumably constant during the observation period, then the complex baseband received signal can be expressed as:

$$\tilde{r}(t) = \sum_{u=0}^{U-1} \sum_{l=0}^{L-1} \tilde{h}_{u,l} \tilde{y}_u(t - \delta t_u - \tau_{u,l}) e^{j2\pi \delta f_u t} + \tilde{n}(t) \tag{3.5}$$

where $\tilde{n}(t)$ is the complex baseband AWGN at the input of the OFDMA receiver and U is total number of ranging users. It is worth noting that we consider scenario where there is no data transmission during the ranging period. The interference caused by ranging channels on data transmission channel is not the interest of this chapter. And since these MSs in data

transmission mode are already synchronized to the BS and using different frequency bands, they should not cause any interference to the ranging channels. Thus, their effect can be neglected in our evaluation. At the receiver, the received signal is sampled at rate $1/\Delta t$, e.g. $\tilde{r}[n] = \tilde{r}(n\Delta t)$. Our task now is to find the independent TOs and CFOs of each active user based on the sampled observation at the BS.

3.4 The Direct Time-Domain Ranging Technique

The DTDR technique uses a bank of correlators to correlate the received and sampled signal with the known time-domain representation of all available ranging codes [57], which are also sampled at the same rate. Figure 3.2 illustrates the block diagram of the DTDR technique. We assume that there is no ranging code used by more than one user at any ranging channel at any given time, i.e. the code collision scenario is not considered. The correlator output corresponding to the mth ranging code at the gth ranging channel, which is referred to as the (m, g) code hereafter, can be expressed as:

$$
\begin{aligned}
\tilde{\Gamma}^{\text{DTDR}}_{m,g}[\lambda] &= \sum_{n=0}^{N_r-1} \tilde{x}_{m,g}[n]\tilde{r}^*\big[(n+\lambda)\big] \\
&= \begin{cases} \tilde{p}_{m,g}[\lambda] + \tilde{w}_{m,g}[\lambda] + \tilde{v}_{m,g}[\lambda] & \exists \text{ user } u \text{ using } (m,g) \text{ code} \\ \tilde{w}_{m,g}[\lambda] + \tilde{v}_{m,g}[\lambda] & \text{Otherwise} \end{cases}
\end{aligned}
\tag{3.6}
$$

where $[.]^*$ denotes complex conjugate, N_r is the length of correlation window, λ is the correlation lag and:

$$
\tilde{x}_{m,g}[n] = \frac{1}{N} \sum_{k \in \Delta_g} c_m\big[\mathcal{M}^g_{k \to i}(k)\big] e^{j2\pi \frac{nk}{N}}
\tag{3.7}
$$

$$
\begin{aligned}
\tilde{p}_{m,g}[\lambda] &= e^{-j2\pi\epsilon f_u \frac{\lambda}{N}} \sum_{l=0}^{L-1} \tilde{h}^*_{u,l} \sum_{n=0}^{N_r-1} \tilde{x}_{m,g}[n] \\
&\times \tilde{y}^*_u\big[n + \lambda - \epsilon t_u - \tau_{u,l}/\Delta t\big] e^{-j2\pi\epsilon f_u \frac{n}{N}}
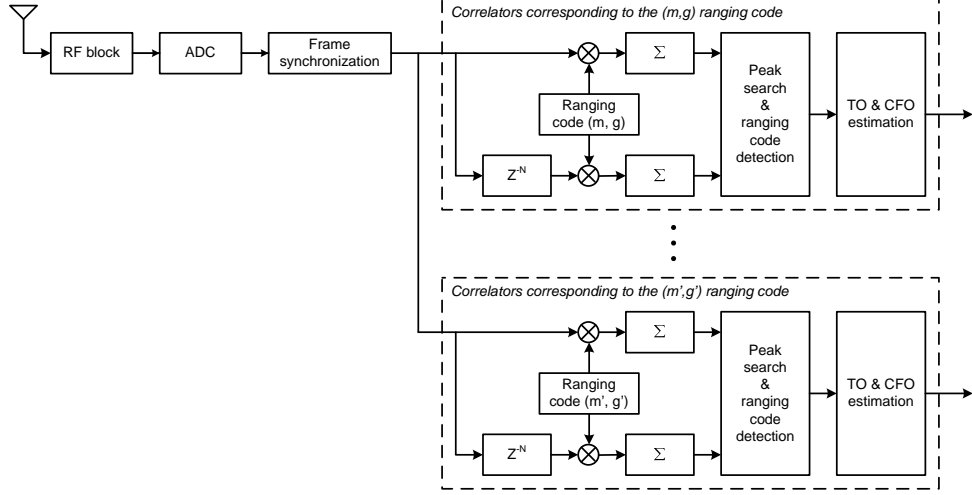\end{aligned}
\tag{3.8}
$$

Figure 3.2: The block diagram of the Direct Time-Domain Ranging scheme

$$
\begin{aligned}
\tilde{w}_{m,g}[\lambda] &= \sum_{u'=0;u'\neq u}^{U-1} \sum_{l=0}^{L-1} \tilde{h}_{u',l}^* \sum_{n=0}^{N_r-1} \tilde{x}_{m,g}[n] \\
&\times \; \tilde{y}_{u'}^*[n+\lambda-\epsilon t_{u'}-\tau_{u',l}/\Delta t] e^{-j2\pi\epsilon f_{u'}\frac{(n+\lambda)}{N}}
\end{aligned}
\tag{3.9}
$$

$$
\tilde{v}_{m,g}[\lambda] = \sum_{n=0}^{N_r-1} \tilde{x}_{m,g}[n] \tilde{n}^*[n+\lambda]
\tag{3.10}
$$

The $\tilde{p}_{m,g}[\lambda]$ indicates the auto-correlation term of the ranging code of interest, while the $\tilde{w}_{m,g}[\lambda]$ and $\tilde{v}_{m,g}[\lambda]$ are the cross-correlation terms between the ranging code of interest with ranging code from other users and with the AWGN, respectively. $\tilde{y}[n+\lambda] = \tilde{y}((n+\lambda)\Delta t)$ is the sampled transmitted signal, while $\tilde{n}[n+\lambda] = \tilde{n}((n+\lambda)\Delta t)$ is the sampled noise. And Δf is the subcarrier spacing, $\epsilon t_u = \frac{\delta t_u}{\Delta t}$ and $\epsilon f_u = \frac{\delta f_u}{\Delta f}$ are normalized TO and CFO, respectively.

Assume that there exists the uth user that using the mth ranging code at the gth ranging channel. And for the sake of simplicity, we assume that the wireless channel has only one tap, i.e. $L = 1$; and the length of the correlation window is equal to the size of the FFT, $N_r = N$. With these assumptions and by expanding Eq. (3.8), we obtain:

$$\tilde{p}_{m,g}[\lambda] = \frac{1}{N^2} e^{-j2\pi\epsilon f_u \frac{\lambda}{N}} \tilde{h}_{u,0}^* \Big\{ \sum_{k_1 \in \Delta_g} |\tilde{X}_u[k_1]|^2 e^{-j2\pi \frac{(\lambda - \epsilon t_u - \tau_{u,0}/\Delta t - N_g^A)k_1}{N}} \tilde{\mathcal{C}}_{(-\epsilon f_u)}$$

$$+ \sum_{k_1 \in \Delta_g} \sum_{k_2 \in \Delta_g; k_2 \neq k_1} \tilde{X}_u[k_1] \tilde{X}_u^*[k_2]$$

$$\times e^{-j2\pi \frac{(\lambda - \epsilon t_u - \tau_{u,0}/\Delta t - N_g^A)k_2}{N}} \tilde{\mathcal{C}}_{(k_1 - k_2 - \epsilon f_u)} \Big\} \tag{3.11}$$

where N_g^A is the number of samples in the CP, and $\tilde{\mathcal{C}}(\phi) = \frac{\sin \pi\phi}{N \sin \pi\phi/N} e^{j\pi\phi(N-1)/N}$ is the periodic sinc-function [37]. When $\lambda = \epsilon t_u + \tau_{u,0}/\Delta t + N_g^A$, the first sum in Eq. (3.11) becomes maximum because its elements are added in-phase together. This introduces an auto-correlation peak as shown in Figure 3.3: the top sub-figure shows the normalized power of the auto-correlation between the ranging code $\tilde{x}_{m,g}[n]$ and the transmitted ranging preamble, $\tilde{y}_u[n]$, in AWGN channel as a function of the correlation lag. It is worth to note that there are four significant correlation peaks, which correspond to the four repeated parts of the preamble as described in Figure 3.1: the CP, the two consecutive OFDMA symbols, and then the cyclic post-fix.

There is another way to explain this phenomenon. In Eq. (3.2), the signal $\tilde{x}_u(t)$ can be seen as a sum of $|\Delta_g|$ independent phasors, where $|\Delta_g|$ is the size of subcarrier set Δ_g. When the number of subcarriers is large, the law of large number can be evoked and $\tilde{x}_u(t)$ can be considered as a random Gaussian noise sequence with some properties of interest. First, the auto-correlation term in Eq. (3.8) is a Dirac Delta function, which has an auto-correlation peak at lag zero and relatively small values otherwise. Second, the cross-correlation terms of the ranging code of interest with the other ranging codes and the AWGN (in Eq. (3.9) and (3.10), respectively) are expected to be small and can be neglected (see Figure 3.3).

Eq. (3.11) shows the auto-correlation peak at a one-tap channel. Should the channel has more than one tap (i.e $L > 1$), multiple auto-correlation peaks shall be introduced: each corresponding to one tap, where the correlation lag depends on the delay of the tap and the correlation power reduces according to the power of the tap. Thus, the power of the correlator output in Eq. (3.6) reaches its maximum at correlation lag $\lambda_{m,g}^{max}$ equal to:

$$\lambda_{m,g}^{max} = \epsilon t_u + \tau_{u,l_{max}}/\Delta t + N_g^A \tag{3.12}$$

where $\tau_{u,l_{max}}$ is the time delay of the strongest multipath component.

From the above discussion, the TO of the uth user transmitting the (m, g) ranging code can be estimated by finding λ that maximizes the power of the (m, g) correlator output [57]:
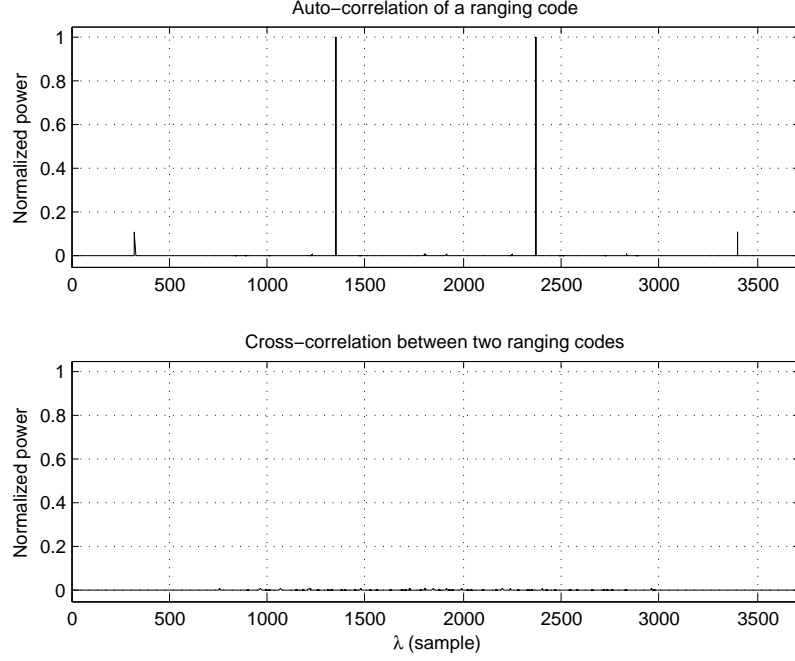
Figure 3.3: The auto- and cross-correlation properties of the ranging code $(N_r = N = 1024)$

$$\hat{\epsilon t}_u^{\text{DTDR}} = \text{argmax}_\lambda \big| \tilde{\Gamma}_{m,g}^{\text{DTDR}}\big[\lambda\big]\big|^2 \qquad (3.13)$$

in which $|.|$ denotes the absolute value of a complex number, λ is integer in the range of $\big[0, D_{max}\big]$, and D_{max} is the maximum value of the normalized delay, $\max(\epsilon t_u)$, plus the maximum delay of the multipath channel, $\max(\tau_{u,l})$. It is worth noting that the estimated TO depends not only on the transmission delay, but also on the time delay of the strongest multipath component.

Due to the fact that the ranging code is successively transmitted in two OFDMA symbol intervals, and the channel is assumed to be constant during this period, the auto-correlation term in Eq. (3.11) is periodic with period of N, except for a phase shift due to the CFO, i.e.:

$$\tilde{p}_{m,g}\big[\lambda + N\big] = e^{-j2\pi\epsilon f_u}\tilde{p}_{m,g}\big[\lambda\big] \qquad (3.14)$$

or:

$$\tilde{\Gamma}_{m,g}^{\text{DTDR}}\big[\lambda + N\big] = e^{-j2\pi\epsilon f_u}\tilde{p}_{m,g}\big[\lambda\big] + \tilde{w}_{m,g}\big[\lambda + N\big] + \tilde{v}_{m,g}\big[\lambda + N\big] \quad (3.15)$$

36

This observation inspires us to propose a CFO estimation scheme for the ranging scenario. We consider N_{ob} observation points at the output of the correlator corresponding to the (m, g) ranging code and define the following vectors:

$$\vec{\boldsymbol{\Gamma}}_{m,g,d_1}^{\mathrm{Ob-DTDR}} = \left[\tilde{\Gamma}_{m,g}^{\mathrm{DTDR}}[\lambda_1], \tilde{\Gamma}_{m,g}^{\mathrm{DTDR}}[\lambda_2], \ldots, \tilde{\Gamma}_{m,g}^{\mathrm{DTDR}}[\lambda_{N_{\mathrm{ob}}}]\right]^T \tag{3.16}$$

$$\vec{\boldsymbol{\Gamma}}_{m,g,d_2}^{\mathrm{Ob-DTDR}} = \left[\tilde{\Gamma}_{m,g}^{\mathrm{DTDR}}[\lambda_1 + N], \tilde{\Gamma}_{m,g}^{\mathrm{DTDR}}[\lambda_2 + N], \ldots, \right.$$

$$\left. \tilde{\Gamma}_{m,g}^{\mathrm{DTDR}}[\lambda_{N_{\mathrm{ob}}} + N]\right]^T \tag{3.17}$$

$$\vec{\mathbf{p}}_{m,g} = \left[\tilde{p}_{m,g}[\lambda_1], \tilde{p}_{m,g}[\lambda_2], \ldots, \tilde{p}_{m,g}[\lambda_{N_{\mathrm{ob}}}]\right]^T \tag{3.18}$$

$$\vec{\mathbf{q}}_{m,g,d_1} = \left[\tilde{w}_{m,g}[\lambda_1] + \tilde{v}_{m,g}[\lambda_1], \tilde{w}_{m,g}[\lambda_2] + \tilde{v}_{m,g}[\lambda_2], \ldots, \right.$$

$$\left. \tilde{w}_{m,g}[\lambda_{N_{\mathrm{ob}}}] + \tilde{v}_{m,g}[\lambda_{N_{\mathrm{ob}}}]\right]^T \tag{3.19}$$

$$\vec{\mathbf{q}}_{m,g,d_2} = \left[\tilde{w}_{m,g}[\lambda_1 + N] + \tilde{v}_{m,g}[\lambda_1 + N], \tilde{w}_{m,g}[\lambda_2 + N] + \tilde{v}_{m,g}[\lambda_2 + N], \right.$$

$$\left. \ldots, \tilde{w}_{m,g}[\lambda_{N_{\mathrm{ob}}} + N] + \tilde{v}_{m,g}[\lambda_{N_{\mathrm{ob}}} + N]\right]^T \tag{3.20}$$

where $\vec{\boldsymbol{\Gamma}}_{m,g,d_i}^{\mathrm{Ob-DTDR}}$ is the N_{ob}-point observation vector selected from the output of the correlator corresponding to the (m, g) code, $\vec{\mathbf{s}}_{m,g}$ is the auto-correlation vector of the ranging code of interest, while $\vec{\mathbf{q}}_{m,g,d_i}$ is the cross-correlation vector of the ranging code of interest with the other active ranging codes and the AWGN ($i = 1, 2$). Then the Eq. (3.6) and (3.15) can be re-written in matricial form as follows:

$$\begin{cases} \vec{\boldsymbol{\Gamma}}_{m,g,d_1}^{\mathrm{Ob-DTDR}} = \vec{\mathbf{p}}_{m,g} + \vec{\mathbf{q}}_{m,g,d_1} \\ \vec{\boldsymbol{\Gamma}}_{m,g,d_2}^{\mathrm{Ob-DTDR}} = \vec{\mathbf{p}}_{m,g} e^{-j2\pi\epsilon f_u} + \vec{\mathbf{q}}_{m,g,d_2} \end{cases} \tag{3.21}$$

This is a known problem, and the Maximum Likelihood (ML) estimate of ϵf_u is given in [46]:

$$
\begin{aligned}
\hat{\epsilon f}_u^{\;\mathrm{DTDR}} &= -\frac{1}{2\pi}\arctan\left\{\frac{\Im\left[(\vec{\boldsymbol{\Gamma}}_{m,g,d_1}^{\mathrm{Ob-DTDR}})^H\vec{\boldsymbol{\Gamma}}_{m,g,d_2}^{\mathrm{Ob-DTDR}}\right]}{\Re\left[(\vec{\boldsymbol{\Gamma}}_{m,g,d_1}^{\mathrm{Ob-DTDR}})^H\vec{\boldsymbol{\Gamma}}_{m,g,d_2}^{\mathrm{Ob-DTDR}}\right]}\right\} \\[2ex]
&= -\frac{1}{2\pi}\arctan\left\{\frac{\sum_{i=1}^{N_{\mathrm{ob}}}\Im\left(\tilde{\Gamma}_{m,g}^{\mathrm{DTDR}}[\lambda_i+N]\tilde{\Gamma}_{m,g}^{\mathrm{DTDR}}[\lambda_i]^*\right)}{\sum_{i=1}^{N_{\mathrm{ob}}}\Re\left(\tilde{\Gamma}_{m,g}^{\mathrm{DTDR}}[\lambda_i+N]\tilde{\Gamma}_{m,g}^{\mathrm{DTDR}}[\lambda_i]^*\right)}\right\} \quad (3.22)
\end{aligned}
$$

where arctan(.) is the inverse tangent function, $\Im(.)$ and $\Re(.)$ are the imaginary and the real parts of a complex number, respectively.

It is worth noting that the estimator performance depends on the selection of the observation points. Since the CFO is estimated based on the phase difference between two correlations, which are disturbed by noise and interference terms, it is desirable that the elements of the observation vectors have high useful CINR, i.e. the ratio between the power of the useful component, $\left|\tilde{p}_{m,g}[\lambda_i]\right|^2$, and the power of the noise and interference, $\left|\tilde{q}_{m,g}[\lambda_i]\right|^2 = \left|\tilde{w}_{m,g}[\lambda_i]+\tilde{v}_{m,g}[\lambda_i]\right|^2$ $(i=1,2,\ldots,N_{\mathrm{ob}})$. As illustrated in Figure 3.4, the higher the CINR, the smaller the phase error, and thus the smaller the CFO estimation error. In the following section, we will discuss the algorithm to select the observation points that maximizes the useful CINR in more details.

Since the inverse tangent function is limited in range $\left[-\pi,\pi\right]$, the theoretical range of our CFO estimator is given by:

$$
|\delta f_u| \le 0.5\Delta f \quad (3.23)
$$

We assume that, prior to the ranging transmission, a coarse frequency synchronization has been performed at the downlink by the MS, using one among the various estimation techniques available for OFDM, such as [47, 46], to bring its CFO down to an acceptable value. Thus, this limitation does not introduce any problem for our proposed algorithm.

3.5 The Indirect Time-Domain Ranging technique

The ITDR technique is proposed in [56, 58], where the correlators are replaced by FFT blocks, as shown in Figure 3.5. The principle behind this technique is the circular correlation theorem [59, 60], which states:
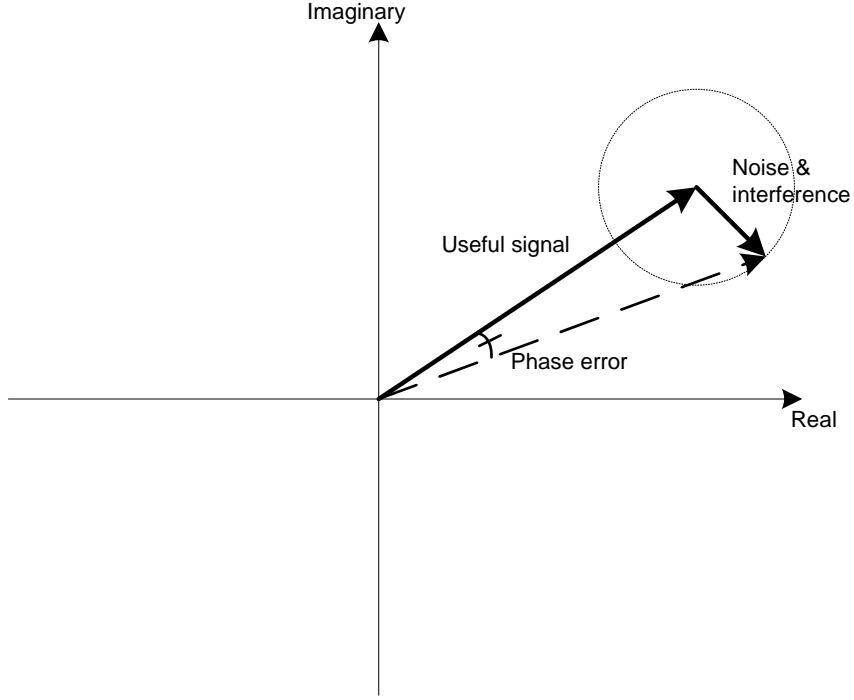
Figure 3.4: The phase error caused by the noise and interference
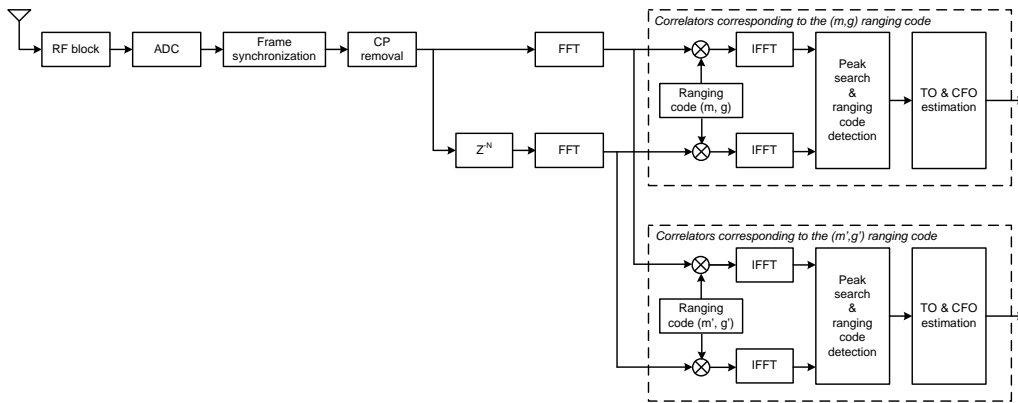
Figure 3.5: The Indirect Time-Domain Ranging scheme
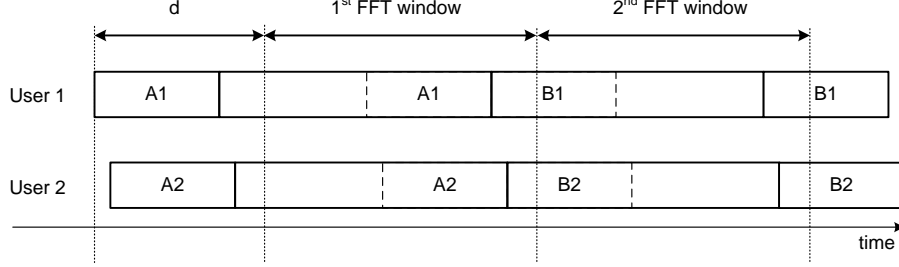
Figure 3.6: Two consecutive N-sample FFT windows with timing offset d.

Theorem 1. *Let $\vec{\mathfrak{a}}$, $\vec{\mathfrak{A}}$, $\vec{\mathfrak{b}}$, $\vec{\mathfrak{B}}$ be finite vectors of length N. Assume $\vec{\mathfrak{A}}$ is the N-point DFT of $\vec{\mathfrak{a}}$ and $\vec{\mathfrak{B}}$ is the N-point DFT of $\vec{\mathfrak{b}}$. Then $\vec{\mathfrak{a}}$ and $\vec{\mathfrak{b}}$ are also the N-point Inverse Discrete Fourier Transform (IDFT) of $\vec{\mathfrak{A}}$ and $\vec{\mathfrak{B}}$, respectively.*

The unnormalized circular cross correlation of two vectors $\vec{\mathfrak{a}}$ and $\vec{\mathfrak{b}}$ is defined as:

$$\vec{\mathfrak{c}}_{ab} \triangleq \left\{ \tilde{c}_{ab}[k] = \sum_{n=0}^{N-1} \tilde{a}[n]^* \times \tilde{b}[(k+n) \mod N], \ k = 0, 1, 2, \ldots, N-1 \right\}^T \tag{3.24}$$

where $[.]_{\mod N}$ denotes modulo N operation, $\tilde{a}[k]$ and $\tilde{b}[k]$ are the kth complex-value elements of two vectors $\vec{\mathfrak{a}}$ and $\vec{\mathfrak{b}}$, respectively.

Then the N-point DFT pair of vector $\vec{\mathfrak{c}}_{ab}$ is given by:

$$\vec{\mathfrak{C}}_{ab} = \vec{\mathfrak{A}}^* \odot \vec{\mathfrak{B}} \tag{3.25}$$

where $\odot$ is Schur product of two vectors or matrices, which performs the element-wise multiplication.

Consider N consecutive samples of the received signal, $\vec{\mathbf{r}}_d = [\tilde{r}_d[0], \ldots, \tilde{r}_d[N-1]]^T$, where $\tilde{r}_d[n] = \tilde{r}\big((d+n)\Delta t\big)$, $n = 0, 1, \ldots, N-1$ and d denotes the timing offset of the observation vector, starting from the earliest arrived signal (as illustrated in Figure 3.6). We assume that d is long enough to accommodate both the transmission delays of all users and the channel delay, thus there is no influence from the adjacent transmitted OFDMA symbol to the observation window. After FFT operation, only the subcarriers belonging to the gth ranging channel is selected, and the output at these subcarriers is given by:

$$\vec{\mathbf{Z}}_{g,d} = \mathbf{S}_g \mathbf{F}_N \vec{\mathbf{r}}_d$$

$$= e^{j2\pi \frac{\epsilon f_u}{N} d} \mathbf{S}_g \mathbf{C}_{(\epsilon f_u)} \mathbf{T}_{(d)} \mathbf{H}_u \vec{\mathbf{X}}_u + \sum_{u_1 \in U_g; u_1 \neq u} e^{j2\pi \frac{\epsilon f_{u_1}}{N} d} \mathbf{S}_g \mathbf{C}_{(\epsilon f_{u_1})} \mathbf{T}_{(d)} \mathbf{H}_{u_1} \vec{\mathbf{X}}_{u_1}$$

$$+ \sum_{u_2 \notin U_g} e^{j2\pi \frac{\epsilon f_{u_2}}{N} d} \mathbf{S}_g \mathbf{C}_{(\epsilon f_{u_2})} \mathbf{T}_{(d)} \mathbf{H}_{u_2} \vec{\mathbf{X}}_{u_2} + \mathbf{S}_g \vec{\mathbf{N}}_d \qquad (3.26)$$

where $\mathbf{F}_N$ stands for the size-N square FFT matrix with entries $\mathbf{F}_N[n,k] = e^{-j2\pi nk/N}/\sqrt{N}$ for $0 \leq n, k \leq N-1$, and $\mathbf{S}_g$ is a diagonal matrix of size $N \times N$, acting as a filter to select only subcarriers belonging to the gth ranging channel, i.e. $\mathbf{S}_g(k,k) = 1$ for $k \in \Delta_g$ and zero elsewhere. $\vec{\mathbf{Z}}_{g,d} = \left[\tilde{Z}_{g,d}[0], \tilde{Z}_{g,d}[1], \ldots, \tilde{Z}_{g,d}[N-1] \right]^T$ and $\vec{\mathbf{N}}_d = \left[\tilde{N}_d[0], \tilde{N}_d[1], \ldots, \tilde{N}_d[N-1] \right]^T$, where $\tilde{Z}_{g,d}[k]$ and $\tilde{N}_d[k]$ are the uth user's observed information and the AWGN contribution at the kth subcarriers, respectively. $\mathbf{H}_u$ is a diagonal matrix of size N, whose k^{th} diagonal entry, $\mathbf{H}_u[k,k] = e^{-j2\pi \frac{k}{N} \epsilon t_u} \sum_{l=0}^{L-1} \tilde{h}_{u,l} e^{-j2\pi \frac{k}{T_o} \tau_{u,l}}$, is the CTF at the kth subcarrier of the uth user. $\vec{\mathbf{X}}_u = \left[\tilde{X}_u[0], \tilde{X}_u[1], \ldots \tilde{X}_u[N-1] \right]^T$ is the uth user's transmitted ranging code. $\mathbf{T}_{(d)}$ is the diagonal matrix of size N, whose k^{th} diagonal element is equal to $e^{j2pi \frac{k}{N} d}$, indicating the phase shift due to the timing offset d. The $N \times N$ matrix $\mathbf{C}_{(\phi)}$ represents the shift due to the normalized CFO ϕ in frequency-domain. It is a circulant matrix representing the circular convolution operation:

$$\mathbf{C}_{(\phi)} = \mathbf{F}_N \mathbf{c}_{(\phi)} \mathbf{F}_N^H$$

$$= \begin{bmatrix} \tilde{\mathcal{C}}(\phi) & \tilde{\mathcal{C}}(1+\phi) & \ldots & \tilde{\mathcal{C}}(N-1+\phi) \\ \tilde{\mathcal{C}}(N-1+\phi) & \tilde{\mathcal{C}}(\phi) & \ldots & \tilde{\mathcal{C}}(N-2+\phi) \\ \vdots & \vdots & \ddots & \vdots \\ \tilde{\mathcal{C}}(1+\phi) & \tilde{\mathcal{C}}(2+\phi) & \ldots & \tilde{\mathcal{C}}(\phi) \end{bmatrix} \qquad (3.27)$$

where $\tilde{\mathcal{C}}(\phi) = \frac{\sin \pi \phi}{N \sin \pi \phi / N} e^{j\pi \phi (N-1)/N}$ is the periodic sinc-function [37] and $\mathbf{c}_{(\phi)}$ is a diagonal matrix of size N representing the CFO in time-domain, whose the nth diagonal element is equal to $e^{j2\pi \frac{n}{N} \phi}$. The output $\vec{\mathbf{Z}}_g$ shall be multiplied element-wise with the complex conjugate of the FFT of the known (m,g) ranging code, $\vec{\mathbf{X}}_{m,g}$, and then be converted back to time-domain to obtain the required correlation:

$$
\begin{aligned}
\vec{\mathbf{\Gamma}}_{m,g,d}^{\mathrm{ITDR}} \;=\;& \mathbf{F}_N^H \left[\vec{\mathbf{X}}_{m,g}^* \odot \vec{\mathbf{Z}}_{g,d} \right] \\[4pt]
=\;& e^{j2\pi \frac{\epsilon f_u}{N} d} \bar{\mathbf{x}}_{m,g} \mathbf{F}_N^H \mathbf{S}_g \mathbf{C}_{(\epsilon f_u)} \mathbf{T}_{(d)} \mathbf{H}_u \vec{\mathbf{X}}_u \\
&+ \sum_{u_1 \in U_g; u_1 \neq u} e^{j2\pi \frac{\epsilon f_{u_1}}{N} d} \bar{\mathbf{x}}_{m,g} \mathbf{F}_N^H \mathbf{S}_g \mathbf{C}_{(\epsilon f_{u_1})} \mathbf{T}_{(d)} \mathbf{H}_{u_1} \vec{\mathbf{X}}_{u_1} \\
&+ \sum_{u_2 \notin U_g} e^{j2\pi \frac{\epsilon f_{u_2}}{N} d} \bar{\mathbf{x}}_{m,g} \mathbf{F}_N^H \mathbf{S}_g \mathbf{C}_{(\epsilon f_{u_2})} \mathbf{T}_{(d)} \mathbf{H}_{u_2} \vec{\mathbf{X}}_{u_2} + \bar{\mathbf{x}}_{m,g} \mathbf{F}_N^H \mathbf{S}_g \vec{\mathbf{N}}_d \\[4pt]
=\;& e^{j2\pi \frac{\epsilon f_u}{N} d} \bar{\mathbf{x}}_{m,g} \mathbf{s}_g \mathbf{c}_{(\epsilon f_u)} \mathbf{t}_{(d)} \mathbf{h}_u \vec{\mathbf{x}}_u + \sum_{u_1 \in U_g; u_1 \neq u} e^{j2\pi \frac{\epsilon f_{u_1}}{N} d} \bar{\mathbf{x}}_{m,g} \mathbf{s}_g \mathbf{c}_{(\epsilon f_{u_1})} \mathbf{t}_{(d)} \mathbf{h}_{u_1} \vec{\mathbf{x}}_{u_1} \\
&+ \sum_{u_2 \notin U_g} e^{j2\pi \frac{\epsilon f_{u_2}}{N} d} \bar{\mathbf{x}}_{m,g} \mathbf{s}_g \mathbf{c}_{(\epsilon f_{u_2})} \mathbf{t}_{(d)} \mathbf{h}_{u_2} \vec{\mathbf{x}}_{u_2} + \bar{\mathbf{x}}_{m,g} \mathbf{s}_g \vec{\mathbf{n}}_d \qquad (3.28)
\end{aligned}
$$

in which:

$$
\vec{\mathbf{X}}_{m,g} = \left\{ \tilde{X}_{m,g}[k] = \sum_{n=0}^{N-1} \tilde{x}_{m,g}[n] e^{-j2\pi \frac{nk}{N}}, \; k = 0, 1, \ldots, N-1 \right\}^T \qquad (3.29)
$$

$$
\begin{aligned}
\bar{\mathbf{x}}_{m,g} \;=\;& \mathbf{F}_N^H \mathrm{diag}\left(\vec{\mathbf{X}}_{m,g}^* \right) \mathbf{F}_N \\[4pt]
=\;& \begin{bmatrix}
\tilde{x}_{m,g}[0]^* & \tilde{x}_{m,g}[1]^* & \ldots & \tilde{x}_{m,g}[N-1]^* \\
\tilde{x}_{m,g}[N-1]^* & \tilde{x}_{m,g}[0]^* & \ldots & \tilde{x}_{m,g}[N-2]^* \\
\vdots & \vdots & \ddots & \vdots \\
\tilde{x}_{m,g}[1]^* & \tilde{x}_{m,g}[2]^* & \ldots & \tilde{x}_{m,g}[0]^*
\end{bmatrix} \qquad (3.30)
\end{aligned}
$$

$$
\mathbf{t}_{(d)} \;=\; \mathbf{F}_N^H \mathbf{T}_{(d)} \mathbf{F}_N \qquad (3.31)
$$

$$
\mathbf{s}_g \;=\; \mathbf{F}_N^H \mathbf{S}_g \mathbf{F}_N \qquad (3.32)
$$

$$
\begin{aligned}
\mathbf{h}_u \;=\;& \mathbf{F}_N^H \mathbf{H}_u \mathbf{F}_N \\[4pt]
=\;& \begin{bmatrix}
\tilde{h}_u^{\mathrm{eff}}[0] & \tilde{h}_u^{\mathrm{eff}}[N-1] & \ldots & \tilde{h}_u^{\mathrm{eff}}[1] \\
\tilde{h}_u^{\mathrm{eff}}[1] & \tilde{h}_u^{\mathrm{eff}}[0] & \ldots & \tilde{h}_u^{\mathrm{eff}}[2] \\
\vdots & \vdots & \ddots & \vdots \\
\tilde{h}_u^{\mathrm{eff}}[N-1] & \tilde{h}_u^{\mathrm{eff}}[N-2] & \ldots & \tilde{h}_u^{\mathrm{eff}}[0]
\end{bmatrix} \qquad (3.33)
\end{aligned}
$$

$$\vec{\mathbf{x}}_u = [\tilde{x}_u[0], \tilde{x}_u[1], \ldots, \tilde{x}_u[N-1]]^T \tag{3.34}$$

$$\vec{\mathbf{n}}_d = [\tilde{n}_d[0], \tilde{n}_d[1], \ldots, \tilde{n}_d[N-1]]^T \tag{3.35}$$

$\vec{\mathbf{\Gamma}}_{m,g,d}^{\text{ITDR}}$ is the correlator's output vector, $\bar{\mathbf{x}}_{m,g}$ indicates the circular correlation corresponding to the (m, g) ranging code, and $\tilde{x}_u[n] = \tilde{x}_u(n\Delta t)$ and $\tilde{n}_d[n] = \tilde{n}((n + d)\Delta t)$ are respectively the nth sample of the uth user's signal and the AWGN, and diag $(\vec{\mathfrak{a}})$ denotes diagonal matrix with the entries of the vector $\vec{\mathfrak{a}}$ on its diagonal. The circulant matrix, $\mathbf{h}_u$, represents the circular convolution of the uth user's effective channel, where $\tilde{h}_u^{\text{eff}}[n]$ is the nth multipath component of the uth user's effective CIR, which is a result of the sampling process and can be expressed as:

$$
\begin{aligned}
\tilde{h}_u^{\text{eff}}[n] &= \sum_{k=0}^{N-1} \mathbf{H}_u[k, k] e^{j2\pi \frac{nk}{N}} \\
&= \sum_{l=0}^{L-1} \tilde{h}_{u,l} \tilde{\mathcal{C}}(n - \epsilon t_u - \zeta_{u,l} - \xi_{u,l})
\end{aligned}
\tag{3.36}
$$

where $\zeta_{u,l}$ and $\xi_{u,l}$ are the integer and the fractional part of the $\tau_{u,l}/\Delta t$, respectively.

In Eq. (3.28), the first term indicates the circular auto-correlation of the (m, g) ranging code, and if expanding it, the kth element will be similar to the one given in Eq. (3.11). And the second, third and last terms are the circular cross-correlation between the (m, g) ranging code and (a) other ranging codes in the same ranging slot, (b) other ranging codes in different ranging slots, and (c) the AWGN vector, respectively. Based on the same argument as presented in section 3.4, we can estimate the TO and CFO by:

$$\hat{\epsilon t}_u^{\text{ITDR}} = \text{argmax}_\lambda \left| \tilde{\Gamma}_{m,g}^{\text{ITDR}}[\lambda] \right|^2 \tag{3.37}$$

$$\hat{\epsilon f}_u^{\text{ITDR}} = -\frac{1}{2\pi} \arctan \left\{ \frac{\Im \left[(\vec{\mathbf{\Gamma}}_{m,g,d_1}^{\text{Ob-ITDR}})^H \vec{\mathbf{\Gamma}}_{m,g,d_2}^{\text{Ob-ITDR}} \right]}{\Re \left[(\vec{\mathbf{\Gamma}}_{m,g,d_1}^{\text{Ob-ITDR}})^H \vec{\mathbf{\Gamma}}_{m,g,d_2}^{\text{Ob-ITDR}} \right]} \right\} \tag{3.38}$$

where $\vec{\mathbf{\Gamma}}_{m,g,d_1}^{\text{Ob-ITDR}}$ and $\vec{\mathbf{\Gamma}}_{m,g,d_2}^{\text{Ob-ITDR}}$ are two N_{ob}-points observation vectors, selected from two consecutive circular correlations, $\vec{\mathbf{\Gamma}}_{m,g,d_1}^{\text{ITDR}}$ and $\vec{\mathbf{\Gamma}}_{m,g,d_2}^{\text{ITDR}}$, which are N samples apart (i.e. $d_2 = d_1 + N$). The theoretical range of this CFO estimator is also the same as Eq. (3.23).

3.6 Implementation of the proposed algorithms

3.6.1 Ranging code detection

In the previous sections, we assume that the (m, g) ranging code is always transmitted, but that is not always the case. Thus, the BS must identify if a particular ranging code is actually present, before concluding that the estimated TO and CFO corresponding to that ranging code are valid. This process is referring to as "ranging code detection".

For the Direct Time-Domain Ranging scheme

The Eq. (3.6) shows the two possible case of the output of the (m, g) correlator: when the (m, g) ranging code is transmitted, and when it is not. Recalling the cross- and auto-correlation properties of the ranging code discussed in section 3.4, we know that, when the code of interest is not present, the power at the correlator's output will be relatively small and constant, due to the low cross-correlation between different ranging codes and the noise. When the code of interest is present, the power at the correlator output will also small, except at correlation lag corresponding to the maximum auto-correlation value. Thus, the code detection problem is equivalent to a search for the peak power caused by the auto-correlation. This search can be done by comparing the ratio between the instantaneous correlation power with the average correlation power to a predefined threshold η_a. Let's consider the following decision variable:

$$\Omega^{\text{DTDR}}_{m,g,d_1}[\lambda] = \frac{\left|\tilde{\Gamma}^{\text{DTDR}}_{m,g,d_1}[\lambda]\right|^2}{\Theta^{\text{DTDR}}_{m,g,d_1}} \tag{3.39}$$

in which

$$\Theta^{\text{DTDR}}_{m,g,d_1} = \frac{1}{N_{\text{ow}}} \sum_{\lambda_1 = \lambda - N_{\text{ow}}}^{\lambda - 1} \left|\tilde{\Gamma}^{\text{DTDR}}_{m,g,d_1}[\lambda_1]\right|^2 \tag{3.40}$$

is the average power of the correlator's output over a window of size N_{ow}. Let the null hypothesis, H_0, be the (m, g) ranging code is not present, and the alternative hypothesis, H_1, be the (m, g) ranging code is present. The code detection test can be expressed as:

$$\begin{aligned} H_0 &: \nexists\hat{\lambda}^{\max}_{m,g} \text{ s.t. } \Omega^{\text{DTDR}}_{m,g,d_1}[\hat{\lambda}^{\max}_{m,g}] \geq \eta_a \quad \Rightarrow \text{Code not present} \\ H_1 &: \exists\hat{\lambda}^{\max}_{m,g} \text{ s.t. } \Omega^{\text{DTDR}}_{m,g,d_1}[\hat{\lambda}^{\max}_{m,g}] \geq \eta_a \quad \Rightarrow \text{Code present} \end{aligned} \tag{3.41}$$
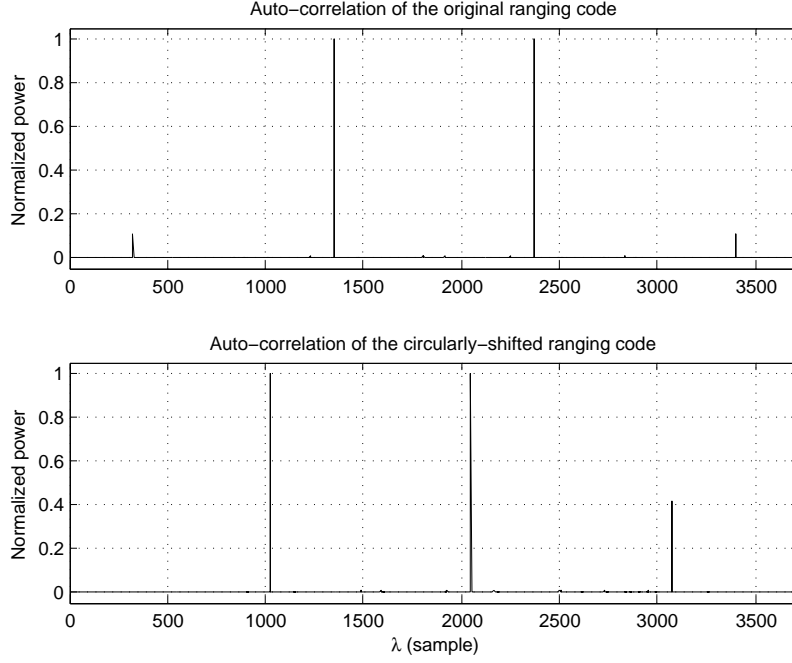
Figure 3.7: The auto-correlation property of the original and circularly-shifted ranging codes ($N_r = N = 1024$)

in which $0 \leq \hat{\lambda}_{m,g}^{\max} \leq D_{max}$. This is referred to as one-peak code detection scheme. Once the code is detected, $\hat{\lambda}_{m,g}^{\max}$ also marks the begining of the ranging transmission, which provides us the TO estimation (i.e. $\hat{\epsilon}t_u = \hat{\lambda}_{m,g}^{\max}$).

Since the preamble was designed in a way that two auto-correlation peaks are available, we can also utilize both peaks to reduce the false detection probability. This test is referred to as two-peak code detection scheme:

$$
\begin{aligned}
H_0 : &\nexists \hat{\lambda}_{m,g}^{\max} \text{ s.t. } \Omega_{m,g,d_1}^{\text{DTDR}}\big[\hat{\lambda}_{m,g}^{\max}\big] \geq \eta_a \\
&\text{and } \Omega_{m,g,d_2}^{\text{DTDR}}\big[\hat{\lambda}_{m,g}^{\max} + N\big] \geq \eta_a \\
&\qquad\qquad\qquad\qquad \Rightarrow \quad \text{Code not present} \\
H_1 : &\exists \hat{\lambda}_{m,g}^{\max} \text{ s.t. } \Omega_{m,g,d_1}^{\text{DTDR}}\big[\hat{\lambda}_{m,g}^{\max}\big] \geq \eta_a \\
&\text{and } \Omega_{m,g,d_2}^{\text{DTDR}}\big[\hat{\lambda}_{m,g}^{\max} + N\big] \geq \eta_a \\
&\qquad\qquad\qquad\qquad \Rightarrow \quad \text{Code present}
\end{aligned}
$$

(3.42)

Referring to Figure 3.7, one can observe that there are four correlation

45

peaks, which are all N samples apart, corresponding to the four repeated parts in the ranging interval: the 1st CP, the 1st OFDMA symbol, the 2nd OFDMA symbol, and the 2nd CP. This phenomena makes both of the above-mentioned peak search algorithms prone to error, as they can mistake the first and the second peaks as the desirable ones. In our implementation, we choose to correlate the received signal with the circularly-shifted version of the ranging code:

$$\tilde{x}'_{m,g}\big[n\big] = \tilde{x}_{m,g}\big[(n - N_{gi}) \mod N\big] \tag{3.43}$$

in which N_{gi} is the number of samples in CP. Comparing the auto-correlation peaks at the top and bottom sub-figures in Figure 3.7, we can see that the first ambiguous peak is now eliminated by using the new N_{gi}-sample circularly-shifted ranging code.

The proposed implementation for code detection and TO and CFO estimation using the DTDR technique with two-peak code detection and circularly-shifted ranging code is illustrated in Figure 3.8.

For the Indirect Time-Domain Ranging scheme

Since the ITDR is based on the correlation principle, similarly to the DTDR technique, the above-mentioned one-peak and two-peak code detection algorithms can also be applied for ITDR. The decision variable for ITDR scheme is as following:

$$\Omega_{m,g,d_i}^{\text{ITDR}}\big[\lambda\big] = \frac{\left|\tilde{\Gamma}_{m,g,d_i}^{\text{ITDR}}\big[\lambda\big]\right|^2}{\Theta_{m,g,d_i}^{\text{ITDR}}} \tag{3.44}$$

in which

$$\Theta_{m,g,d_i}^{\text{ITDR}} = \frac{1}{N} \sum_{\lambda_1=0}^{N-1} \left|\tilde{\Gamma}_{m,g,d_i}^{\text{ITDR}}\big[\lambda_1\big]\right|^2 \tag{3.45}$$

is the average power and $\tilde{\Gamma}_{m,g,d_i}^{\text{ITDR}}\big[\lambda\big]$ is the λth element of the correlation vector $\vec{\Gamma}_{m,g,d_i}^{\text{ITDR}}$ $(i = 1, 2)$, respectively. The two-peak code detection test for ITDR, therefore, can be written as:
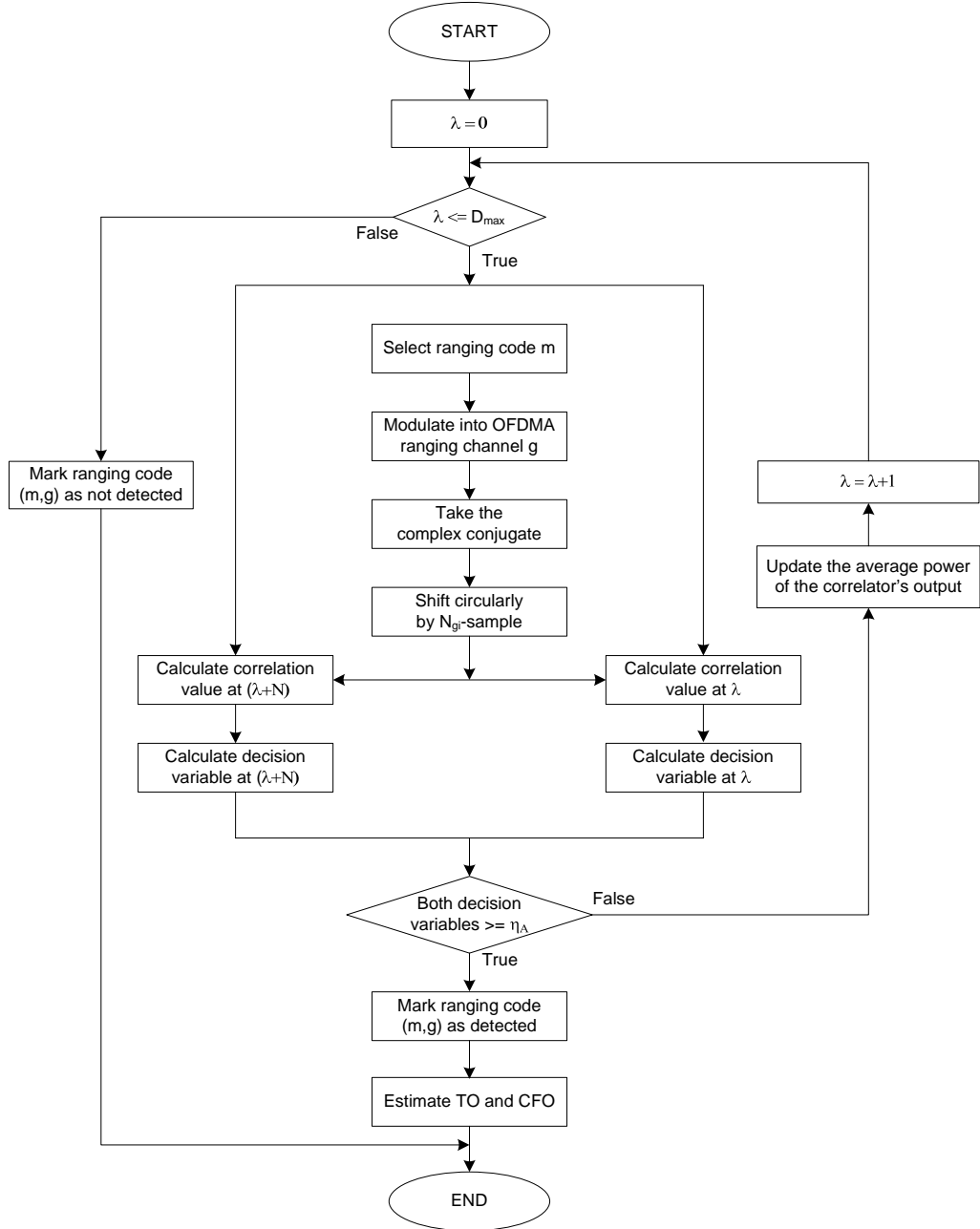
Figure 3.8: The DTDR scheme with circularly-shifted ranging code and two-peak code detection algorithm

$$
\begin{aligned}
H_0 : \nexists \hat{\lambda}_{m,g}^{\max} \text{ s.t. } & \Omega_{m,g,d_1}^{\text{ITDR}}\left[\hat{\lambda}_{m,g}^{\max}\right] \geq \eta_a \\
\text{and } & \Omega_{m,g,d_2}^{\text{DTDR}}\left[\hat{\lambda}_{m,g}^{\max}\right] \geq \eta_a \\
& \Rightarrow \quad \text{Code not present} \\
H_1 : \exists \hat{\lambda}_{m,g}^{\max} \text{ s.t. } & \Omega_{m,g,d_1}^{\text{DTDR}}\left[\hat{\lambda}_{m,g}^{\max}\right] \geq \eta_a \\
\text{and } & \Omega_{m,g,d_2}^{\text{DTDR}}\left[\hat{\lambda}_{m,g}^{\max}\right] \geq \eta_a \\
& \Rightarrow \quad \text{Code present}
\end{aligned}
\tag{3.46}
$$

However, due to the nature of the FFT-implemented circular correlation, complete N-sample correlation output vectors are available in ITDR technique, which allows us to utilize the argmax(.) function - which returning the maximum value in a vector - to search for the correlation peak. Let's consider the decision vectors:

$$
\vec{\boldsymbol{\Omega}}_{m,g,d_i}^{\text{ITDR}} = \left\{ \left|\tilde{\Gamma}_{m,g,d_i}^{\text{ITDR}}\left[\lambda\right]\right|^2, \lambda = 0, 1, \ldots, N \right\}^T \quad (i = 1, 2)
\tag{3.47}
$$

With the assumption that the two auto-correlation peaks are exactly N samples apart, and they corresponds to the two maxima of the decision vectors, a maximum-based code detection test can be described as follows:

$$
\begin{aligned}
H_0 : \nexists \hat{\lambda}_{m,g}^{\max} \text{ s.t. } \hat{\lambda}_{m,g}^{\max} = \text{argmax}_\lambda \left\{\vec{\boldsymbol{\Omega}}_{m,g,d_1}^{\text{ITDR}}\right\} &= \text{argmax}_\lambda \left\{\vec{\boldsymbol{\Omega}}_{m,g,d_2}^{\text{ITDR}}\right\} \\
&\Rightarrow \text{Code not present} \\
H_1 : \exists \hat{\lambda}_{m,g}^{\max} \text{ s.t. } \hat{\lambda}_{m,g}^{\max} = \text{argmax}_\lambda \left\{\vec{\boldsymbol{\Omega}}_{m,g,d_1}^{\text{ITDR}}\right\} &= \text{argmax}_\lambda \left\{\vec{\boldsymbol{\Omega}}_{m,g,d_2}^{\text{ITDR}}\right\} \\
&\Rightarrow \text{Code present}
\end{aligned}
\tag{3.48}
$$

This test indicates that if the two maxima of the two correlation vectors are not at the same correlation lag, then those two maxima are due to noise and interference, and the code is not present. However, the above-mentioned assumption is not always valid: due to the fact that the noise and interference added to the two correlations are independent, the two maxima of the correlation output's vectors can be at different correlation lags at those vectors. A less restricted rule, "double-peak distance restriction rule", can be applied, where the two maxima can be at different lags, but they must be very close in distance [61]:

$$H_0 : \nexists \hat{\lambda}_{m,g,d_1}^{\max}, \hat{\lambda}_{m,g,d_2}^{\max} \text{ s.t. } \hat{\lambda}_{m,g,d_1} = \text{argmax}_\lambda \left\{ \vec{\boldsymbol{\Omega}}_{m,g,d_1}^{\text{ITDR}} \right\}$$

$$\hat{\lambda}_{m,g,d_2} = \text{argmax}_\lambda \left\{ \vec{\boldsymbol{\Omega}}_{m,g,d_2}^{\text{ITDR}} \right\}$$

$$\text{and } |\hat{\lambda}_{m,g,d_1}^{\max} - \hat{\lambda}_{m,g,d_2}^{\max}| \le N_{\text{pd}}$$

$$\Rightarrow \quad \text{Code not present}$$

$$H_1 : \exists \hat{\lambda}_{m,g,d_1}^{\max}, \hat{\lambda}_{m,g,d_2}^{\max} \text{ s.t. } \hat{\lambda}_{m,g,d_1} = \text{argmax}_\lambda \left\{ \vec{\boldsymbol{\Omega}}_{m,g,d_1}^{\text{ITDR}} \right\}$$

$$\hat{\lambda}_{m,g,d_2} = \text{argmax}_\lambda \left\{ \vec{\boldsymbol{\Omega}}_{m,g,d_2}^{\text{ITDR}} \right\}$$

$$\text{and } |\hat{\lambda}_{m,g,d_1}^{\max} - \hat{\lambda}_{m,g,d_2}^{\max}| \le N_{\text{pd}}$$

$$\Rightarrow \quad \text{Code present}$$

$$\tag{3.49}$$

where N_{pd} is the maximum allowable distance between two auto-correlation peaks. Since there are two correlation lags now, another rule is adopted, which selects the smaller correlation lag of the two as the estimated start of the auto-correlation peak, i.e. $\hat{\epsilon t}_u = \min\left(\hat{\lambda}_{m,g,d_1}^{\max}, \hat{\lambda}_{m,g,d_2}^{\max} \right)$, where $\min(.)$ return the minimum value selected from input arguments.

In this section, we also propose a method to calculate the adaptive threshold η_a^{ad} for the two-peak code detection algorithm. The advantage of an adaptive threshold is that it will automatically scale according to the received signal power. Assume that σ_p^2 is the average power of the correlator outputs when the code of interest is present and at the correct correlation lag to achieve the auto-correlation peak, and σ_{ni}^2 is the average power of the correlator outputs when the code of interest is not present, or when the auto-correlation peak is not achieved. If such statistical information is available, then a good adaptive threshold can be simply set at the mid-point between these two values. However, these values cannot be obtained in practice, therefore, we have to approximate them from the received signal. First, all potential auto-correlation peaks are detected from the decision vectors, $\vec{\boldsymbol{\Omega}}_{m,g,d_1}^{\text{ITDR}}$ and $\vec{\boldsymbol{\Omega}}_{m,g,d_2}^{\text{ITDR}}$, using the $\max(.)$ function and double-peak power restriction rule. The double-peak power restriction rule is based on the assumption that, if the code is present and its auto-correlation peak corresponds to the maximum value of any correlation output's vector, it is expected that the value at the same correlation lag in the other vector cannot be significantly lower. This rule states that, if $\exists \hat{\lambda}_{m,g,d_i}^{\max}$ s.t. $\hat{\lambda}_{m,g,d_i}^{\max} = \text{argmax}_\lambda \left\{ \vec{\boldsymbol{\Omega}}_{m,g,d_i}^{\text{ITDR}} \right\}$ and

$\dfrac{\vec{\boldsymbol{\Omega}}_{m,g,d_i'}^{\text{ITDR}}\left[\hat{\lambda}_{m,g,d_i}^{\max}\right]}{\vec{\boldsymbol{\Omega}}_{m,g,d_i}^{\text{ITDR}}\left[\hat{\lambda}_{m,g,d_i}^{\max}\right]} < \eta_b$ and $\dfrac{\vec{\boldsymbol{\Omega}}_{m,g,d_i}^{\text{ITDR}}\left[\hat{\lambda}_{m,g,d_i}^{\max}\right]}{\vec{\boldsymbol{\Omega}}_{m,g,d_i'}^{\text{ITDR}}\left[\hat{\lambda}_{m,g,d_i}^{\max}\right]} < \eta_b$, where $i = 1, 2$, $i' = 1, 2$ and

$i' \neq i$, then we mark a potential auto-correlation peak at $(m, g, i, \hat{\lambda}_{m,g,d_i}^{\max})$, by adding these values to the expected code set Δ_{ec}. The threshold $\eta_b \geq 1$ denotes the maximum allowable power ratio between the high and the low value of a correlation peak. Second, we calculate the average power of all potential auto-correlation peaks by:

$$\Omega_{\text{avg}} = \frac{1}{2N_{\text{np}}} \sum_{(m,g,\hat{\lambda}_{m,g,d_i}^{\max}) \in \Delta_{\text{ec}}} \left(\vec{\Omega}_{m,g,d_1}^{\text{ITDR}} \left[\hat{\lambda}_{m,g,d_i}^{\max} \right] + \vec{\Omega}_{m,g,d_2}^{\text{ITDR}} \left[\hat{\lambda}_{m,g,d_i}^{\max} \right] \right) \quad (3.50)$$

where N_{np} is the size of the estimated code set Δ_{ec}, denoting the number of the potential auto-correlation peaks. Ω_{avg} gives an approximation for σ_p^2. Thirdly, the average power of the noise and interference is calculated by using the following equation:

$$\Theta_{\text{avg}} = \frac{1}{2GM - N_{\text{np}}} \sum_{(m,g,i) \notin \Delta_{\text{ec}}} \Theta_{m,g,d_i}^{\text{ITDR}} \quad (3.51)$$

This denotes taking the average power of all correlator's outputs in which a potential auto-correlation peak was not found, which is an approximation of σ_n^2. Finally, the adaptive threshold is calculated as follows:

$$\eta_a^{\text{ad}} = \frac{1}{2} \frac{\Omega_{\text{avg}}}{\Theta_{\text{avg}}} \quad (3.52)$$

The code detection test is similar to Eq. (3.46), except that η_a is replaced by η_a^{ad}, which is re-calculated on every ranging cycle.

3.6.2 The selection of observation vectors for CFO estimation

After the code detection process, the transmitted code is detected, and the auto-correlation peak is identified. The correlation lag corresponding to the auto-correlation peak gives the TO estimation, and the ML estimate of the CFO is calculated based on Eq. (3.22) or (3.38). This section discusses how to select the N_{ob}-point observation vectors for CFO estimation.

As discussed earlier, the performance of the CFO estimator depends on the number of observation points and also the useful CINR of the elements of the observation vectors. The higher the useful CINR, the more accurate the estimate. The high useful CINR condition can be satisfied by selecting

only correlation lags corresponding to the auto-correlation peaks. Due to the multipath channel, the single auto-correlation peak in AWGN channel is spread in time into a number of peaks, whose powers depend on the channel's Power Delay Profile (PDP). These peaks can be exploited as elements of the observation vectors in our algorithm.

The algorithm is proposed as follows: First, we consider the correlation lag range $\left[\hat{\lambda}_{m,g}^{\max}, \hat{\lambda}_{m,g}^{\max} + N_{\mathrm{os}}\right]$, where N_{os} is a parameter deciding the size of the observation point search. This should be large enough to contain most of the channel power, for example a recommended value is equal to the total delay spread of the channel. Over this correlation lag range, all the λ point that satisfies condition $(\vec{\boldsymbol{\Omega}}_{m,g,d_1}^{\mathrm{ITDR}}[\lambda] \geq \eta_o)$ and $(\vec{\boldsymbol{\Omega}}_{m,g,d_2}^{\mathrm{ITDR}}[\lambda] \geq \eta_o)$ will be selected as observation point. η_o is another parameter deciding how large the auto-correlation peak should the algorithm choose. For convenient, we set it equal to the code detection threshold η_a or η_a^{ad}. This ensures that only auto-correlation peaks that are significantly larger than the noise and interference floor will be selected for CFO estimation.

3.6.3 Computational complexity comparison

The DTDR scheme requires $2(N_r - 1)$ complex additions and $2N_r$ complex multiplications for each search step of one correlator. Assume that the TO is distributed uniformly over $[0, D_{\max}]$, and all available ranging codes are used at any given time, then on average each correlator has to perform $\frac{D_{\max}+1}{2}$ search steps to find a code. Since there are total of $G \times M$ ranging codes, the DTDR scheme needs $(GM(N_r - 1)D_{\max} + 1)$ complex additions and $(GMN_rD_{\max} + 1)$ complex multiplications per ranging cycle. Therefore, the complexity of DTDR scheme is in the order of $\mathcal{O}\left(GMN_rD_{\max}\right)$.

The ITDR scheme requires two FFT conversion to convert the two received OFDMA symbols into frequency-domain, and $2GM$ IFFT operations to convert the signals back to time-domain. The complexity of the ITDR is in the order of $\mathcal{O}\left(GMN \log_2 N\right)$.

We observe that one advantage of the DTDR scheme is that the length of the correlation windows, N_r, can be flexible. The shorter the length, the lower the computational complexity, but also the lower the correlation peak. If $N_r = N$, the ratio between the complexity of DTDR with that of ITDR scheme is only $\mathcal{O}\left(D_{\max}/\log_2 N\right)$. If $N = 2048$, then $\log_2 N = 11$, which is really small compared to a practical value for $D_{\max}$ (recall that $D_{\max}$ is the maximum value of the normalized delay plus the maximum delay of the multipath channel, which is often as large as the guard interval). Therefore, we can conclude that the ITDR has lower computational complexity than

the DTDR scheme.

In addition, due to the nature of the FFT-based circular correlation, the ITDR technique offers complete correlation output vectors, which facilitates the usage of different algorithms, such as calculation of the adaptive threshold or selection of the observation vectors. Although these algorithm can also be applied in DTDR scheme, they require that more correlation steps be performed, and thus an increased complexity.

3.7 Numerical Evaluation

In this section, we evaluate the performance of both DTDR and ITDR schemes under various settings. The evaluation are based on the following metrics: (a) the successful detection probability, P_{succ}, which is the ratio between the number of successfully-detected ranging codes and the total number of ranging attempts; (b) the false alarm probability, P_{fa} indicating the possibility of incorrect detections, in which a particular ranging code is detected, when actually it was not sent; (c) the Standard Deviation (STD) of the TO estimation error, $\sigma_{\hat{\epsilon t}_u}$; and (d) the Mean Square Error (MSE) of the CFO estimation, $\sigma^2_{\hat{\epsilon f}_u}$. It is worth noting that only the successfully-detected ranging codes are taken into account when calculating the TO and CFO estimation errors. Therefore, the standard deviation of the TO estimation error and the MSE of the CFO estimate are respectively defined as follows:

$$\sigma_{\hat{\epsilon t}_u} = \sqrt{\frac{1}{N_{\text{sm}}} \sum_{i=1}^{N_{\text{sm}}} (\hat{\epsilon t}_u - \epsilon t_u - \tau_{u,l_{max}})^2} \tag{3.53}$$

$$\sigma^2_{\hat{\epsilon f}_u} = \frac{1}{N_{\text{sm}}} \sum_{i=1}^{N_{\text{sm}}} (\hat{\epsilon f}_u - \epsilon f_u)^2 \tag{3.54}$$

where N_{sm} is the number of successfully-detected ranging transmission. The miss detection probability, which is the ratio between the number of undetected ranging code and the total ranging attempts, is not presented here, because it can be deduced directly from the successful detection probability, i.e. $P_{\text{miss}} = 1 - P_{\text{succ}}$.

Table 3.1 summaries the common parameters and their values used in simulation. All users signal arrive at the BS with equal received power. The system bandwidth is 40MHz, which corresponds to the sampling interval of 25ns. We use QPSK modulation for the ranging channel. The applied wideband channel model is 7-tap exponential decay Rayleigh [43], with rms delay spread of 1us. The cell size is assumed to be 1km, which gives the

maximum round-trip transmission delay of 6.67us, or $\epsilon t_{max} \approx 267$ sample. The TOs are generated uniformly between 0 and ϵt_{max}, whereas the CFOs are uniformly distributed in the $\left[-\epsilon f_{max}, +\epsilon f_{max}\right]$ range, where ϵf_{max} represents the maximum tolerable CFO value of the system during ranging period. The CP and cyclic post-fix are 512 samples in total, so that they are longer than the sum of the transmission delay and five times the channel's rms delay spread. The maximum number of available ranging codes $G \times M$ is 28, i.e. the system will search for 28 possible ranging codes per ranging cycle. Note that the ranging code collision problem is not considered in our simulation, therefore there is no need to implement a larger search space in the simulation, which only increases simulation time. The ranging codes are truncated from a m-sequence of length $2^{15}-1$, as defined in [44]. All available subcarriers in the system are utilized for ranging, i.e. during ranging period no data transmission will occur. For DTDR technique, we set $N_r = N$ to maximize its performance, so that we can compare the two techniques side by side.

Table 3.1: Common simulation parameters

Parameter	Value
System bandwidth	40MHz
Sampling interval (Δt)	25ns
Number of subcarriers	1024
Modulation	QPSK
Channel model	7-tap exponential decay Rayleigh
Channel's rms delay spread	1us
Maximum round-trip delay	6.67us
Length of CP plus cyclic post-fix	512 samples
Number of available ranging codes $(G \times M)$	28

Figure 3.9 indicates the success and the false alarm probabilities as a function of detection threshold η_a for both DTDR and ITDR schemes using one-peak and two-peak code detection algorithms, as discussed in section 3.6.1. In addition, the STD of the TO error and the MSE of the CFO error are shown in Figure 3.10, while the probability that the absolute value of the CFO error is less than or equal to 2% of subcarrier spacing, which is the requirement in [44], is plotted in Figure 3.11. There are 10 active ranging MSs, the CNR is 20dB, and the ϵf_{max} is 30% of the subcarrier spacing. Since the testing condition of the two-peak code detection rule is stricter than one-peak one, its false alarm probabilities are reduced significantly than those of the
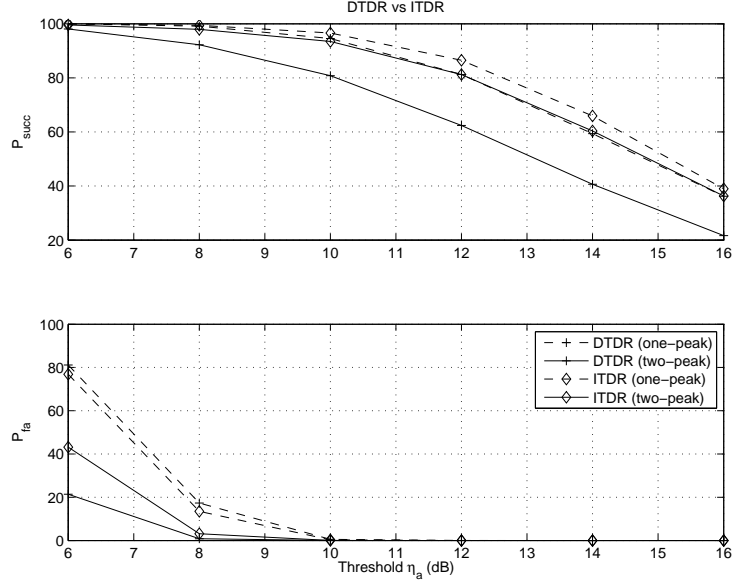
Figure 3.9: Success and false alarm probabilities for DTDR and ITDR schemes as function of the detection threshold
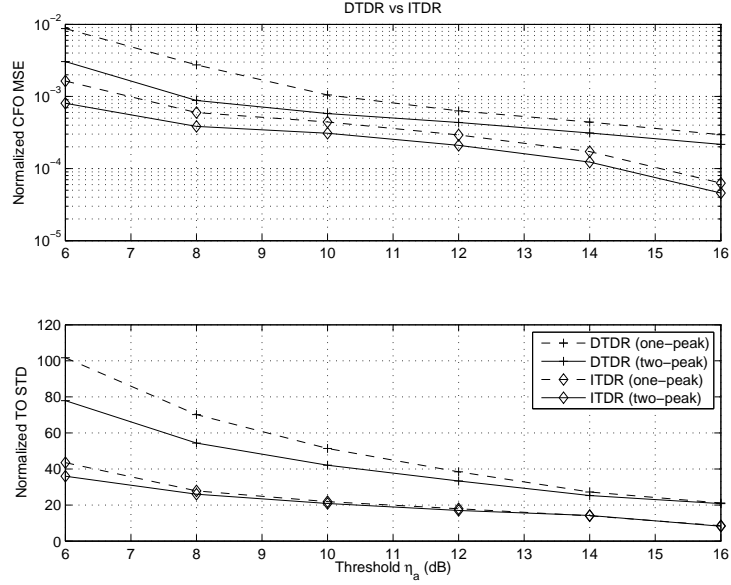

Figure 3.10: TO and CFO estimation errors for DTDR and ITDR schemes as function of the detection threshold
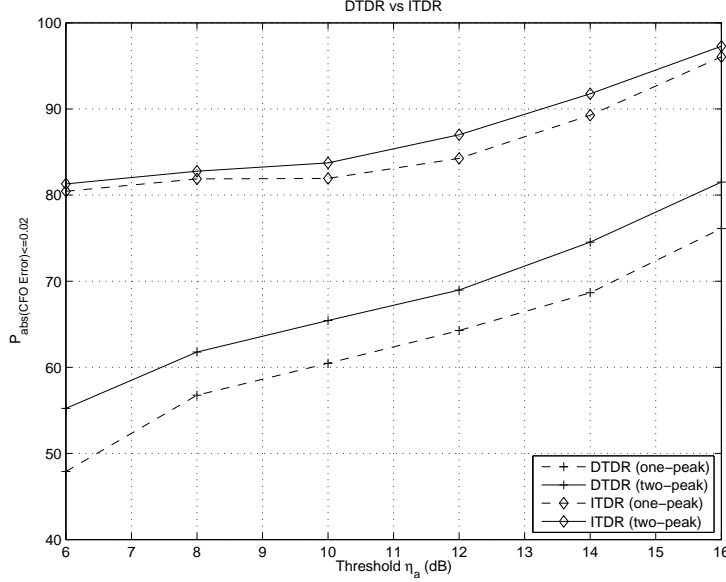
54

Figure 3.11: Performance of the CFO estimation for DTDR and ITDR schemes

one-peak code detection algorithm, at the cost of lower successful detection probabilities. Nevertheless, the performance of the TO and CFO estimator in DTDR and ITDR are also improved with two-peak code detection algorithm, comparing to the corresponding one-peak's ones (see Figure 3.10 and 3.11). As a result, we shall mainly use the two-peak code detection algorithm for further evaluation of the DTDR and ITDR schemes in this section.

From Figure 3.9, we can see that when the predefined peak detection threshold η_a increases, the success and false alarm probabilities are decreased for both DTDR and ITDR schemes. A high threshold means that only very high correlation peaks can pass the code detection test, and therefore the TO and CFO estimator's performance are also improved, which is illustrated in Figure 3.10 and 3.11. Therefore, the choice of threshold is a trade-off between the success detection rate and accurate TO and CFO estimation. In our particular setting, the optimum threshold should be around 10 - 12dB. For example, at threshold $\eta_a = 10$dB, the success probability of two-peak ITDR scheme is 93%, the false-alarm probability is 0%, the TO STD is 20 samples, and the CFO MSE is 0.03% subcarrier spacing, in which the probability that the absolute CFO estimation error is less than 2% is around 84%. We can also observe that the DTDR performs worst than the ITDR scheme in both aspects, namely code detection and parameter estimation. This can
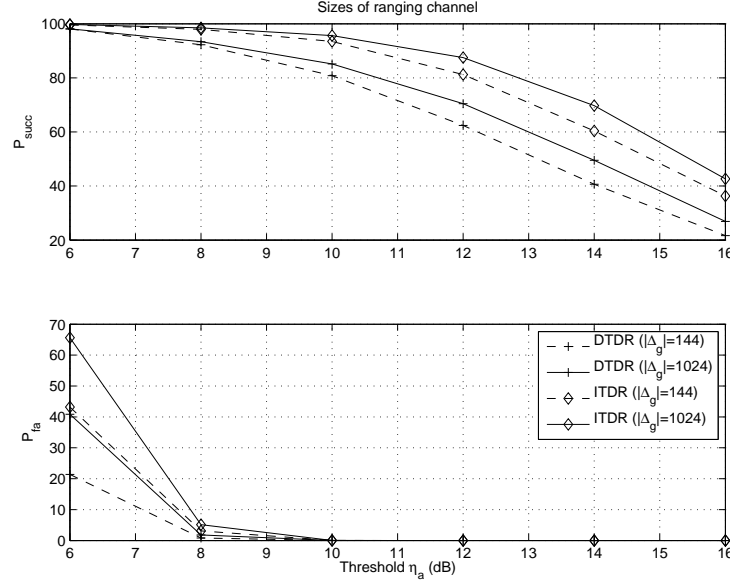
55

Figure 3.12: Success and false alarm probabilities for DTDR and ITDR schemes with respect to the size of ranging channel

be explained by comparing Eq. (3.40) and (3.45): The average power of the correlator's output in ITDR scheme is calculated over an observation window of size N, while in DTDR it is window of size $N_{\text{ow}} < N$ (in our simulation, N_{ow} is set equal to $N/4$). The larger the observation window, the closer the average power of the correlator's output to the noise and interference floor, and thus the better the peak detection. We can increase the observation window in DTDR scheme to achieve better performance, but at the cost of higher number of correlation steps, or higher computational complexity.

Figure 3.12, 3.13 and 3.14 show the performance of two ranging scenarios with different sizes of ranging channel, namely 144 and 1024 subcarriers. Again, there are 10 active ranging users in each system, and the CNR is 20dB. In 144-subcarrier ranging scenario, there are 7 ranging channels and 4 available ranging codes; while in 1024-subcarrier ranging scenario there are one ranging channel and 28 available ranging code, so that the product $G \times M$ does not change in both scenarios. The success probability is slightly higher, the false-alarm probability is lower, and the STD of the TO estimation is lower in the case of 1024-subcarrier scenario. This is due to the fact that the auto-correlation peaks are higher in 1024-subcarrier ranging channel than in 144-subcarrier one. However, the cross-correlations between the ranging code of interest and the other codes and the noise are also fluctuating with
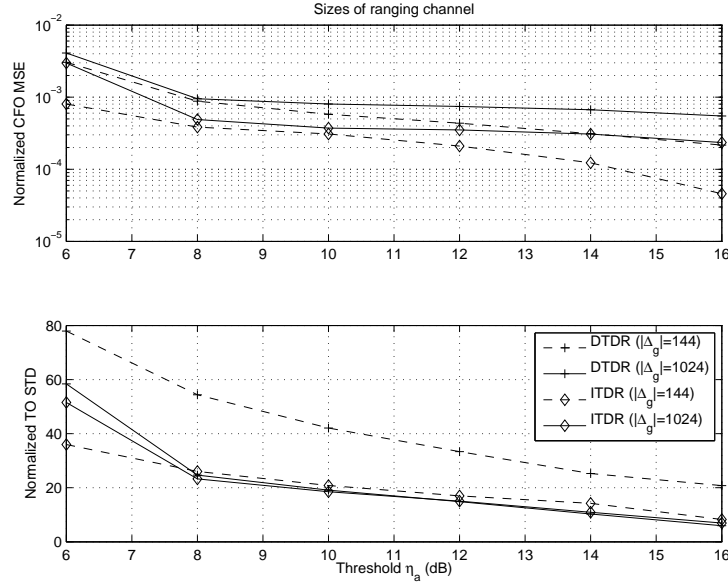
56

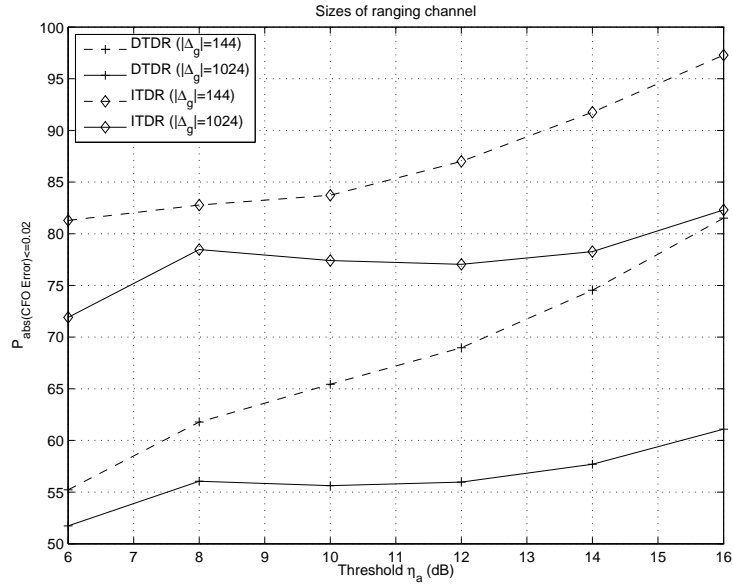Figure 3.13: TO and CFO estimation errors with respect to the size of ranging channel

Figure 3.14: Performance of the CFO estimation for DTDR and ITDR schemes with respect to the size of ranging channel
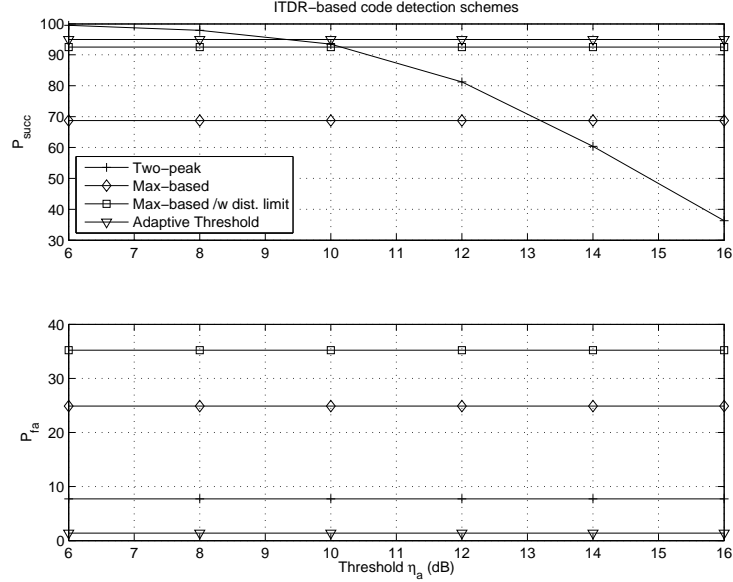
Figure 3.15: Success and false alarm probabilities for ITDR-based code detection schemes

greater variances. This causes a degradation in term of CFO estimation, which can be seen in Figure 3.14: The two-peak ITDR scheme in 1024-subcarrier ranging scenario can only achieve 83% at $\eta_a = 16$dB, while that number is 98% in 144-subcarrier ranging scenario. It is worth noting that the overall performance of the DTDR is worst than those of the ITDR in both scenarios. As a result, we will select the ITDR as the preferred scheme, and only evaluate this scheme from now on.

In Figure 3.15, 3.16 and 3.17 are the performance of the ITDR-based code detection schemes discussed in section 3.6.1. The advantage of the code detection schemes based on max(.) function or using an adaptive threshold is that they do not depend on the choice of threshold η_a, which allows them to adapt to various channel conditions or transmit power variation. The maximum-based code detection scheme offers the most accurate TO and CFO estimation among the three, namely maximum-based, maximum-based with double-peak distance restriction, and adaptive threshold. However, its probability of false alarm is high, up to 25%; and the miss detection probability is very high, around 30%. The maximum-based with double-peak distance restriction helps increase the success detection rate, but it also increase the false alarm probability to 35%. Finally, the proposed adaptive threshold offers the highest success probability among the three, up to 95%; and a false alarm probability close to zero. The adaptive threshold also shows
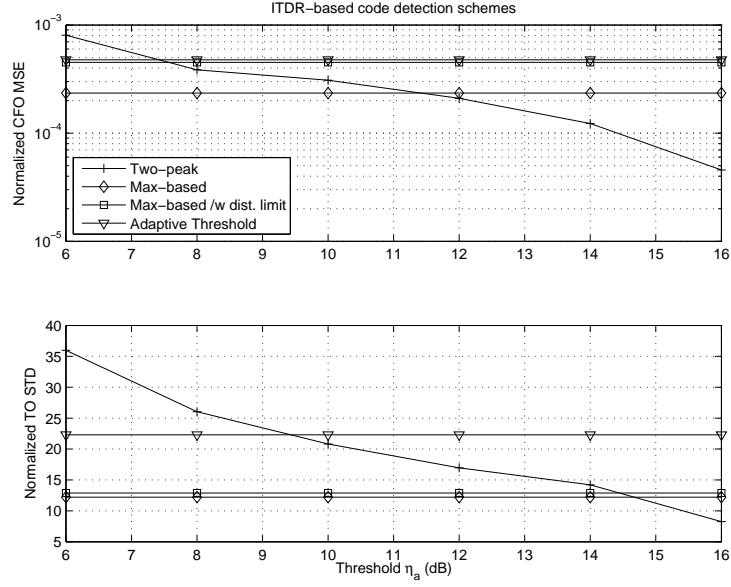
Figure 3.16: TO and CFO estimation errors for ITDR-based code detection schemes
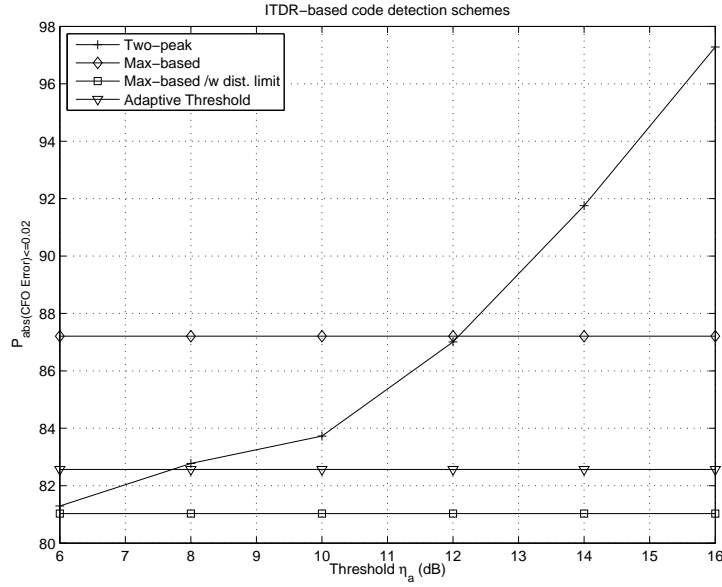
Figure 3.17: Performance of the CFO estimator for ITDR-based code detection schemes
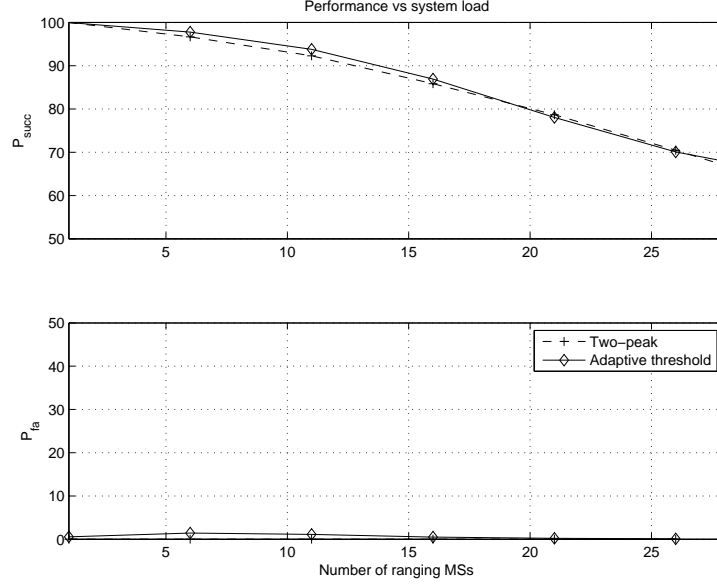
Figure 3.18: Success and false alarm probabilities for ITDR-based schemes as function of system load

to be slightly more accurate than the maximum-based with double-peak distance restriction in term of CFO estimation. As a result, we will only focus on the two preferred code detection algorithms for ITDR scheme, namely the two-peak using fixed-threshold and the adaptive threshold.

Figure 3.18, 3.19 and 3.20 show the performance of the two-peak and adaptive threshold code detection schemes with regards to the number of active ranging MSs in the system. With the increase of the number of users, the probability of successful code detection and the accuracy of CFO estimation are greatly reduced, but the TO estimate becomes more accurate. Recall from Eq. (3.53) that the reference timing for measuring the TO error is $(\epsilon t_u + \tau_{u,l_{max}})$, in which $\tau_{u,l_{max}}$ is the time delay of the strongest multipath component of the channel. When the system load increases, so does the interference floor, and therefore it is more difficult to detect an auto-correlation peak, unless it corresponds to a very strong multipath component of the channel. In this case, the strongest multipath component is often detected, and thus the TO error is reduced.

In Figure 3.21, 3.22 and 3.23 are the performance of the ITDR-based schemes as a function of ϵf_{max}. As we can see, the overall performance is degraded significantly with the increment of CFO. The increase of CFO value causes a larger linear phase shift in the time-domain, which reduces the effec-

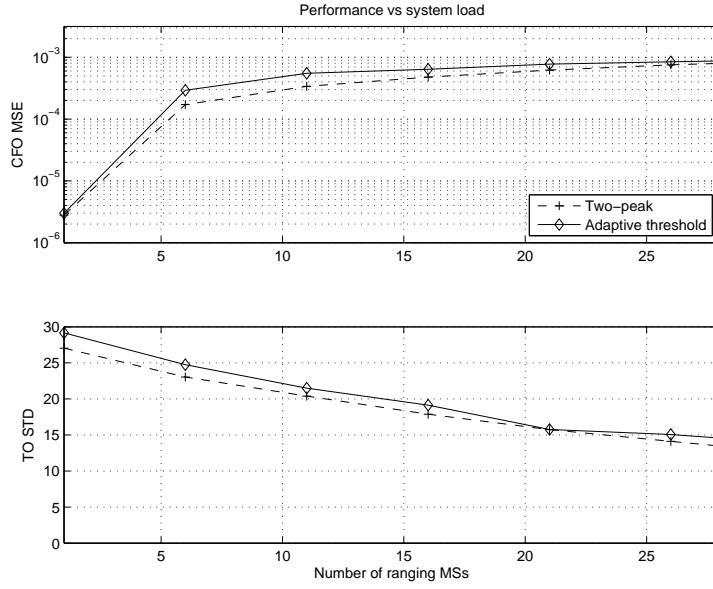Figure 3.19: TO and CFO estimation errors for ITDR-based schemes as function of system load
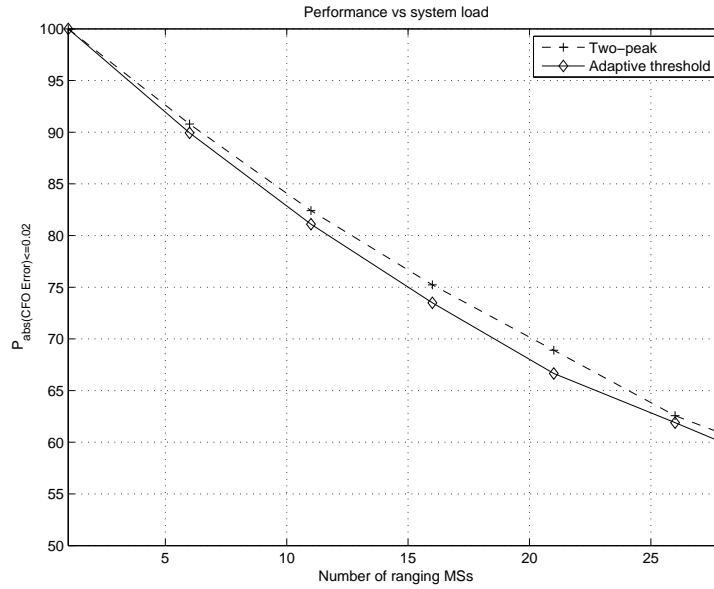
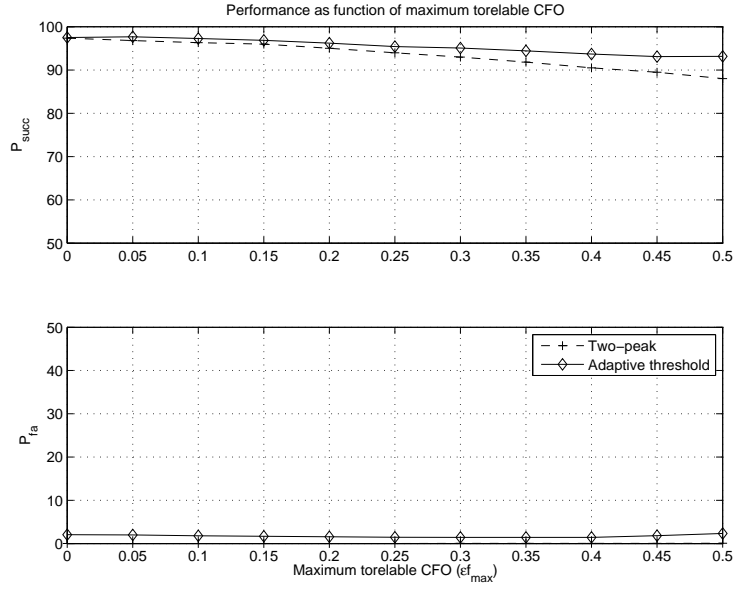Figure 3.20: Performance of the CFO estimator for ITDR-based schemes as function of system load

Figure 3.21: Success and false alarm probabilities for ITDR-based schemes as function of the maximum tolerable CFO

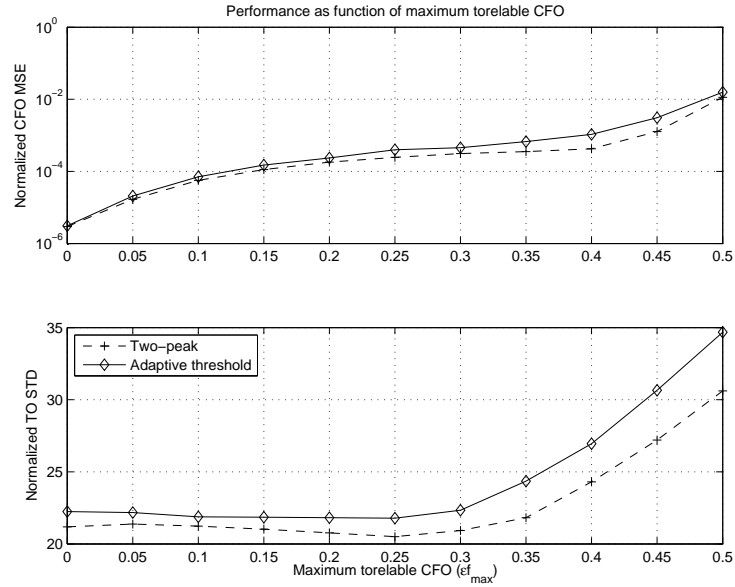Figure 3.22: TO and CFO estimation errors for ITDR-based schemes as function of the maximum tolerable CFO
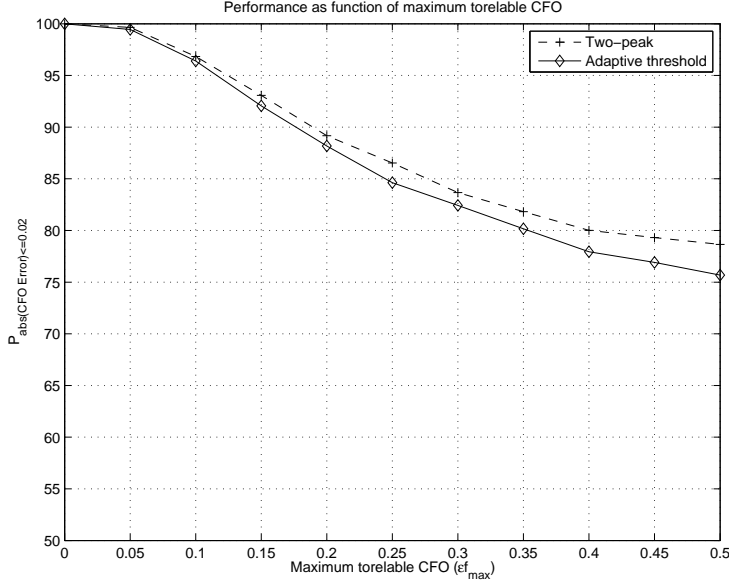
Figure 3.23: Performance of the CFO estimator for ITDR-based schemes as function of the maximum tolerable CFO

tive peak of the correlator output. To avoid this problem, a coarse frequency synchronization before uplink transmission is necessary at the user's side to bring the CFO to a tolerable range. Nevertheless, when the value of ϵf_{max} is as high as 40% of the subcarrier spacing, both schemes can still achieve 90% successful detection rate, while the TO estimation error is less than 30 samples and the MSE of the CFO estimation is in the order of 10^{-3}, and the probability that the absolute CFO error is less than 2% subcarrier spacing is 80%.

Finally, the performance of the above-mentioned code detection and estimation schemes under various CNR values are presented in Figure 3.24, 3.25 and 3.26. For both schemes, their performance improve diminishingly with the increase of CNR level. There is little difference in performance between CNR of 10dB and CNR of 30dB, due to the fact that the interference, caused by the cross-correlation between active ranging codes, is the more dominant source of performance degradation than the AWGN.

We observe that, under all discussed scenarios, the performance of the two-peak using adaptive threshold is equivalent to that of the two-peak using fixed-threshold with threshold $\eta = 10$dB. However, this observation might not hold if another channel model is applied, or the assumption that the all users signal arrives at the BS with equal received power is relaxed, due to the
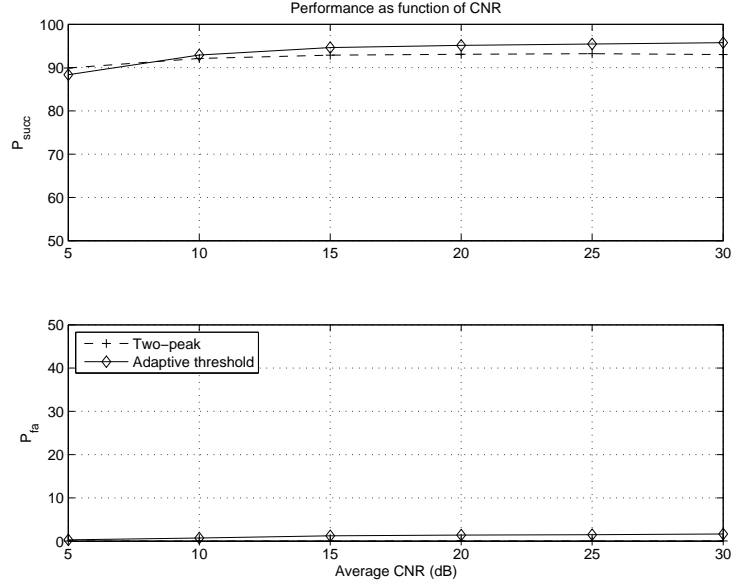
Figure 3.24: Success and false alarm probabilities for ITDR-based schemes as function of the average CNR
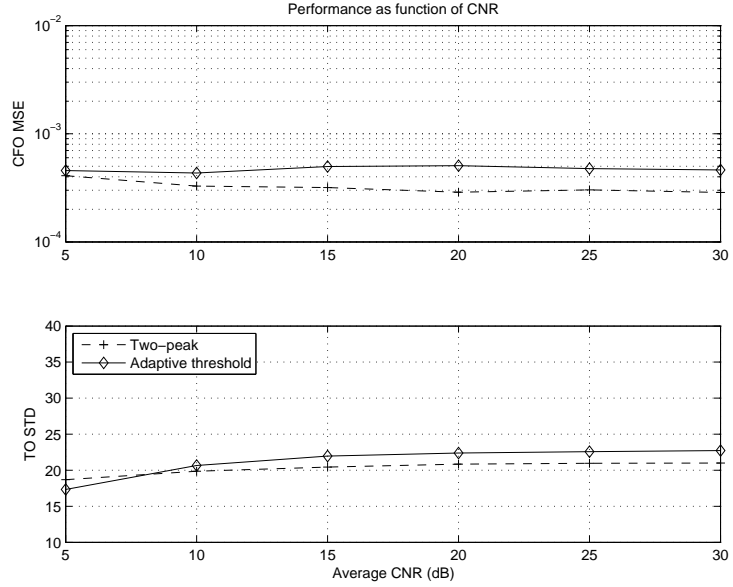
Figure 3.25: TO and CFO estimation errors for ITDR-based schemes as function of the average CNR
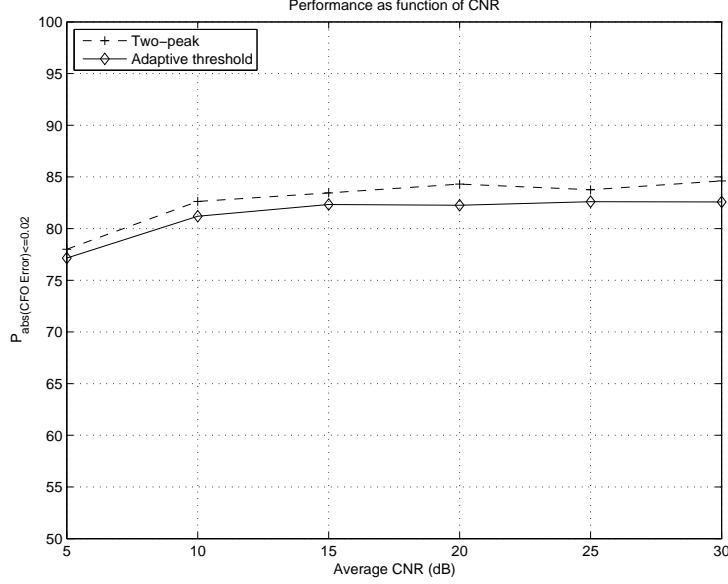
Figure 3.26: Performance of the CFO estimator for ITDR-based schemes as function of the average CNR

fact that the adaptive threshold scheme will adapt accordingly to the received signal powers. This could be an interesting topic for the future works.

3.8 Conclusions

In this chapter, our focus is the code detection and TO and CFO estimation for ranging MSs in an OFDMA-based system. The two techniques discussed here, namely Direct Time-Domain Ranging (DTDR) and Indirect Time-Domain Ranging (ITDR), are based on CDMA principle. While DTDR utilizes a bank of correlator for code detection and parameter estimation, the ITDR employs FFT blocks to perform the required correlations. As a result, ITDR is not only less computationally complex than the DTDR, but also able to offer a complete correlation vector, which facilitates the usage of more advanced detection and estimation algorithms. Simulation shows that ITDR performs slightly better than DTDR, due to the fact that more information is available for ITDR-based schemes. As a result, we conclude that the ITDR is a prefered method for code detection and TO estimation in the initial ranging scenario.

Our contribution in this chapter is the proposal of a CFO estimation

65

algorithm that can be applied for both DTDR and ITDR techniques. The CFO is estimated using ML criterion from the phase difference between two sets of auto-correlation peaks at N-sample apart. Numerical results have shown that our proposed CFO estimator can achieve very high probability, up to 97%, that the CFO estimation error is less than 2% of the subcarrier spacing, which is a requirement in the IEEE 802.16e standard.

In this chapter, we also investigated the performance of different code detection algorithms, namely one-peak code detection, two-peak code detection with fixed threshold, maximum-based code detection, maximum-based code detection with double-peak distance restriction and the two-peak code detection with adaptive threshold. Among these algorithms, the two-peak code detection with fixed and adaptive threshold has shown numerically to be able to offer the best overall performance. The choice of threshold is a trade-off between the successful detection rate and the accuracy of the TO and CFO estimates. If a strict requirement on TO and CFO estimation is applied, the two-peak code detection with a high fixed threshold should be used to guarantee such a requirement, at the cost of lower successful detection rate.

In the future, we are interested in studying the behavior of the adaptive threshold scheme under different channel models, or in scenario where the received signals at the BS do not have equal powers. Developing the Cramer-Rao Bound (CRB) for the parameter estimation in ranging channel, and comparing the performance of our CFO estimator with the bound, is also an interesting topic for the future works.

Chapter 4

Synchronization in data transmission phase

This chapter discusses two CFO estimation techniques for the uplink of OFDMA-based systems during the data transmission phase, where each MS has been allocated a unique time-frequency block for data transmission. The first estimation scheme is a generalized version of the estimator proposed by Moose [46], while the second one is based on the ITDR technique discussed in the previous chapter. Both schemes estimate the CFO using the phase difference between two observation vectors observed at distance less than the length of an OFDMA symbol. Thus, they offer the possibility to shorten the OFDMA preamble required for synchronization, which reduces the overhead in packet-based wireless communications.

Our contributions in this chapter include:

- Generalization of the Moose estimation technique to a class of frequency-domain ML estimators, where the distance between observation vectors can be less than the length of an OFDMA symbol.

- Proposal of a correlation-based CFO estimation technique, also with the shortened observation distance.

- Introduction of an Iterative Estimation and Adjustment (IEA) algorithm, which aims at improving the performance of the above-mentioned techniques in certain scenarios.

4.1 Introduction

As discussed in Chapter 2, the major drawback of OFDMA technique is its sensitivity to TO and CFO, especially in the uplink [36, 50, 40, 62]. While

the TO problem can be overcome by using a sufficiently long CP [34], the CFO problem is more difficult to deal with. In this chapter, we consider a quasi-synchronous scenario, where MSs are synchronized in time, but not in frequency. We also assume that MSs has already been given unique time-frequency blocks for their data transmission. Due to oscillator inaccuracy and Doppler frequency shift, each user in the uplink of OFDMA-based systems experiences an independent CFO, which destroys the orthogonality among subcarriers and produces ICI and MUI. These CFOs must be estimated and accounted for before decoding data at the receiver, or severe performance degradation will occur.

4.2 The state of the art

Only a few methods to estimate the independent CFOs for the uplink of OFDMA-based systems have been studied in the literature. Firstly, a straightforward solution is to employ a bank of filters to separate users' signals, so that each user can be synchronized individually using known synchronization techniques for OFDM-based systems. These estimators, for example in [36] and [63], only work with contiguous subcarrier allocation scheme, and their performance largely depend on the characteristics of the filters used to separate users' signals, as well as the size of the frequency guard band between users [63]. And even with ideal brick-wall filters, perfect signals' separation is not achievable due to energy leakage caused by the CFOs, and thus some performance loss is experienced comparing to the single-user case [34]. The estimator in [36] utilizes the redundant information carried by the CP to estimate the TO and CFO for each user. When the channel is time-dispersive, the performance of this method degrades considerably, which characterizes by a floor at high CNR for the variance of its CFO estimate [63]. On the other hand, the scheme in [63] operates by searching for a CFO value that minimizes the measured energy on a set of *null* subcarriers. A drawback of this method is that it requires a large frequency guard band between users when the CFO of each user are large to limit the performance loss due to MUI, and this would reduce the system efficiency [63]

Secondly, high-resolution array signal processing techniques can also be used for CFO estimation in the uplink of OFDMA-based systems, due to the fact that the formulation of the multiple CFOs estimation problem is similar to the estimation of the directions of arrival of narrowband signals at an array antenna. For instance, a blind technique based on the principle of Multiple Signal Classification (MUSIC) is introduced in [50], which exploits the periodic structure of the received signals for CFO estimation and thus

only works with interleaved subcarrier allocation scheme. Another CFO estimation method is presented in [64], which is based on Space-Alternating Generalized Expectation-Maximization (SAGE) technique and works with both interleaved or contiguous subcarrier allocation schemes. Although this method is shown to have performance close to the Cramer-Rao's lower bound in a quasi-synchronous OFDMA uplink transmission, its computational complexity is an obstacle for practical implementation [34].

Finally, a frequency-domain CFO estimation technique has been proposed in [46] for OFDM systems, which is referred to as the Moose estimator in this paper (Paul Moose is name of the author). Although it was designed for single-user scenario, the estimator has been discussed and used in multiuser scenario in various papers, such as in [65, 40, 66]. The Moose technique estimates the CFO from the differential phase between two or more repeated versions of the same OFDM symbol using ML criterion. The distance between the these observations is N samples, therefore at least two OFDM symbols are required in the preamble for CFO estimation.

In this chapter, we generalize the Moose technique to a class of frequency-domain ML estimator, where distance between observations can be selected arbitrarily. We also propose a CFO estimation technique based on the correlation of known pilots, which can be seen as an extension of the ITDR technique discussed in Chapter 3. These techniques open the possibility to shorten the preamble required in the data transmission phase, thus reduce the overall overhead and increase the system's efficiency. To enhance the performance of the proposed CFO estimators in certain scenarios, an Iterative Estimation and Adjustment (IEA) algorithm is introduced. Analytical and numerical evaluation of the proposed estimators shall be presented in comparison with the original Moose technique.

4.3   System Model

Let's consider an OFDMA system using a FFT of size N. The uth user is given an independent set of subcarriers, denoted as Δ_u and $\Delta_u \bigcap \Delta_{u'} = \emptyset, \forall u \neq u'$. We assume that, before the actual data transmission, a known preamble is sent to assist the CFO and channel estimation process on the same set of given subcarriers. As a result, our proposed estimators are considered as data-aided techniques. During the preamble, the transmitted information on the kth subcarrier of the uth user is given by:

$$\tilde{X}_u[k] = \begin{cases} c_{\Delta_u}\left[\mathcal{M}_{k \to i}^{\Delta_u}(k)\right] & k \in \Delta_u \\ 0 & \text{otherwise} \end{cases} \tag{4.1}$$
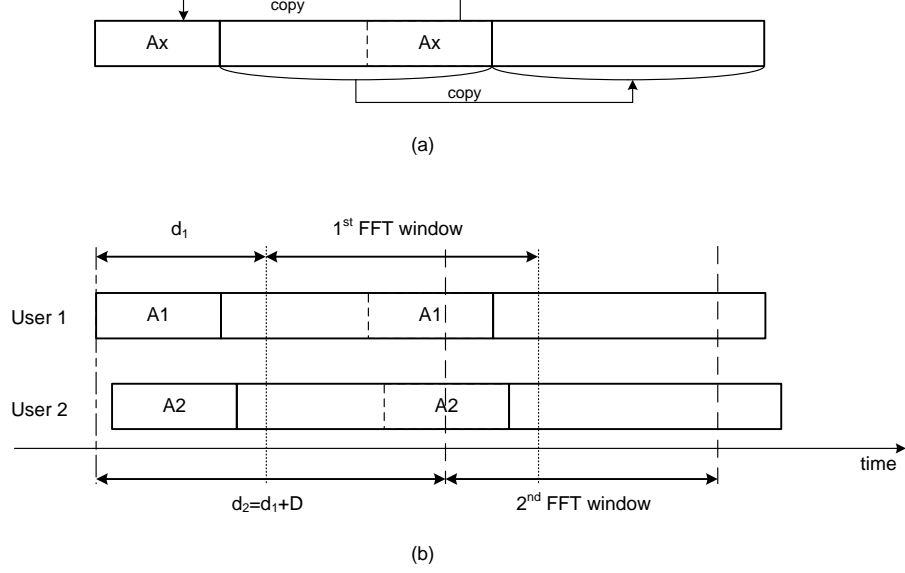
Figure 4.1: (a) Construction of the OFDMA preamble symbol, (b) Positions of the two observation FFT windows

where $k = 0, 1, \ldots, N-1$ is the subcarrier index, $c_{\Delta_u}[i]$ is the ith pilot symbol and $\mathcal{M}^{\Delta_u}_{k \to i}(.)$ is a function that maps k to i depending on the specified set of subcarriers, Δ_u.

After the IFFT operation, the output is extended cyclically as illustrated Figure 4.1 to obtain the required preamble consisting of two consecutive OFDMA symbols with a CP:

$$\tilde{x}_u(t) = \frac{1}{N} \sum_{k \in \Delta_u} \tilde{X}_u[k] e^{j2\pi \frac{k}{T_o}(t-T_g)} \Xi_{T_s}(t) \tag{4.2}$$

where T_o is the duration of the original OFDMA symbol, T_g is the guard interval, and $\Xi_{T_s}(t)$ is the unity amplitude gate pulse of length $T_s = T_g + 2T_o$.

Assume that the uth user experiences an independent TO, δt_u, and frequency-selective fading channel, which are constant during the observation period, the complex received signal from the uth user is:

$$\tilde{y}_u(t) = \sum_{l=0}^{L-1} \tilde{h}_{u,l} \tilde{x}_u(t - \delta t_u - \tau_{u,l}) \tag{4.3}$$

where $\tilde{h}_{u,l}$ and $\tau_{u,l}$ are the complex gain and time delay of the lth multipath component experienced by the uth user, respectively. In the OFDMA uplink,

the received signal is the sum of the signal from multiple users, which can be expressed as:

$$\tilde{r}(t) = \sum_{u=0}^{U-1} \tilde{y}_u(t) e^{j2\pi\delta f_u t} + \tilde{n}(t) \tag{4.4}$$

where δf_u is the CFO of the uth user and $\tilde{n}(t)$ is the complex baseband AWGN at the input of the OFDMA receiver.

At the receiver, the received signal is sampled at rate $1/\Delta t$ and an observation vector is formed by performing FFT operation on N consecutive samples with a timing offset d, i.e. $\mathbf{r}_d = [\tilde{r}_d[0], \tilde{r}_d[1], \ldots \tilde{r}_d[N-1]]^T$ where $\tilde{r}_d[n] = \tilde{r}((d+n)\Delta t)$. The timing offset d is measured from the earliest arrived signal (see Figure 4.1), and we assume that d is long enough to accommodate both the maximum TO of all the users and the channel delay spread, thus there is no influence from the adjacent transmitted OFDM symbols to the observation vector. After FFT, the observation vector of the uth user, which corresponds to the timing offset d, can be written in matricial form as follows:

$$\vec{\mathbf{Z}}_{u,d} = \vec{\mathbf{A}}_{u,d} + \vec{\mathbf{B}}_{u,d}^I + \vec{\mathbf{B}}_{u,d}^M + \mathbf{S}_u\vec{\mathbf{N}}_d \tag{4.5}$$

where $\vec{\mathbf{A}}_{u,d}$ is the useful signal of the uth user, whereas $\vec{\mathbf{B}}_{u,d}^I$ and $\vec{\mathbf{B}}_{u,d}^M$ are the self-interference (i.e. the ICI due to subcarriers belonging to the same user) and the cross-interference (the ICI caused by subcarriers of the other users), respectively:

$$\vec{\mathbf{A}}_{u,d} = e^{j2\pi\frac{\epsilon f_u}{N}d}\mathbf{T}_{(d)}\mathbf{S}_u\mathbf{C}_{(\epsilon f_u)}^p\vec{\mathbf{Y}}_u \tag{4.6}$$

$$\vec{\mathbf{B}}_{u,d}^I = e^{j2\pi\frac{\epsilon f_u}{N}d}\mathbf{S}_u\mathbf{C}_{(\epsilon f_u)}^s\mathbf{T}_{(d)}\vec{\mathbf{Y}}_u \tag{4.7}$$

$$\vec{\mathbf{B}}_{u,d}^M = \sum_{u_1=0;u_1\neq u}^{U-1} e^{j2\pi\frac{\epsilon f_{u_1}}{N}d}\mathbf{S}_u\mathbf{C}_{(\epsilon f_{u_1})}\mathbf{T}_{(d)}\mathbf{Y}_{u_1} \tag{4.8}$$

and $\vec{\mathbf{Z}}_{u,d} = \left[\tilde{Z}_{u,d}[0], \tilde{Z}_{u,d}[1], \ldots \tilde{Z}_{u,d}[N-1]\right]^T$ and $\vec{\mathbf{N}}_d = \left[\tilde{N}_d[0], \tilde{N}_d[1], \ldots \tilde{N}_d[N-1]\right]^T$; $\tilde{Z}_{u,d}[k]$ and $\tilde{N}_d[k] = \sum_{n=0}^{N-1} \tilde{n}((d+n)\Delta t)e^{j2\pi\frac{nk}{N}}$ are the uth user's output signal at the kth subcarrier and the AWGN contribution at the kth subcarrier, respectively. $\vec{\mathbf{Y}}_u = \left[\tilde{Y}_u[0], \tilde{Y}_u[1], \ldots \tilde{Y}_u[N-1]\right]^T$ is the uth user's received signal under the effect of the channel, i.e. $\tilde{Y}_u[k] = \tilde{H}_u[k]\tilde{X}_u[k]$. $\tilde{H}_u[k] = e^{-j2\pi\frac{k}{N}\epsilon t_u}\sum_{l=0}^{L-1}\tilde{h}_{u,l}e^{-j2\pi\frac{k}{T_o}\tau_{u,l}}$ is the CTF at the kth subcarrier of the uth user. $\epsilon t_u = \delta t_u/\Delta t$ and $\epsilon f_u = \delta f_u/\Delta f$ are the normalized TO and CFO

of the uth user, respectively. $\mathbf{S}_u$ is a diagonal matrix of size $N \times N$, acting as a filter to select only subcarriers belonging to the uth user, i.e. $\mathbf{S}_u(k,k) = 1$ for $k \in \Delta_u$ and zero elsewhere. $\mathbf{T}_{(d)}$ is also a diagonal matrix of size N, whose k^{th} diagonal element is $e^{j2\pi\frac{k}{N}d}$, indicating the phase-shift due to the timing offset d. The $N \times N$ matrix $\mathbf{C}_{(\phi)}$ represents the amplitude and phase change due to the normalized CFO, ϕ, in frequency-domain. It is a circulant matrix denoting the circular convolution operation, and can be written as:

$$\mathbf{C}_{(\phi)} = \mathbf{F}_N \mathbf{c}_{(\phi)} \mathbf{F}_N^H \tag{4.9}$$

$$\mathbf{C}_{(\phi)} = \mathbf{C}_{(\phi)}^p + \mathbf{C}_{(\phi)}^s \tag{4.10}$$

$$\mathbf{C}_{(\phi)}^p = \tilde{\mathcal{C}}(\phi) \times \mathbf{I}_{N \times N} \tag{4.11}$$

$$\mathbf{C}_{(\phi)}^s = \begin{bmatrix} 0 & \tilde{\mathcal{C}}(1+\phi) & \dots & \tilde{\mathcal{C}}(N-1+\phi) \\ \tilde{\mathcal{C}}(N-1+\phi) & 0 & \dots & \tilde{\mathcal{C}}(N-2+\phi) \\ \vdots & \vdots & \ddots & \vdots \\ \tilde{\mathcal{C}}(1+\phi) & \tilde{\mathcal{C}}(2+\phi) & \dots & 0 \end{bmatrix} \tag{4.12}$$

where $\mathbf{F}_N$ stands for the size-N FFT matrix with entries $\mathbf{F}_N[n,k] = e^{-j2\pi nk/N}/\sqrt{N}$, $\tilde{\mathcal{C}}(\phi) = \frac{\sin\pi\phi}{N\sin\pi\phi/N}e^{j\pi\phi(N-1)/N}$ is the periodic sinc-function [37], $[.]^H$ in the superscript denotes the transpose operation, and $\mathbf{c}_{(\phi)}$ is a diagonal matrix of size N representing the CFO in time-domain, whose k^{th} diagonal element is equal to $e^{j2\pi\frac{k}{N}\phi}$. In the next section, our goal is to derive the CFO estimation from two observation vectors, $\vec{\mathbf{Z}}_{u,d_1}$ and $\vec{\mathbf{Z}}_{u,d_2}$, which are observed at two different timing offsets, d_1 and d_2, respectively.

4.4 Our proposed estimators

4.4.1 The Moose-based Shortened Observation Distance Estimator

Consider two FFT windows, which are taken at two different timing offsets, d_1 and d_2, as in Figure 4.1. We defines the "observation distance", $D = d_2 - d_1$, which denotes the distance between the two observations. If the timing offsets are neither too short nor too long, so that both FFT windows are kept within the ISI-free region of the preamble, we can show the following relation:

$$\vec{\mathbf{A}}_{u,d_2} = e^{j2\pi\frac{\epsilon f_u}{N}D}\mathbf{T}_{(D)}\vec{\mathbf{A}}_{u,d_1} \tag{4.13}$$

where $\mathbf{T}_{(D)}$ is a diagonal matrix of size N, whose the kth diagonal element is $e^{j2\pi \frac{k}{N}D}$. In another words, the useful signal parts of two observations separated by observation distance D are the same, except for their differential phase, which is a deterministic function of the CFO and the observation distance. Based on this relation, we can multiply $\vec{\mathbf{Z}}_{u,d_2}$ with $\mathbf{T}_{(D)}^{-1}$ to remove the effect of the observation distance and thus be able to estimate the CFO. It is worth noting that the inverse of the diagonal matrix $\mathbf{T}_{(D)}$ is simply equal to $\mathbf{T}_{(-D)}$. The modified observation vectors, $\vec{\mathbf{\Gamma}}_{u,d_1}^{\text{MSOD}}$ and $\vec{\mathbf{\Gamma}}_{u,d_2}^{\text{MSOD}}$, are given below:

$$\begin{cases} \vec{\mathbf{\Gamma}}_{u,d_1}^{\text{MSOD}} &= \vec{\mathbf{Z}}_{u,d_1} = \vec{\mathbf{A}}_{u,d_1} + \vec{\mathbf{W}}_{u,d_1} \\ \vec{\mathbf{\Gamma}}_{u,d_2}^{\text{MSOD}} &= \mathbf{T}_{(D)}^{-1}\vec{\mathbf{Z}}_{u,d_2} = e^{j2\pi \frac{\epsilon f_u}{N}D}\vec{\mathbf{A}}_{u,d_1} + \vec{\mathbf{W}}_{u,d_2} \end{cases} \tag{4.14}$$

in which $\vec{\mathbf{W}}_{u,d_1}$ and $\vec{\mathbf{W}}_{u,d_2}$ are the interference and noise vectors:

$$\vec{\mathbf{W}}_{u,d_1} = \vec{\mathbf{B}}_{u,d_1}^I + \vec{\mathbf{B}}_{u,d_1}^M + \mathbf{S}_u\vec{\mathbf{N}}_{d_1} \tag{4.15}$$

$$\vec{\mathbf{W}}_{u,d_2} = \mathbf{T}_{(D)}^{-1}\vec{\mathbf{B}}_{u,d_2}^I + \mathbf{T}_{(D)}^{-1}\vec{\mathbf{B}}_{u,d_2}^M + \mathbf{T}_{(D)}^{-1}\mathbf{S}_u\vec{\mathbf{N}}_{d_2} \tag{4.16}$$

The kth elements of the self- and cross-interference vectors, $\vec{\mathbf{B}}_{u,d_i}^I$ and $\vec{\mathbf{B}}_{u,d_i}^M$ ($i = 1, 2$), are assumed to be complex Gaussian distributions with zero mean and variance $\sigma_k^{I^2}$ and $\sigma_k^{M^2}$, respectively. This assumption is based on the fact that each element is the sum of the ICI and MUI from the other subcarriers, each of which experienced a random and independent channel and transmitted data, so that the Central Limit Theorem can be applied. The noise vector, $\vec{\mathbf{N}}_{d_i}$ ($i = 1, 2$), is also zero-mean complex Gaussian distribution with variance σ_N^2. Since rotating the phases of a circular symmetric complex random Gaussian vector does not change its statistical properties and the sum of random Gaussian vector gives a Gaussian vector [67, 68], $\vec{\mathbf{W}}_{u,d_1}$ and $\vec{\mathbf{W}}_{u,d_2}$ are also vectors whose element are complex Gaussian distribution with zero mean and variance $\sigma_W^2 = (\sigma_I^2 + \sigma_M^2 + \sigma_N^2)$. The maximum likelihood estimate of the differential phase of two observation vectors similar to Eq. (4.26) has been derived in [46], and the result can be expressed:

$$\hat{\epsilon f}_u = \frac{N}{2\pi D}\arctan\left\{\frac{\sum_{k\in\Delta_u}\Im\left[(\vec{\mathbf{\Gamma}}_{u,d_2}^{\text{MSOD}})^H\vec{\mathbf{\Gamma}}_{u,d_1}^{\text{MSOD}}\right]}{\sum_{k\in\Delta_u}\Re\left[(\vec{\mathbf{\Gamma}}_{u,d_2}^{\text{MSOD}})^H\vec{\mathbf{\Gamma}}_{u,d_1}^{\text{MSOD}}\right]}\right\} \tag{4.17}$$

where arctan(.) is arctangent function, $\Im(.)$ and $\Re(.)$ are respectively the imaginary and real parts of a complex, and $(.)^H$ denotes the Hermitian transpose.

It is worth noting that the Moose estimator is a special case of the proposed scheme, where the observation distance D is equal to N. In this case, $\mathbf{T}_{(D)} = \mathbf{T}_{(N)} = \mathbf{I}$, or the two observations in Eq. (4.26) can be re-written as:

$$\begin{cases} \vec{\mathbf{\Gamma}}_{u,d_1}^{\mathrm{ME}} &= \left(\vec{\mathbf{A}}_{u,d_1} + \vec{\mathbf{B}}_{u,d_1}^{I} \right) + \vec{\mathbf{W}}_{u,d_1}^{\mathrm{ME}} \\ \vec{\mathbf{\Gamma}}_{u,d_2}^{\mathrm{ME}} &= e^{j2\pi \frac{\epsilon f_u}{N} D} \left(\vec{\mathbf{A}}_{u,d_1} + \vec{\mathbf{B}}_{u,d_1}^{I} \right) + \vec{\mathbf{W}}_{u,d_2}^{\mathrm{ME}} \end{cases} \tag{4.18}$$

in which

$$\vec{\mathbf{W}}_{u,d_1}^{\mathrm{ME}} = \vec{\mathbf{B}}_{u,d_1}^{M} + \mathbf{S}_u \vec{\mathbf{V}}_{d_1} \tag{4.19}$$

$$\vec{\mathbf{W}}_{u,d_2}^{\mathrm{ME}} = \vec{\mathbf{B}}_{u,d_2}^{M} + \mathbf{S}_u \vec{\mathbf{V}}_{d_2} \tag{4.20}$$

and the $(.)^{\mathrm{ME}}$ in the superscript denotes variables used in the Moose estimator. The Eq. (4.18) indicates that both the signal and the self-interference term in Moose estimator are altered in exactly the same way between two observations, by a phase shift proportional to the frequency offset [46]. Thus, in the Moose estimator, the self-interference term will be an useful part of the estimation; whereas in the case where $D < N$, it is regarded as interference. The role of cross-interference term, however, is unchanged for both $D = N$ and $D < N$ cases. From now on, we treat these two cases separately as Moose estimator and Moose-based Shortened Observation Distance (MSOD) estimator, respectively.

Since the phase is limited in the range $[-\pi, \pi]$, the theoretical range of MSOD estimator is given by:

$$|\hat{\epsilon f}_u{}^{\mathrm{MSOD}}| \le \frac{N}{2D} \Delta f \tag{4.21}$$

Since $D < N$, the range of the proposed estimator is larger than half of subcarrier spacing, which is the limit of the Moose estimator. However, a larger estimation range would also mean that the MSOD estimator is more sensitive to noise and interference, because the same amount of phase error due to noise and interference results in a larger frequency offset error in this case.

4.4.2 The Correlation-based Shortened Observation Distance Estimator

In chapter 3, we have discussed a CFO estimation scheme for the initial ranging scenario, which is based on correlation of the received signal with known ranging code. Although the scheme was designed for situations where

users are allowed to overlap in a time-frequency block, it can also be applied for the data transmission phase, where each MS has been assigned a separate time-frequency block for uplink communication. In this chapter, we shall modify the above-mentioned scheme so that it works with the observation distance of less than a OFDM symbol. The modified scheme is referred to as the Correlation-based Shortened Observation Distance (CSOD) estimator hereafter.

Consider the correlation of the known code with the transmitted version of itself presented in Eq. (3.11). The lag $\lambda_{max} = \epsilon t_u + \tau_{u,0}/\Delta t + N_g^A$ corresponds to the peak of $\tilde{p}_{m,g}[\lambda]$, which is equal to:

$$
\begin{aligned}
\tilde{p}_{m,g}[\lambda_{max}] &= \frac{1}{N^2} e^{-j2\pi\epsilon f_u \frac{\lambda}{N}} \tilde{h}_{u,0}^* \Big\{ \sum_{k_1 \in \Delta_g} |\tilde{X}_u[k_1]|^2 \tilde{\mathcal{C}}_{(-\epsilon f_u)} \\
&\quad + \sum_{k_1 \in \Delta_g} \sum_{k_2 \in \Delta_g; k_2 \neq k_1} \tilde{X}_u[k_1] \tilde{X}_u^*[k_2] \tilde{\mathcal{C}}_{(k_1-k_2-\epsilon f_u)} \Big\} \quad (4.22)
\end{aligned}
$$

And the correlation value at lag $(\lambda_{max} + D)$ is given by:

$$
\begin{aligned}
\tilde{p}_{m,g}[\lambda_{max} + D] &= \frac{1}{N^2} e^{-j2\pi\epsilon f_u \frac{D}{N}} e^{-j2\pi\epsilon f_u \frac{\lambda}{N}} \tilde{h}_{u,0}^* \Big\{ \sum_{k_1 \in \Delta_g} |\tilde{X}_u[k_1]|^2 e^{-j2\pi\frac{Dk_1}{N}} \tilde{\mathcal{C}}_{(-\epsilon f_u)} \\
&\quad + \sum_{k_1 \in \Delta_g} \sum_{k_2 \in \Delta_g; k_2 \neq k_1} \tilde{X}_u[k_1] \tilde{X}_u^*[k_2] \\
&\quad \times e^{-j2\pi\frac{Dk_2}{N}} \tilde{\mathcal{C}}_{(k_1-k_2-\epsilon f_u)} \Big\} \quad (4.23)
\end{aligned}
$$

Due to the rotated phase $e^{-j2\pi\frac{Dk_1}{N}}$, the elements in the first sum in Eq. (4.23) do not add coherently, and therefore the auto-correlation peak cannot be achieved unless D is multiple of N. In order to obtain another auto-correlation peak at D less than N, we propose that the known code is replaced by a D-sample circularly-shifted version of itself in Eq. (3.7):

$$
\begin{aligned}
\tilde{x}_{m,g}'[n] &= \tilde{x}_{m,g}\big[(n+D) \mod N\big] \\
&= \frac{1}{N} \sum_{k \in \Delta_g} \tilde{X}_u[k] e^{j2\pi\frac{Dk}{N}} e^{j2\pi\frac{nk}{N}} \quad (4.24)
\end{aligned}
$$

The corresponding auto-correlation at $(\lambda_{max} + D)$ can be expressed as:

$$
\begin{aligned}
\tilde{p}'_{m,g}\big[\lambda_{max} + D\big] &= e^{-j2\pi\epsilon f_u \frac{\lambda+D}{N}} \tilde{h}^*_{u,0} \sum_{n=0}^{N-1} \tilde{x}_{m,g}\big[n\big] \\
&\times \quad \tilde{y}^*_u\big[n + \lambda + D - \epsilon t_u - \tau_{u,1}/\Delta t\big] e^{-j2\pi\epsilon f_u \frac{n}{N}} \\
&= \frac{1}{N^2} e^{-j2\pi\epsilon f_u \frac{D}{N}} e^{-j2\pi\epsilon f_u \frac{\lambda}{N}} \tilde{h}^*_{u,0} \Big\{ \sum_{k_1 \in \Delta_g} |\tilde{X}_u\big[k_1\big]|^2 \tilde{\mathcal{C}}_{(-\epsilon f_u)} \\
&\quad + \sum_{k_1 \in \Delta_g} \sum_{k_2 \in \Delta_g; k_2 \neq k_1} \tilde{X}_u\big[k_1\big] \tilde{X}^*_u\big[k_2\big] \\
&\quad \times e^{j2\pi \frac{D(k_1-k_2)}{N}} \tilde{\mathcal{C}}_{(k_1-k_2-\epsilon f_u)} \Big\}
\end{aligned}
\tag{4.25}
$$

The rotated phase now disappears in the first sum in Eq. (4.25), making it equivalent to the first sum in Eq. (4.22). Although the second term in these two equations are different, it is insignificant and thus we can treat it as interference in our algorithm.

The above analysis inspires us to propose a CFO estimation scheme based on the correlation of known preamble in time-domain, with the observation distance less than N. We consider two correlation vectors for the CSOD scheme as given below:

$$
\begin{cases}
\vec{\mathbf{\Gamma}}^{\text{CSOD}}_{u,d_1} &= \mathbf{F}^H_N \Big[\vec{\mathbf{X}}_u \odot \vec{\mathbf{Z}}^*_{u,d_1} \Big] = \vec{\mathbf{P}}_{u,d_1} + \vec{\mathbf{Q}}_{u,d_1} \\
\vec{\mathbf{\Gamma}}^{\text{CSOD}}_{u,d_2} &= \mathbf{F}^H_N \Big[\mathbf{T}_{(D)} \vec{\mathbf{X}}_u \odot \vec{\mathbf{Z}}^*_{u,d_2} \Big] = e^{j2\pi \frac{\epsilon f_u}{N} D} \vec{\mathbf{P}}_{u,d_1} + \vec{\mathbf{Q}}_{u,d_2}
\end{cases}
\tag{4.26}
$$

in which $d_2 = d_1 + D$, $\vec{\mathbf{X}}_u = \Big[\tilde{X}_u\big[0\big], \tilde{X}_u\big[1\big], \ldots, \tilde{X}_u\big[N-1\big]\Big]^T$ is the vector of transmitted pilots, $\vec{\mathbf{P}}_{u,d_1} = \Big[\tilde{p}_{u,d_1}\big[0\big], \tilde{p}_{u,d_1}\big[1\big], \ldots, \tilde{p}_{u,d_1}\big[N-1\big]\Big]^T$ is the vector of useful signal part, and $\vec{\mathbf{Q}}_{u,d_i} = \Big[\tilde{q}_{u,d_i}\big[0\big], \tilde{q}_{u,d_i}\big[1\big], \ldots, \tilde{q}_{u,d_i}\big[N-1\big]\Big]^T$ $(i = 1, 2)$ is the vector of noise and interference, and:

$$
\begin{aligned}
\tilde{p}_{u,d_1}\big[\lambda\big] &= \frac{1}{N^2} e^{-j2\pi\epsilon f_u \frac{d_1+\lambda}{N}} \sum_{l=0}^{L-1} h^*_{u,l} \sum_{k_1 \in \Delta_u} \Big|\tilde{X}_u\big[k_1\big]\Big|^2 \\
&\times e^{-j2\pi \frac{(d_1+\lambda-\epsilon t_u - \tau_{u,l}/\Delta t - N^A_g)k_1}{N}} \tilde{\mathcal{C}}_{(-\epsilon f_u)}
\end{aligned}
\tag{4.27}
$$

$$
\begin{aligned}
\tilde{q}_{u,d_1}\left[\lambda\right] &= \frac{1}{N^2}e^{-j2\pi\epsilon f_u\frac{d_1+\lambda}{N}}\sum_{l=0}^{L-1}h_{u,l}^*\sum_{k_1\in\Delta_u}\sum_{k_2\in\Delta_u;k_2\neq k_1}\tilde{X}_u\left[k_1\right]\tilde{X}_u^*\left[k_2\right]\\
&\times e^{-j2\pi\frac{(d_1+\lambda-\epsilon t_u-\tau_{u,l}/\Delta t-N_g^A)k_2}{N}}\tilde{\mathcal{C}}_{(k_1-k_2-\epsilon f_u)}\\
&+\frac{1}{N^2}\sum_{u'=0;u'\neq u}^{U-1}e^{-j2\pi\epsilon f_{u'}\frac{d_1+\lambda}{N}}\sum_{l=0}^{L-1}h_{u',l}^*\sum_{k_1\in\Delta_u}\sum_{k_2\in\Delta_{u'}}\tilde{X}_u\left[k_1\right]\tilde{X}_{u'}^*\left[k_2\right]\\
&\times e^{-j2\pi\frac{(d_1+\lambda-\epsilon t_{u'}-\tau_{u',l}/\Delta t-N_g^A)k_2}{N}}\tilde{\mathcal{C}}_{(k_1-k_2-\epsilon f_{u'})}\\
&+\frac{1}{N^2}\sum_{k_1\in\Delta_u}\tilde{X}_u\left[k_1\right]\tilde{N}_{d_1}\left[k_1\right]
\end{aligned}
\tag{4.28}
$$

$$
\begin{aligned}
\tilde{q}_{u,d_2}\left[\lambda\right] &= \frac{1}{N^2}e^{-j2\pi\epsilon f_u\frac{d_2+\lambda}{N}}\sum_{l=0}^{L-1}h_{u,l}^*\sum_{k_1\in\Delta_u}\sum_{k_2\in\Delta_u;k_2\neq k_1}\tilde{X}_u\left[k_1\right]\tilde{X}_u^*\left[k_2\right]\\
&\times e^{j2\pi\frac{Dk_1}{N}}e^{-j2\pi\frac{(d_2+\lambda-\epsilon t_u-\tau_{u,l}/\Delta t-N_g^A)k_2}{N}}\tilde{\mathcal{C}}_{(k_1-k_2-\epsilon f_u)}\\
&+\frac{1}{N^2}\sum_{u'=0;u'\neq u}^{U-1}e^{-j2\pi\epsilon f_{u'}\frac{d_2+\lambda}{N}}\sum_{l=0}^{L-1}h_{u',l}^*\sum_{k_1\in\Delta_u}\sum_{k_2\in\Delta_{u'}}\tilde{X}_u\left[k_1\right]\tilde{X}_{u'}^*\left[k_2\right]\\
&\times e^{j2\pi\frac{Dk_1}{N}}e^{-j2\pi\frac{(d_2+\lambda-\epsilon t_{u'}-\tau_{u',l}/\Delta t-N_g^A)k_2}{N}}\tilde{\mathcal{C}}_{(k_1-k_2-\epsilon f_{u'})}\\
&+\frac{1}{N^2}\sum_{k_1\in\Delta_u}\tilde{X}_u\left[k_1\right]\tilde{N}_{d_2}\left[k_1\right]e^{j2\pi\frac{Dk_1}{N}}
\end{aligned}
\tag{4.29}
$$

In Eq. (4.28) and (4.29), the first term indicates the self-interference, causing by the power leakage from the other subcarriers of the same user to the subcarrier of interest. If the CFO is not present, this term will go to zero due to the periodic sinc-function. The second term is the cross-interference, causing by the power leakage from the subcarriers of the other active users in the system to the subcarrier of interest. Finally, the last term is the cross-correlation between the pilot and the AWGN noise. Eq. (4.26) indicates that the FFT is used to implement the circular-correlation, but the direct usage of a bank of correlators can also be used since they are equivalent (see Chapter 3).

In order to estimate the CFO, we need to find the correlation lag corresponding to the auto-correlation peak. One method is to use the argmax(.) function:

$$
\lambda_{max} = \text{argmax}_\lambda\left\{\left|\tilde{\Gamma}_{u,d_2}[\lambda]\tilde{\Gamma}_{u,d_1}^*[\lambda]\right|^2\right\}
\tag{4.30}
$$

where $\tilde{\Gamma}_{u,d_i}[\lambda]$ is the λth element of vector $\vec{\mathbf{\Gamma}}_{u,d_i}^{\text{CSOD}}$ ($i = 1, 2$). This method is referred to as the "max-based" algorithm. The CFO is then calculated from the peak:

$$\hat{\epsilon f}_u = \frac{N}{2\pi D} \arctan\left(\tilde{\Gamma}_{u,d_2}[\lambda_{max}]\tilde{\Gamma}_{u,d_1}^*[\lambda_{max}]\right) \tag{4.31}$$

Another method involves comparing the correlation output with a pre-defined threshold η_A, which is referred to as "threshold-based" algorithm. All the correlation lag λ that satisfies the condition $(\tilde{\Gamma}_{u,d_1}[\lambda] > \eta_A)$ and $(\tilde{\Gamma}_{u,d_2}[\lambda] > \eta_A)$ will be selected as an observation point. This creates two observation vectors, $\vec{\mathbf{\Gamma}}_{u,d_1}^{\text{Ob}-\text{CSOD}}$ and $\vec{\mathbf{\Gamma}}_{u,d_1}^{\text{Ob}-\text{CSOD}}$, which is a subset of $\vec{\mathbf{\Gamma}}_{u,d_1}^{\text{CSOD}}$ and $\vec{\mathbf{\Gamma}}_{u,d_1}^{\text{CSOD}}$, respectively. And the CFO estimate is then given by:

$$\hat{\epsilon f}_u = \frac{N}{2\pi D} \arctan\left\{ \frac{\Im\left[(\vec{\mathbf{\Gamma}}_{u,d_1}^{\text{Ob}-\text{CSOD}})^H \vec{\mathbf{\Gamma}}_{u,d_2}^{\text{Ob}-\text{CSOD}}\right]}{\Re\left[(\vec{\mathbf{\Gamma}}_{u,d_1}^{\text{Ob}-\text{CSOD}})^H \vec{\mathbf{\Gamma}}_{u,d_2}^{\text{Ob}-\text{CSOD}}\right]} \right\} \tag{4.32}$$

It is worth to note that if there is no λ satisfying the above-mentioned condition, the "threshold-base" algorithm will have to choose a λ using the argmax(.) function, or in another words, it falls back to "max-based" in that particular case.

We can see that the estimator in this section has the same theoretical range as the MSOD estimator in section 4.4.1.

4.4.3 The Iterative Estimation and Adjustment Algorithm

When the observation distance D is not a multiple of the length of OFDM symbol, N, the self-interference becomes different between two observation windows, and therefore must be treated as interference in both above-mentioned algorithms, namely the MSOD and CSOD. By reducing the CFO of the user of interest, we can limit the level of self-interference, and thus increase the performance of the estimators. In addition, large CFO causes the reduction of the received power of the pilot signal on each subcarrier, which also degrades the performance of the estimators.

To alleviate the negative effect of large CFO in the MSOD and CSOD estimators, we propose the Iterative Estimation and Adjustment (IEA) algorithm as follows:

IEA algorithm

Initialization:

Step 1: Set $i = 0$ and $\hat{\epsilon f_i} = 0$

Loop:

Step 2: $i = i + 1$

Step 3: Adjust the CFO of the received preamble vector by multiplying it with $\mathbf{c}_{(\hat{\epsilon f_i})}$

Step 4: Perform FFT on the preamble and estimate the new CFO, $\hat{\epsilon f_i}$, by using Eq. (4.17) or Eq. (4.31) or Eq. (4.32).

Step 5: Go back to *Loop* until $i = N_{loop}$

This algorithm aims at reducing the CFO of the current user close to zero, thus decreasing the level of self-interference and removing the peak reduction issue, so as to improve the accuracy of both estimators. The performance of this algorithm is discussed in more details in the next section.

4.4.4   Computational complexity comparison

The MSOD requires $N \log_2 N$ operations to convert the time-domain received signal into frequency-domain. Then it needs $|\Delta_u|$ complex multiplications to obtain the second observation vector in Eq. (4.26), and another $|\Delta_u|$ complex multiplications to estimate the CFO in Eq. (4.17) for the uth user, where $|\Delta_u|$ is the size of the set of subcarriers Δ_u. In total, the MSOD scheme requires $N \log_2 N + 2N$ operations, or the complexity of MSOD is $\mathcal{O}(N \log_2 N)$.

The CSOD, on the other hand, is more complex than the MSOD scheme. It must convert the time-domain received signal into frequency-domain, multiply with the known code, and the convert back to time-domain again for each user separately. In general, the complexity of CSOD is $\mathcal{O}(UN \log_2 N)$

If the IEA is implemented, the complexity of the MSOD and CSOD schemes become $\mathcal{O}(N_{loop}N \log_2 N)$ and $\mathcal{O}(N_{loop}UN \log_2 N)$, respectively. In case of the CSOD scheme using IEA and "max-based" algorithm, computational complexity can be reduced by implementing the direct correlation in time-domain instead of the FFT-based implementation, once the correlation lag corresponding to the auto-correlation peak has been found. From the second iteration, the time-domain version of the preamble can be correlated directly with the CFO-adjusted received signal only at the maximum correlation lag to give the auto-correlation peaks, and then using them to estimate the new CFO. Correlation at one lag requires only N complex multiplication, thus the complexity in this special case is $\mathcal{O}(UN \log_2 N + (N_{loop} - 1)UN)$.

Table 4.1: Simulation parameters

Parameter	Value
Number of subcarriers	512
Number of users	4
Number of subcarriers per user	128
Subcarrier allocation scheme	Contiguous and Non-contiguous
Modulation	Binary Phase Shift Keying (BPSK)
Channel model	7-tap exponential decay Rayleigh fading channel [43]

4.5   Numerical Results

In this section, numerical evaluation is presented to shed some light on the performance of the proposed scheme. Table 5.2 summaries the parameters used in our Monte Carlo simulation. The performance measure is the MSE, defined as:

$$\sigma^2_{\epsilon f_u} = \frac{1}{N_{meas}} \sum_{i=1}^{N_{meas}} (\epsilon \hat{f}_u - \epsilon f_u)^2 \tag{4.33}$$

where N_{meas} is the number of Monte Carlo trials. All users are assumed to have equal transmitting power and to be at the same distance from BS. The CFOs are generated uniformly in the $[-\epsilon f_{max}, \epsilon f_{max}]$ range, where ϵf_{max} is the maximum tolerable CFO of the system, which is normalized to subcarrier spacing. In the CSA scheme, each user is assigned a block of subcarriers that are adjacent to each other, while in the NCSA scheme, the subcarriers are interleaved uniformly across the spectrum. The Moose estimator's performance is shown in the figures as MSOD scheme with $D = N$.

4.5.1   Singe-user scenario

First, we evaluate the effect of the observation distance, D, on the performance of the proposed schemes in Figure 4.2. In this scenario, only one user is active in the system, and thus there is no cross-interference occurring. The CNR is 20dB, while the maximum tolerable CFO is equal to 30% of the subcarrier spacing. It is clear that the performance of the estimators are improved with the increase of observation distance. This is due to the fact that shorter D increases the estimation range for both estimators, but that also makes them more sensitive to noise and interference: The same phase error will cause larger MSE error when observation distance is smaller.
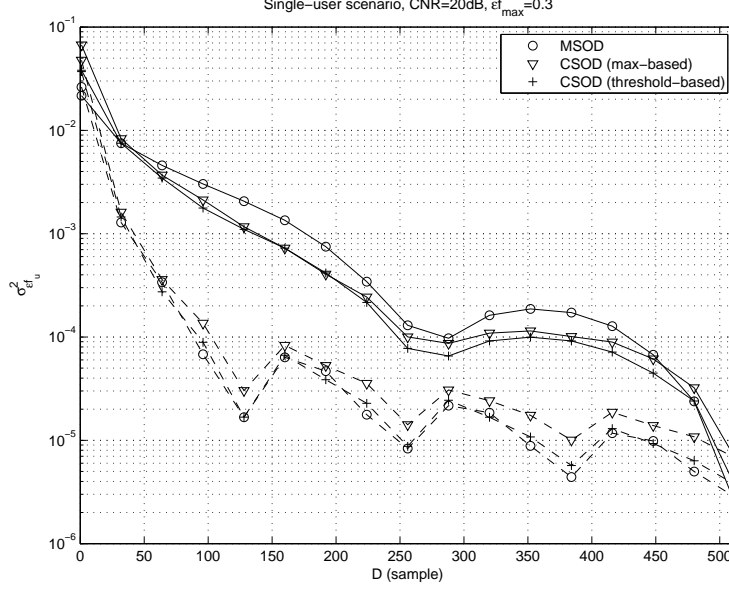
Figure 4.2: The MSE performance vs observation distance for single-user scenario. Solid lines indicate contiguous subcarrier allocation, while dashed lines present the non-contiguous subcarrier allocation.

Shorter D also causes the noise and interference in two observations to be more correlated, which undermines the efficiency of the ML estimator.

To evaluate the effect of self-interference, we plot the performance of the NCSA scheme on the Figure using the dashed lines. As we can see, when there are guard band between subcarriers of the user, which reduces the self-interference, the performance of the estimators increases significantly. When $D = N$, the two subcarrier allocation schemes perform exactly the same. If we take a closer look, the MSOD seems to be more affected by the self-interference than the CSOD scheme. Its performance degrades more significantly when changing from NCSA to CSA scheme. This agrees with the fact that CSOD is a correlation-based scheme, which requires heavier computation, but also offers greater processing gain and less degradation due to noise and interference.

In single-user scenario, the performance of the two estimators are very close. They all shows the same trend, for example a particularly good performance ad $D = N/2$. This gives a guideline when designing the MSOD and CSOD in practice. And we can see that CSOD with threshold-based algorithm is better than the max-based one. In this figure, the predefined threshold is fixed as 10dB.
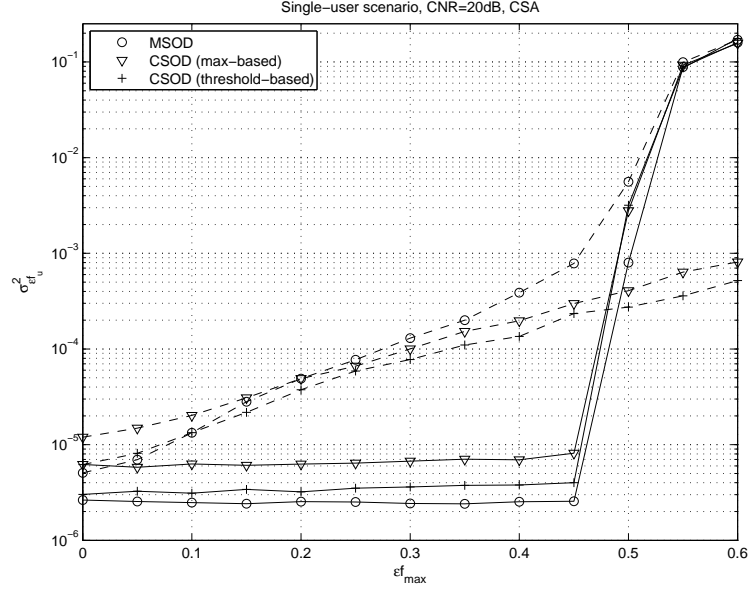
81

Figure 4.3: The MSE performance vs maximum tolerable CFO for single-user scenario. Solid lines indicate observation distance $D = N$, and dashed lines present $D = N/2$.

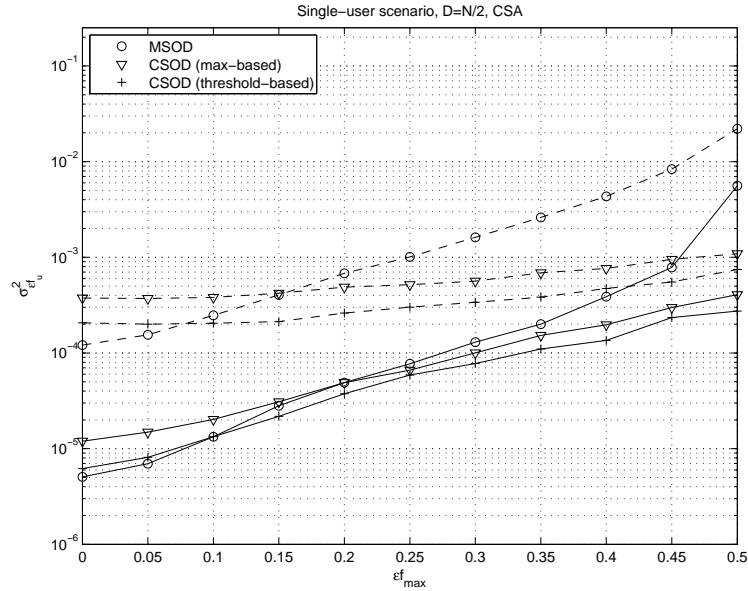Figure 4.4: The MSE performance vs maximum tolerable CFO for single-user scenario. Solid lines indicate the carrier-to-noise ratio (CNR) of 20dB, while the dashed lines present CNR=5dB.
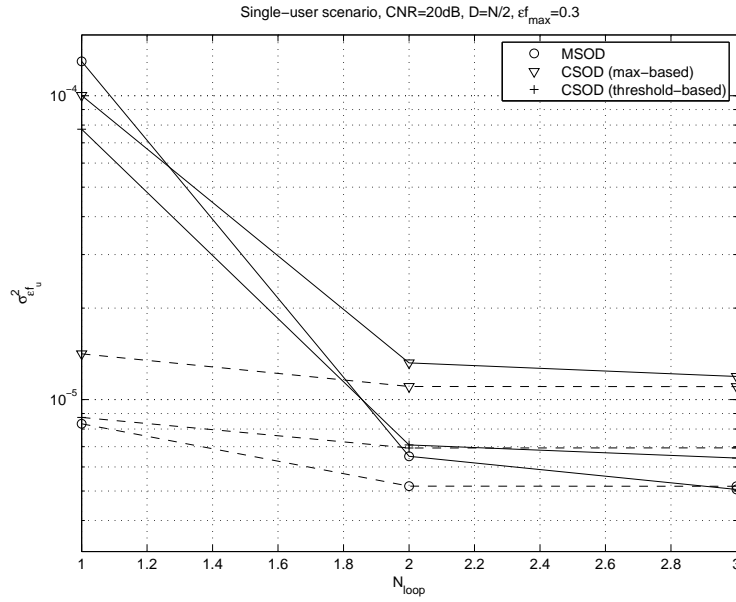
Figure 4.5: The MSE performance vs the number of iterations of the IEA algorithm for single-user scenario. Solid lines indicate contiguous subcarrier allocation, while dashed lines present the non-contiguous subcarrier allocation.

Secondly, we evaluate the performance of the estimators under different CFO range in Figure 4.3. This is still single-user scenario, where CSA scheme is used. The maximum tolerable CFO varies from 0 to 0.6 of subcarrier spacing. The solid lines indicates observation distance $D = N$, while the dashed lines shows the performance with $D = N/2$. The performance of all estimators with $D = N$ is relatively constant with the increase of the CFO until a certain point, due to the fact that the self-interference is now a part of the useful signal used in estimation process [46]. However, their performance suddenly breaks when they reach their theoretical estimation range, which is 0.5 of the subcarrier spacing.

On the other hand, the performance of the estimators with $D = N/2$ gradually degrades with the increase of the CFO. This causes by the increase of self-interference, which is no longer a part of the useful signal used for estimation process, and also the reduction of the power of the pilot signals due to CFO. The MSOD is more prone to interference, and thus its performance degrades much more than the CSOD at high CFO values. In contrast, both CSOD schemes offers reasonable accurate estimates at high CFO values, for example up to 0.6 of the subcarrier spacing.

Thirdly, the proposed estimators are evaluated with different CNR values in Figure 4.4. The observation distance is fixed at $D = N/2$, and the solid line shows CNR of 20dB, while the dashed line presents the CNR value of 5dB. We can see that the effect of the AWGN is only significant at low CFO values, which indicates by the difference in performance between the dashed lines and the solid ones at CFO less than 0.2 subcarrier spacing. At high CFO, the interference becomes more dominant, and the performance of the dashed and solid lines converges.

Finally, the convergence of the IEA algorithm is shown in Figure 4.5 for both CSA and NCSA schemes. We can see that all estimators converge only after 2 or 3 iterations. In single user scenario, the CSA scheme benefits more from the IEA algorithm than the NCSA one, as the self-interference is more dominant in this scheme.

4.5.2 Multi-user Scenario

In this section, we evaluate the performance of the proposed estimators in the multi-user scenario. There are 4 active users in the system, and the subcarrier allocation scheme is either CSA or NCSA. Figure 4.6 show the performance as a function of the observation distance. The CNR is 20dB, and the maximum CFO is 0.3 subcarrier spacing - the same setting as in Figure 4.2 for single-user scenario. We can see that, under the CSA scheme, the MSEs of all estimators are relatively unchanged comparing to the single-
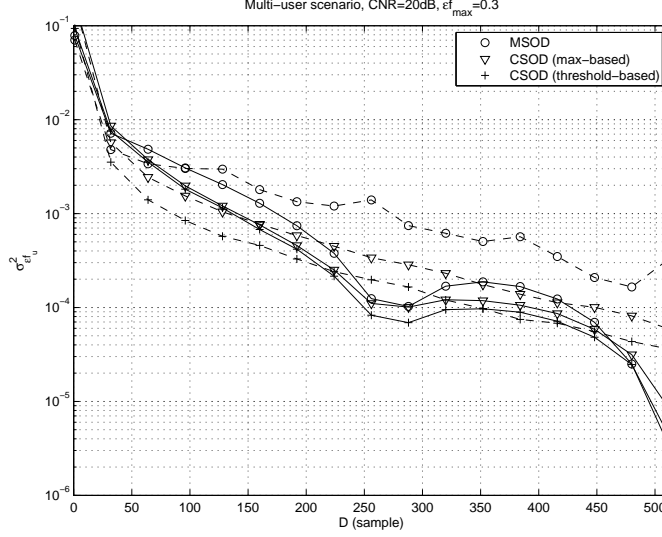
Figure 4.6: The MSE performance vs observation distance for multi-user scenario. Solid lines indicate contiguous subcarrier allocation, while dashed lines present the non-contiguous subcarrier allocation.

user scenario. Due to the fact that each user is allocated a block of contiguous subcarriers for transmission, the MUI only affects a few subcarriers at the edge of the block, and therefore their effect is insignificant. On the other hand, the NCSA scheme experiences a great penalty in performance when going from single-user to multi-user scenario. The MSOD scheme shows the worst performance, while the threshold-based CSOD is the best among the three, both for CSA and NCSA, in the multi-user scenario.

Figure 4.7 and 4.8 are the MSEs of the proposed estimators as a function of the maximum tolerable CFO in multi-user scenario, with CSA and NCSA scheme, respectively. The performance of the estimators with $D = N$ is no longer constant with the increase of CFO values, due to the fact that the cross-interference also increases with the increase of CFO. This cross-interference has very negative impact on the MSOD scheme, especially in NCSA scheme. Here the MSE of the MSOD increases much quicker than those of the CSOD scheme, even with the full observation distance, i.e. $D = N$. In both subcarrier allocation schemes, the CSOD with $D = N/2$ offers an acceptable performance at high CFO values, for example around 10^{-3} at CFO of 0.6 subcarrier spacing

The impact of CNR on the proposed estimators in multi-user scenario is illustrated in Figure 4.9. CNR of 5dB and 20dB is evaluated with the CSA scheme. We observe the same tendency as in single-user scenario: The effect

Figure 4.7: The MSE performance vs maximum tolerable CFO for multi-user scenario with contiguous subcarrier allocation. Solid lines indicate observation distance $D = N$, and dashed lines present $D = N/2$.

Figure 4.8: The MSE performance vs maximum tolerable CFO for multi-user scenario with non-contiguous subcarrier allocation. Solid lines indicate observation distance $D = N$, and dashed lines present $D = N/2$.
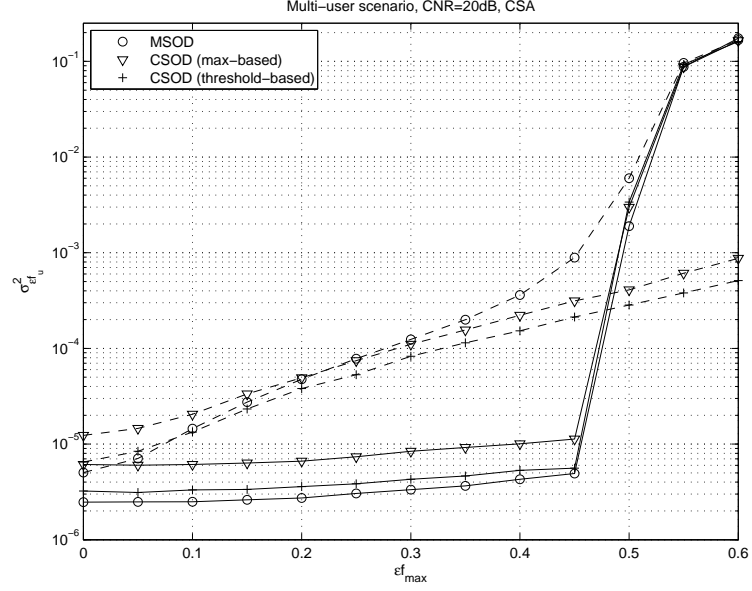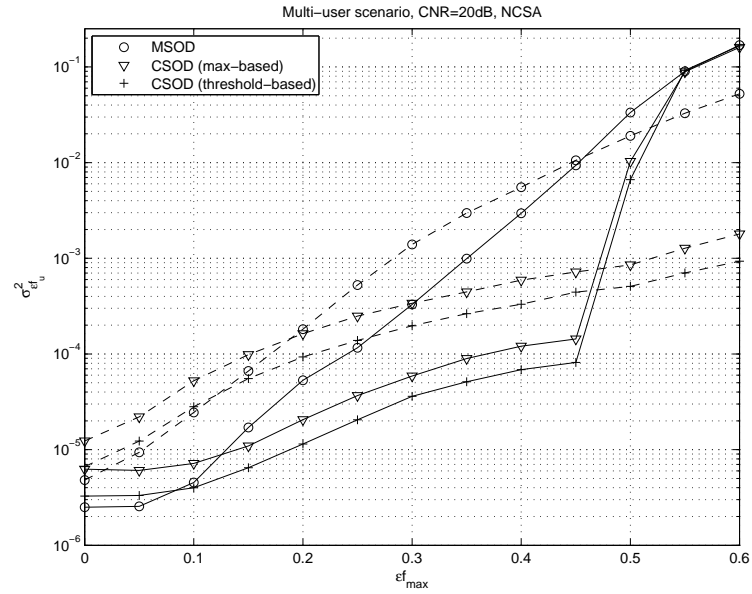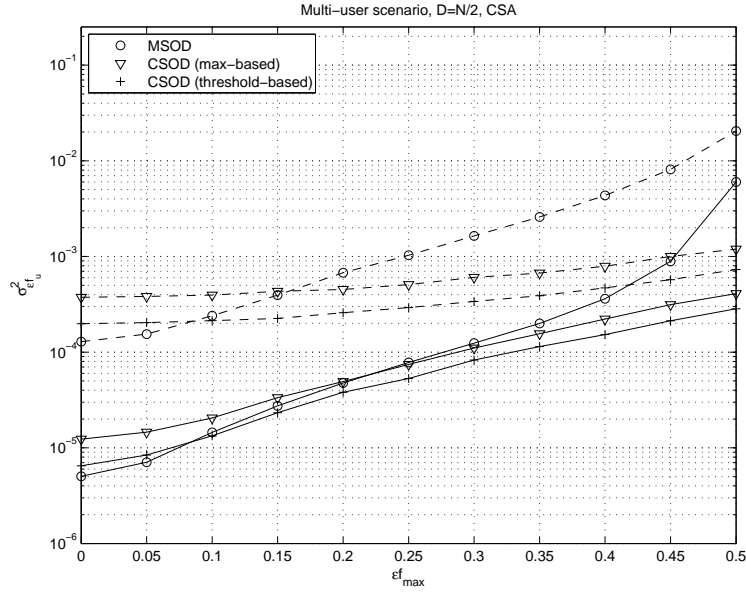
Figure 4.9: The MSE performance vs maximum tolerable CFO for multi-user scenario with contiguous subcarrier allocation. Solid lines indicate the carrier-to-noise ratio (CNR) of 20dB, while the dashed lines present CNR=5dB.
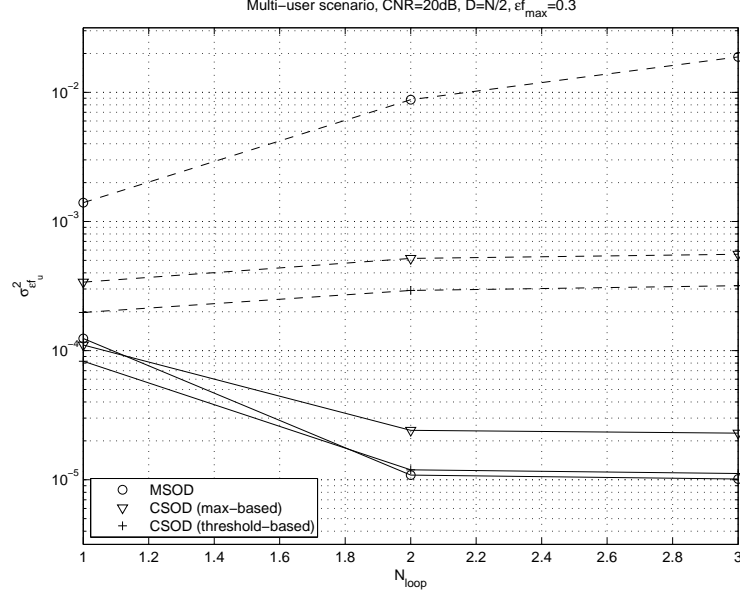
Figure 4.10: The MSE performance vs the number of iterations of the IEA algorithm for multi-user scenario. Solid lines indicate contiguous subcarrier allocation, while dashed lines present the non-contiguous subcarrier allocation.

of AWGN is only significant at low CFO values. At high CFO, the self- and cross-interference becomes the dominant source of MSE, and thus the dashed and the solid lines converges.

Figure 4.10 illustrates the convergence property of the IEA scheme. The CNR is 20dB, while the maximum CFO is fixed at 0.3 of subcarrier spacing. We can see that the IEA converges after 2 or 3 iterations in CSA scheme. Nevertheless, since the main source of interference in NCSA scheme is cross-interference, the IEA algorithm - which only reduces self-interference - does not perform very well. Applying the IEA algorithm in NCSA scheme even degrades the performance of the MSOD and CSOD estimator, because the CFO correction for one user in IEA could increase the CFO of the other users in the system, thus introduce even more interference in NCSA scheme [65].

Figure 4.11 presents the performance of MSOD and threshold-based CSOD as a function of the observation distance. The number of iterations here is two, i.e. $N_{loop} = 2$. The IEA offers a significant performance gain when the CSA is used and the observation distance is less than the length of OFDM symbol, i.e. $D < N$. For example, at $D = N/4$, the MSE of the proposed estimators with IEA algorithm is close to 10^{-4}.
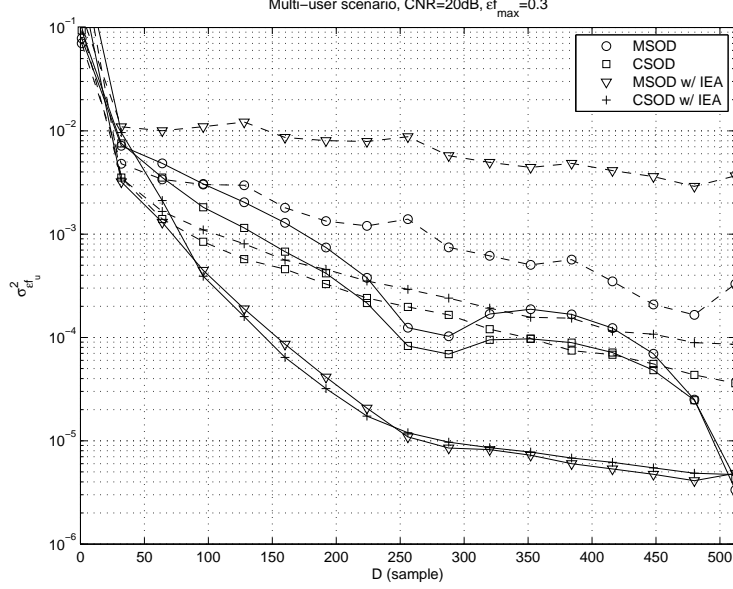
Figure 4.11: The MSE performance vs the observation distance for multi-user scenario. Solid lines indicate contiguous subcarrier allocation, while dashed lines present the non-contiguous subcarrier allocation.

4.6   Conclusions

In this chapter, we discussed the CFO estimation problem for the data transmission phase of an uplink OFDMA-based system, during which MSs have been allocated independent time-frequency block for communications.

Our contribution in this chapter is the proposal of two CFO estimators, namely the Moose-based Shortened Observation Distance (MSOD) and Correlation-based Shortened Observation Distance (CSOD). The first one is a generalized version of the Moose CFO estimation technique, where the observation distance D between two FFT windows can be selected arbitrary and less than the length of the OFDM symbol. The second is based on time-domain correlation technique, which has previously proposed for initial ranging scenario. Both schemes offer the possibility to shorten the length of the OFDMA preamble required for synchronization, and thus reduces the overhead in packet-based wireless communications. We also introduce an Iterative Estimation and Adjustment (IEA) algorithm in this chapter, which aims at improving the performance of the above-mentioned techniques in scenarios where self-interference is the dominant source of estimation error.

We evaluated the performance of the proposed schemes in various scenarios. The shorten observation distance estimators have shown to offer

reasonable accurate estimates at D is equal to only half of the length of the OFDMA symbol. Especially in the CSA scheme, the MSE of the proposed schemes with IEA algorithm is close to 10^{-4} at D equal to one fourth of the length of the OFDMA symbol. The CSOD requires heavier computational complexity, but it also offers a better performance than the MSOD scheme.

Chapter 5

Multi-user interference cancellation

As mentioned in Chapter 2, each user in the uplink of an OFDMA-based system experiences an independent Carrier Frequency Offset (CFO). These CFOs, if not corrected, destroy the orthogonality among subcarriers, causing ICI and MUI, which could degrade the system's performance severely.

In this chapter, we focus on the techniques to alleviate the negative effects of the multiple CFOs in the uplink of OFDMA-based wireless communications. Our contribution includes:

- Proposal of novel time-domain multi-user interference cancellation schemes, which employ an architecture with multiple OFDMA demodulators to compesate for the impacts of multi-user CFOs at the receiver's side.

- Analytical and numerical evaluation of the proposed schemes in comparisons with the existing techniques in literature. We show that the proposed schemes outperform existing techniques with only a reasonable increase in complexity.

5.1 Introduction

In chapter 2, we have shown that the OFDMA inherits from OFDM the sensitivity to CFO and phase noise [28]. The carrier frequency mis-alignment destroys the orthogonality of the subcarriers, which causes ICI and consequently produces MUI among users [42]. While the CFO can be estimated and corrected relatively easily in the downlink, preserving orthogonality in the uplink is much more demanding. In the uplink, the received signal is

the sum of multiple signals coming from different users, each of which experiences a different CFO due mainly to oscillator instability and/or Doppler shift [40]. These relative CFOs among users must be corrected, otherwise the system performance could degrade severely. Downlink CFO correction methods, which are designed for single-user scenario, are unable to correct multiple CFOs in the uplink, as correction to one user's CFO would misalign the other users [36].

In this chapter, we consider a quasi-synchronous scenario, where MSs are synchronized in time, but not in frequency. Each MS has been assigned a separate time-frequency block for their data transmission. Assuming that the estimates of multiple CFOs is available, the focus of this chapter is to provide the receiver with the technique to combat the ICI and MUI problem due to those CFOs.

5.2 The state of the art

Various studies have been carried out to tackle the multiple CFO problems in the OFDMA uplink scenario, which can be divided into two categories: Interference Avoidance (IA) and Interference Cancellation (IC) methods. Examples of IA schemes includes windowing, self-ICI cancellation and feedback-and-adjust approaches. The windowing approach in [69, 70] shapes the output of the IDFT by a window to suppress the side-lobes of the subcarriers, thus reduces the sensitivity to frequency errors. This approach normally causes CNR loss, and ICI in the case of no CFOs [71]. The self-ICI cancellation approach is performed in frequency-domain, where a set of codewords with low ICI is used to reduce the side-lobes of the output spectrum. Since the code rate is less than one, the spectrum efficiency is reduced [72]. The feedback-and-adjust schemes are described in [40, 36], which suggest that the BS performs only TO and CFO estimation, whereas adjustment of the synchronization parameters is made at the mobile station's side based on instruction transmitted on the base station's control channel. The feedback-and-adjust approach requires an established connection between BS and MS, which is not applicable for some scenarios, and additional signalling overhead, which reduces the system throughput. Also note that, in this approach, there is always a delay between the estimation and adjustment processes, during which the CFO estimation can be outdated (e.g. because of Doppler frequencies) [66].

On the other hand, the IC schemes aim at removing the unwanted ICI and recovering the ideal waveform: In [73, 50], a multiple CFOs estimation and compensation algorithm is introduced based on subspace method. This

scheme works only with interleaved subcarrier allocation. A linear multiuser detection scheme is proposed in [42], hereby referred to as Cao-Tureli-Yao-Honan (CTYH), which attempts to restore the orthogonality among users by applying a linear transformation to the FFT output. The interference due to CFOs is suppressed at the price of additional complexity [34]. In [66], a MUI cancellation scheme in frequency-domain is proposed, hence it is referred to as Frequency-Domain Multi-User Interference Cancellation (FD-MUIC) in this chapter. In this scheme, circular convolutions are employed after the FFT processing to correct the CFOs, and to calculate the MUI terms, which are then subtracted from the subcarrier of interest. This scheme suffers from the loss of subcarrier's power when the CFOs are large, and it is unable to completely remove the self-ICI, which occurs among subcarriers of the same user [66].

In this chapter, we propose simple but effective IC schemes to mitigate the effects of different CFOs coming from multiple users in the uplink of OFDMA systems. The proposed schemes consist of two stages: Prior to uplink transmission, MS performs a coarse synchronization to BS, using well-known single-user CFO estimation techniques, such as [47, 46], so that the CFO is within a tolerable range. In the second stage, novel signal processing techniques are employed at the BS's side to estimate and correct the residual CFOs, and to compensate for the ICI. The ICI compensation is performed in time-domain, thus our proposals are hereafter referred to as Time-Domain Multi-User Interference Cancellation (TD-MUIC) schemes. No further adjustment at MS's side is needed, thus, no additional signalling overhead is required. The maximum tolerable CFO can be as large as 25% of the subcarrier spacing, which is a significant improvement compared to the stringent requirement in IEEE 802.16a, which is 2% of the subcarrier spacing [74]. A loose CFO requirement means low-cost and simple terminals are allowed in the system. The scheme works with both block and interleaved subcarrier allocations, and does not require special processing block, except the basic and readily-available FFT. Analytical and numerical results show that the proposed schemes offer much better performance compared to the FD-MUIC scheme.

This chapter is organized as follows. The system model and conventional receiver structures for the OFDMA uplink are presented in section 5.3. Section 5.4 provides the proposed schemes, along with numerical evaluation assuming perfect CFO knowledge. Simulation results with a practical CFO estimation technique are reported in section 5.5, and finally conclusions are drawn in section 5.6.

5.3 The receiver structures in OFDMA up-link

Let's consider an OFDMA system using a FFT of size N. In this system, the uth user is given a set of subcarriers, denoted as Δ_u, which is independent from the other users, i.e. $\Delta_u \bigcap \Delta_{u'} = \emptyset$ for $u \neq u'$. The transmitted information of the uth user, after an inverse Fast Fourier Transform (IFFT) operation and cyclic prefix (CP) insertion, is given by:

$$\tilde{x}_u(t) = \frac{1}{N} \sum_{k \in \Delta_u} \tilde{X}_u[k] e^{j2\pi \frac{k}{T_o}(t-T_g)} \Xi_{T_s}(t) \tag{5.1}$$

where T_o is the OFDMA symbol duration without guard interval, T_g is the guard interval, and $\Xi_{T_s}(t)$ is the unity amplitude gate pulse of length $T_s = T_o + T_g$. $\tilde{X}_u[k]$ denotes the information symbol for the kth subcarrier of the uth user. We assume that the transmitted symbols on each subcarrier have zero mean and are uncorrelated, i.e. $E\{\tilde{X}_u[k]\} = 0$ and:

$$E\{\tilde{X}_u[k]\tilde{X}_{u'}[k']^*\} = \begin{cases} \sigma_{\tilde{X}_u}^2 & \text{for } u = u', k = k' \\ 0 & \text{otherwise} \end{cases} \tag{5.2}$$

Assume that the uth user experiences an independent TO, δt_u, and frequency-selective fading channel, which are constant during the observation period, the received signal from the uth user is:

$$\tilde{y}_u(t) = \sum_{l=0}^{L-1} \tilde{h}_{u,l} \tilde{x}_u(t - \delta t_u - \tau_{u,l}) \tag{5.3}$$

where $\tilde{h}_{u,l}$ and $\tau_{u,l}$ are the complex gain and time delay of the lth multipath component experienced by the uth user, respectively. In the OFDMA uplink, the received signal is the sum of the signal from multiple users, which can be expressed as:

$$\tilde{r}(t) = \sum_{u=0}^{U-1} \tilde{y}_u(t) e^{j2\pi \delta f_u t} + \tilde{v}(t) \tag{5.4}$$

where δf_u is the CFO of the uth user and $\tilde{v}(t)$ is the complex baseband Additive White Gaussian Noise (AWGN) at the input of the OFDMA receiver.

At the receiver, the received signal is sampled at rate $1/\Delta t$ and the CP is removed to form the received vector $\vec{r} = [\tilde{r}[0], \tilde{r}[1], \dots \tilde{r}[N-1]]^T$, where $\tilde{r}[n] = \tilde{r}(n\Delta t)$. We assume that the CP is long enough to accommodate both the maximum TO and the channel delay spread, and thus there is no influence from the adjacent transmitted OFDM symbols.

5.3.1 Single-FFT receiver

In conventional single-FFT receiver, one FFT block is used to demodulate all users at the same time. The output of the single-FFT corresponding to the uth user can be written in matricial form as follows [42, 66]:

$$
\begin{aligned}
\vec{\mathbf{Z}}_u &= \mathbf{A}_u \mathbf{F}_N \vec{\mathbf{r}} \\
&= \mathbf{A}_u \bigg(\mathbf{C}^p_{(\epsilon f_u)} \vec{\mathbf{Y}}_u + \mathbf{C}^s_{(\epsilon f_u)} \vec{\mathbf{Y}}_u \\
&\quad + \sum_{u_1=0; u_1 \neq u}^{U-1} \mathbf{C}_{(\epsilon f_{u_1})} \vec{\mathbf{Y}}_{u_1} + \vec{\mathbf{V}} \bigg)
\end{aligned}
\tag{5.5}
$$

in which $\mathbf{F}_N$ stands for the size-N FFT matrix with entries $\mathbf{F}_N[n,k] = e^{-j2\pi nk/N}/\sqrt{N}$; $\vec{\mathbf{Z}}_u = \left[\tilde{Z}_u[0], \tilde{Z}_u[1], \dots \tilde{Z}_u[N-1] \right]^T$ and $\vec{\mathbf{V}} = \left[\tilde{V}[0], \tilde{V}[1], \dots \tilde{V}[N-1] \right]^T$, where $Z_u[k]$ and $V[k]$ are the uth user's observed information and the AWGN contribution at the kth subcarriers, respectively. The vector of the received signal from the uth user without the effects of CFO is denoted as $\vec{\mathbf{Y}}_u = \mathbf{H}_u \vec{\mathbf{X}}_u = \left[\tilde{Y}_u[0], \tilde{Y}_u[1], \dots \tilde{Y}_u[N-1] \right]^T$. $\mathbf{H}_u$ is diagonal matrix of size N, whose the kth non-zero diagonal entry, $\tilde{H}_u[k,k] = e^{-j2\pi \frac{k}{N} \epsilon t_u} \sum_{l=0}^{L-1} \tilde{h}_{u,l} e^{-j2\pi \frac{k}{T_o} \tau_{u,l}}$ for all $k \in \Delta_u$, is the CTF at the kth subcarrier of the uth user. $\vec{\mathbf{X}}_u = \left[\tilde{X}_u[0], \tilde{X}_u[1], \dots \tilde{X}_u[N-1] \right]^T$ is the uth user's transmitted symbol vector. $\epsilon t_u = \delta t_u / \Delta t$ and $\epsilon f_u = \delta f_u / \Delta f$ are the normalized TO and CFO of the uth user. $\mathbf{A}_u$ is a diagonal matrix of size N, acting as a filter to select only subcarriers belonging to the uth user, i.e. $\mathbf{A}_u(k,k) = 1$ for $k \in \Delta_u$, and all other diagonal elements are zero.

The $N \times N$ matrix $\mathbf{C}_{(\phi)}$ represents the shift due to the normalized CFO ϕ in frequency-domain. It is a circulant matrix respresenting the circular convolution operation:

$$
\begin{aligned}
\mathbf{C}_{(\phi)} &= \mathbf{F}_N \mathbf{c}_{(\phi)} \mathbf{F}_N^H \\
&= \begin{bmatrix}
\tilde{\mathcal{C}}(\phi) & \tilde{\mathcal{C}}(1+\phi) & \dots & \tilde{\mathcal{C}}(N-1+\phi) \\
\tilde{\mathcal{C}}(N-1+\phi) & \tilde{\mathcal{C}}(\phi) & \dots & \tilde{\mathcal{C}}(N-2+\phi) \\
\vdots & \vdots & \ddots & \vdots \\
\tilde{\mathcal{C}}(1+\phi) & \tilde{\mathcal{C}}(2+\phi) & \dots & \tilde{\mathcal{C}}(\phi)
\end{bmatrix}
\end{aligned}
\tag{5.6}
$$

where $\tilde{\mathcal{C}}(\phi) = \frac{\sin \pi\phi}{N \sin \pi\phi/N} e^{j\pi\phi(N-1)/N}$ is the periodic sinc-function [37], $[.]^H$ in the superscript denotes the Hermitian transpose operation, and $\mathbf{c}_{(\phi)}$ is a

diagonal matrix of size N representing the CFO in time-domain, whose the nth diagonal element is equal to $e^{j2\pi\frac{n}{N}\phi}$. The size N diagonal matrix $\mathbf{C}^p_{(\phi)}$ takes the principal diagonal entries of $\mathbf{C}_{(\phi)}$, while $\mathbf{C}^s_{(\phi)} = \mathbf{C}_{(\phi)} - \mathbf{C}^p_{(\phi)}$.

In the uplink of an OFDMA system with non-zero CFOs, the first term in (5.5) indicates an attenuation of the received signal, since $|\tilde{\mathcal{C}}(\epsilon f_u)|$ is always less than one if ϵf_u is non-zero. The second term represents the ICI among subcarriers of the same user, which is referred to as self-interference. And the third term is the cross-interference, which is the ICI among active users operating in the uplink. It is important to note that the conventional single-FFT receiver is not effective in multiple CFOs scenario, as it can be aligned to only one user at a given time, and the rest are mis-aligned [40].

5.3.2 The FD-MUIC receiver

In [65], the Choi-Lee-Jung-Lee (CLJL) scheme is proposed as an extension to the single-FFT receiver, which allows CFO correction after the FFT using circular convolution. The output of the CLJL demodulator can be expressed as:

$$
\begin{aligned}
\vec{\mathbf{Z}}^{\text{CLJL}}_u &= \mathbf{A}_u \mathbf{C}_{(-\epsilon f_u)} \vec{\mathbf{Z}}_u \\
&= \mathbf{A}_u \bigg(\mathbf{C}_{(-\epsilon f_u)} \mathbf{A}_u \mathbf{C}_{(\epsilon f_u)} \vec{\mathbf{Y}}_u \\
&\quad + \sum_{u_1=0; u_1 \neq u}^{U-1} \mathbf{C}_{(-\epsilon f_u)} \mathbf{A}_u \mathbf{C}_{(\epsilon f_{u_1})} \vec{\mathbf{Y}}_{u_1} + \mathbf{C}_{(-\epsilon f_u)} \mathbf{A}_u \vec{\mathbf{V}} \bigg)
\end{aligned} \tag{5.7}
$$

where $\mathbf{C}_{(-\epsilon f_u)}$ represents the frequency-domain CFO correction by $-\epsilon f_u$. In [66], the Carrier to Interference-plus-Noise Ratio (CINR)) analysis for CLJL scheme is given as follows:

$$
\text{CINR}^{\text{CLJL}}_{u,k} = \frac{\sigma^2_{\tilde{H}_u} \sigma^2_{\tilde{X}_u} \left| \sum_{k_1 \in \Delta_u} \tilde{\mathcal{C}}^2(k_1 - k - \epsilon f_u) \right|^2}{\sigma^2_{I^{\text{CLJL}}_{u,\text{self}}[k]} + \sigma^2_{I^{\text{CLJL}}_{u,\text{cross}}[k]} + N_o} \tag{5.8}
$$

$$
\sigma^2_{I^{\text{CLJL}}_{u,\text{self}}[k]} = \sigma^2_{\tilde{H}_u} \sigma^2_{\tilde{X}_u} \times
$$

$$
\sum_{k_2 \in \Delta_u; k_2 \neq k} \left| \sum_{k_1 \in \Delta_u} \tilde{\mathcal{C}}(k_2 - k_1 + \epsilon f_u) \tilde{\mathcal{C}}(k_1 - k - \epsilon f_u) \right|^2 \tag{5.9}
$$

$$\sigma^2_{I^{\text{CLJL}}_{u,\text{cross}}[k]} = \sum_{u_1=0;u_1\neq u}^{U-1} \sigma^2_{\tilde{H}_{u_1}} \sigma^2_{\tilde{X}_{u_1}} \times$$

$$\sum_{k_2\in\Delta_{u_1}} \left| \sum_{k_1\in\Delta_u} \tilde{\mathcal{C}}(k_2 - k_1 + \epsilon f_{u_1})\tilde{\mathcal{C}}(k_1 - k - \epsilon f_u) \right|^2 \qquad (5.10)$$

where $\sigma^2_{\tilde{H}_u} = E[|\tilde{H}_u|^2]$ is the average gain of the uth user's channel, and $N_o/2$ is the power spectral density of the AWGN. (5.8) shows that, when the CFO is large, the CLJL scheme suffers from attenuation of the signal of interest, due to the fact that signal power does not concentrate in the prescribed subcarrier positions [66]. In addition, there exists residual self- and cross-interference terms, which cause the degradation of the system performance. The FD-MUIC scheme proposed in [66] is a Parallel Interference Cancellation (PIC) scheme, which aims at removing the cross-interference. The output of the FD-MUIC demodulator at the ith iteration is given by:

$$\vec{Z}^{\text{FD}-\text{MUIC}}_{u,i} = \vec{Z}^{\text{CLJL}}_u - \sum_{u_1=0;u_1\neq u}^{U-1} \mathbf{A}_u \mathbf{C}_{(-\epsilon f_u)} \mathbf{A}_u \mathbf{C}_{(\epsilon f_{u_1})} \vec{Z}^{\text{FD}-\text{MUIC}}_{u_1,i-1}$$

$$= \mathbf{A}_u \Bigg[\mathbf{C}_{(-\epsilon f_u)} \mathbf{A}_u \mathbf{C}_{(\epsilon f_u)} \vec{Y}_u$$

$$+ \sum_{u_1=0;u_1\neq u}^{U-1} \mathbf{C}_{(-\epsilon f_u)} \mathbf{A}_u \mathbf{C}_{(\epsilon f_{u_1})} (\vec{Y}_{u_1} - \vec{Z}^{\text{FD}-\text{MUIC}}_{u_1,i-1})$$

$$+ \mathbf{C}_{(-\epsilon f_u)} \mathbf{A}_u \vec{V} \Bigg] \qquad (5.11)$$

and $\vec{Z}^{\text{FD}-\text{MUIC}}_{u,0} = \vec{Z}^{\text{CLJL}}_u$. Since the CINR analysis for FD-MUIC scheme in [66] does not account for the fact that the signal of interest is attenuated with non-zero CFO, hence a closer approximation of CINR is introduced here:

$$\text{CINR}^{\text{FD}-\text{MUIC}}_{u,k,i} = \frac{\sigma^2_{\tilde{H}_u} \sigma^2_{\tilde{X}_u} \left| \sum_{k_1\in\Delta_u} \tilde{\mathcal{C}}^2(k_1 - k - \epsilon f_u) \right|^2}{\sigma^2_{I^{\text{CLJL}}_{u,\text{self}}[k]} + \sigma^2_{I^{\text{FD}-\text{MUIC}}_{u,\text{cross},i}[k]} + N_o} \qquad (5.12)$$

$$
\begin{aligned}
\sigma^2_{I^{\mathrm{FD-MUIC}}_{u,\mathrm{cross},i}[k]} \approx & \sum_{u_1=0;u_1\neq u}^{U-1} \sum_{k_2\in\Delta_{u_1}} \left[\sigma^2_{\tilde{H}_{u_1}} \sigma^2_{\tilde{X}_{u_1}} \left(1 - \left| \sum_{k_3\in\Delta_{u_1}} \tilde{\mathcal{C}}^2(k_3 - k_2 - \epsilon f_{u_1}) \right| \right)^2 \right. \\
& \left. + \sigma^2_{I^{\mathrm{CLJL}}_{u_1,\mathrm{self}}[k_2]} + \sigma^2_{I^{\mathrm{FD-MUIC}}_{u_1,\mathrm{cross},i-1}[k_2]} + N_o \right] \left| \sum_{k_1\in\Delta_u} \tilde{\mathcal{C}}(k_2 - k_1 + \epsilon f_{u_1})\tilde{\mathcal{C}}(k_1 - k - \epsilon f_u) \right|^2 \\
& \text{for } i >= 1 \quad\quad\quad\quad\quad\quad\quad\quad\quad\quad\quad\quad\quad\quad\quad (5.13)
\end{aligned}
$$

where $\sigma^2_{I^{\mathrm{FD-MUIC}}_{u,\mathrm{cross},0}[k]} = \sigma^2_{I^{\mathrm{CLJL}}_{u,\mathrm{cross}}[k]}$.

To provide comparable results with [66], we consider the same OFDMA uplink system, where the number of user is $U = 4$. Each user is allocated 16 subcarriers ($N = 64$), and the CFOs are $\epsilon f_1 = 0.10$, $\epsilon f_2 = -0.10$, $\epsilon f_3 = -0.05$ and $\epsilon f_4 = 0.05$, respectively. Two subcarrier allocation schemes are considered: Block- and interleaved-allocation. In block allocation, the spectrum is uniformly divided into U blocks, where each user is assigned one block. In interleaved allocation, the subcarriers are uniformly interleaved across all the users. The CNR is 40dB, and we assume perfect CFO knowledge at the receiver. In Fig. 5.1, the average CINR performance of the FD-MUIC scheme is plotted against the number of iterations. The average CINR is computed by averaging the CINR at all subcarrier from all users. Two methods of CINR analysis are compared to simulation results: Huang-Letaief (HL) refers to the analysis provided in [66], while Nguyen-Carvalho-Prasad (NCP) refers to equation (5.12). Both methods are named after their authors. It can be seen that our method provides much closer approximation, since the power loss due to filtering process has been taken into account. It is also worthy to note that, in FD-MUIC scheme, the interleaved allocation outperforms the block after few iterations. This is due to the fact that self-interference term, which cannot be removed by FD-MUIC scheme, is smaller in the case of interleave allocation, compared to the block case.

5.3.3   CTYH receiver

The CTYH receiver is based on a single-FFT receiver, which aims at reconstructing the orthogonality among users in frequency-domain [42]. This goal is obtained by means of a linear transformation applied to:

$$
\vec{\mathbf{Z}} = \sum_{u=0}^{U-1} \vec{\mathbf{Z}}_u = \mathbf{\Pi}\mathbf{H}\vec{\mathbf{X}} + \vec{\mathbf{V}} \quad\quad\quad (5.14)
$$

where $\vec{\mathbf{Z}}_u$ is defined in (5.5), $\mathbf{\Pi} = \sum_{u=0}^{U-1} \mathbf{C}_{(\epsilon f_u)}\mathbf{A}_u$ is the $N \times N$ interference matrix, $\mathbf{H} = \sum_{u=0}^{U-1} \mathbf{H}_u$ is CTF matrix and $\vec{\mathbf{X}} = \sum_{u=0}^{U-1} \vec{\mathbf{X}}_u$ is the transmitted
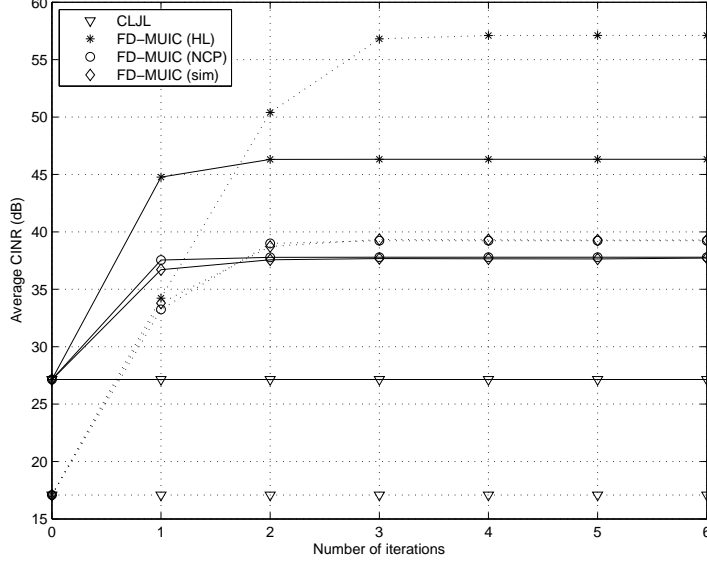
Figure 5.1: Average CINR performance of the FD-MUIC scheme. Solid line indicates block allocation, and dotted line represents interleaved allocation.

symbol vector. The linear unbiased Minimum Mean Square Error (MMSE) estimator [75] is chosen for performance comparison in section 5.4.1. The output CINR of the linear unbiased MMSE estimator at the kth subcarrier is given by [75, 76]:

$$\text{CINR}_{MMSE,k}^{\text{CTYH}} = \frac{\sigma_X^2}{\left[(\mathbf{H}^H \mathbf{\Pi}^H \mathbf{\Pi} \mathbf{H} + \frac{N_o}{\sigma_X^2} \mathbf{I})^{-1} N_o\right]_{kk}} - 1 \qquad (5.15)$$

where all users transmit with equal power (i.e. $\sigma_{X_u}^2 = \sigma_X^2$ for all u) and $[.]_{kk}$ denotes the kth diagonal element. It is worth noting that the CTYH receiver cannot achieve CFO-free performance, because it is based on a linear transformation technique.

5.3.4   Multi-FFT receiver

In multi-FFT receiver structure, each active user is assigned one OFDM-demodulator block, so that their CFOs can be compensated for independently in the time-domain. After CFO compensation, the output of the OFDM

demodulator belonging to the uth user can be expressed as [62]:

$$\vec{\mathbf{Z}}_u^{\text{mFFT}} = \mathbf{A}_u \mathbf{F}_N \mathbf{c}_{(-\epsilon f_u)} \vec{\mathbf{r}}$$

$$= \mathbf{A}_u \left(\vec{\mathbf{Y}}_u + \sum_{u_1=0; u_1 \neq u}^{U-1} \mathbf{C}_{(\epsilon f_{u_1-u}^{\text{mFFT}})} \vec{\mathbf{Y}}_{u_1} + \mathbf{C}_{(-\epsilon f_u)} \vec{\mathbf{V}} \right) \qquad (5.16)$$

where $\mathbf{c}_{(-\epsilon f_u)}$ represents the time-domain CFO correction by $-\epsilon f_u$, and $[.]^{\text{mFFT}}$ in superscript refers to the fact that multiple FFT blocks are employed. $\epsilon f_{u_1-u}^{\text{mFFT}} = \epsilon f_{u_1} - \epsilon f_u$ denotes the relative CFO between the uth and u_1^{th} user. (5.5) and (5.16) show that, by using the multi-FFT receiver, the attenuation factor and the self-interference have disappeared for the desired u^{th} user, provided that its CFO, ϵf_u, is estimated correctly. However, the cross-interference term is still present, and can sometimes become larger due to the fact that the new CFO, $\epsilon f_{u_1-u}^{\text{mFFT}}$, might be larger than the original one, ϵf_{u_1}. This tends to cause significant performance degradation [65], and the aim of the this chapter is to further remove such interference to achieve the CFO-free performance.

5.4   Our proposals

(5.16) indicates that the cross-interference term is a deterministic function, which depends on the transmitted data symbols, the channel frequency responses, the TOs and CFOs of all other active users in the OFDMA system. In the case of cellular's uplink, these parameters are estimated by, and therefore, available to the BS, which inspires the idea of applying the principle of multiuser interference cancellation. In this section, two MUI receiver structures are proposed for the OFDMA uplink, namely Simple Time-Domain Multi-User Interference Cancellation Scheme (SI-MUIC) and Code-Aided Time-Domain Multi-User Interference Cancellation Scheme (CA-MUIC) schemes. They are both based on the multi-FFT receiver, as illustrated in Fig. 5.2, 5.3 and 5.4, and their algorithms are explained as follows:

5.4.1   The SI-MUIC scheme

Assume that users are sorted in order of their Received Signal Strength (RSS), and the BS processes from the user with the strongest received power to the one with lowest power, thus increases the chance of correct estimation and decoding. The iterative Successive Interference Cancellation (SIC) implementation of SI-MUIC scheme can be shown as following:
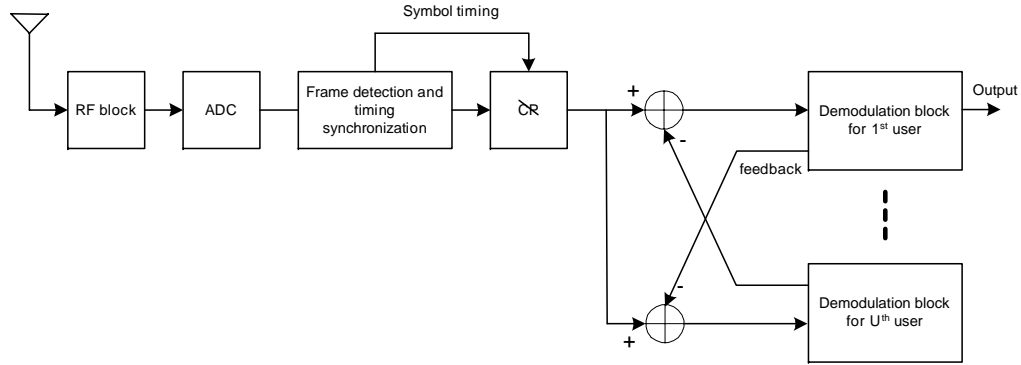   **SI-MUIC's SIC Algorithm**

Figure 5.2: General receiver structure for the Time-domain multi-user interference cancellation schemes
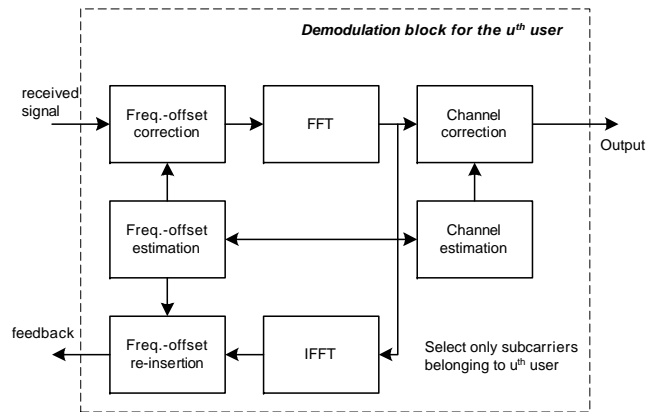

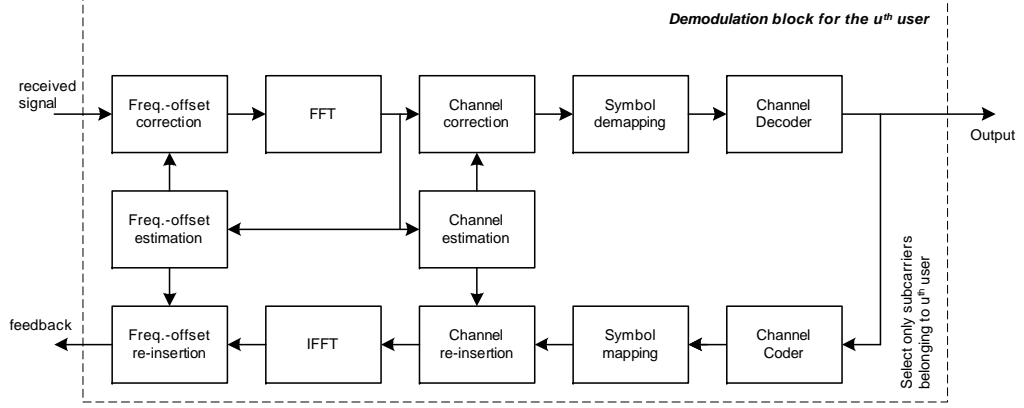Figure 5.3: Demodulation block for SI-MUIC scheme

Figure 5.4: Demodulation block for CA-MUIC scheme

Initialization: Set $i = 0$

$$\hat{\mathbf{r}}_{u,i}^{\text{SI}-\text{MUIC}} = 0 \text{ for } u = 0, 1, \ldots U - 1 \tag{5.17}$$

Loop A: $i = i + 1$ and $u = 0$
   Loop B:

$$\vec{\mathbf{Z}}_{u,i}^{\text{SI}-\text{MUIC}} = \mathbf{A}_u \mathbf{F}_N \mathbf{c}_{(\epsilon f_u)} \times$$
$$\left(\vec{\mathbf{r}} - \sum_{u_1=0}^{u-1} \hat{\mathbf{r}}_{u_1,i}^{\text{SI}-\text{MUIC}} - \sum_{u_2=u+1}^{U-1} \hat{\mathbf{r}}_{u_2,i-1}^{\text{SI}-\text{MUIC}} \right) \tag{5.18}$$

$$\hat{\mathbf{r}}_{u,i}^{\text{SI}-\text{MUIC}} = \mathbf{c}_{(-\epsilon f_u)} \mathbf{F}_N^H \vec{\mathbf{Z}}_{u,i}^{\text{SI}-\text{MUIC}} \tag{5.19}$$

   $u = u + 1$
   Go to Loop B until $u > U - 1$
   Go to Loop A until $i > N_{loop}$
   In the algorithm, $\hat{\mathbf{r}}_{u,i}^{\text{SI}-\text{MUIC}}$ denotes the feedback signal from the uth user at the ith step. The demodulation and calculation of the feedback signal in the SI-MUIC scheme is illustrated in Fig 5.3. (5.18) can be re-written as:

$$\vec{\mathbf{Z}}_{u,i}^{\text{SI}-\text{MUIC}} = \mathbf{A}_u \bigg(\vec{\mathbf{Y}}_u + \sum_{u_1=0}^{u-1} \mathbf{C}_{(\epsilon f_{u_1-u}^{\text{mFFT}})} \vec{\mathbf{I}}_{u_1,i}^{\text{SI}-\text{MUIC}}$$
$$+ \sum_{u_2=u+1}^{U-1} \mathbf{C}_{(\epsilon f_{u_2-u}^{\text{mFFT}})} \vec{\mathbf{I}}_{u_2,i-1}^{\text{SI}-\text{MUIC}} + \mathbf{C}_{(-\epsilon f_u)} \vec{\mathbf{V}} \bigg) \tag{5.20}$$
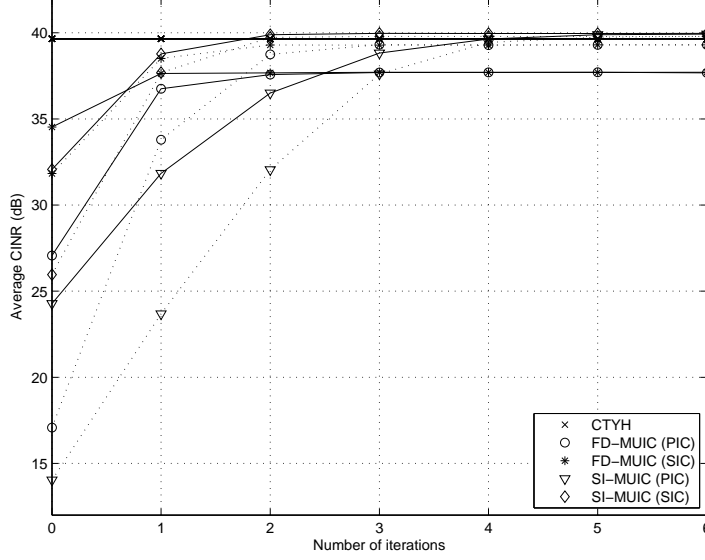
Figure 5.5: Average CINR performance of the PIC and SIC implementations of the FD-MUIC and SI-MUIC schemes. Solid line indicates block allocation, and dotted line represents interleaved allocation.

$$
\vec{\mathbf{I}}_{u,i}^{\mathrm{SI-MUIC}} = \begin{cases} \vec{\mathbf{Y}}_u & i = 0 \\ \vec{\mathbf{Y}}_u - \mathbf{A}_u \vec{\mathbf{Z}}_{u,i}^{\mathrm{SI-MUIC}} & i > 0 \end{cases} \tag{5.21}
$$

where $\vec{\mathbf{I}}_{u,i}^{\mathrm{SI-MUIC}}$ is the residual estimation error after the ith iteration. (5.16) and (5.20) are identical, except that, for $i > 0$, the received signal $\vec{\mathbf{Y}}_{u_1}$ has been replaced by the estimation error, $\vec{\mathbf{I}}_{u_1,i}^{\mathrm{SI-MUIC}}$ or $\vec{\mathbf{I}}_{u_2,i-1}^{\mathrm{SI-MUIC}}$. This indicates the gain from using the SI-MUIC scheme: The cross-interference term shall be reduced, provided that the estimation error for the uth user is small, or $\mathbf{A}_u \vec{\mathbf{Z}}_{u,i}^{\mathrm{SI-MUIC}}$ is a good estimate of $\vec{\mathbf{Y}}_u$. We observe that the estimation error at the ith iteration is the sum of the other users' estimation errors from current or previous iteration, attenuated by a periodic sinc function, $\mathbf{C}_{(\epsilon f_{u_1-u}^{\mathrm{mFFT}})}$ or $\mathbf{C}_{(\epsilon f_{u_2-u}^{\mathrm{mFFT}})}$, respectively. In general, thanks to this attenuation, the estimation error is reduced with the increased number of iterations, which is shown afterwards by numerical evaluation.

Fig. 5.5 illustrates the convergence property of the SIC implementation of the SI-MUIC scheme, under the same OFDMA system's setting as in section 5.3.2, where $U = 4$, $N = 64$ and the CFOs are fixed. The PIC implementation of the SI-MUIC, which is similar to the one described in [66] and section 5.3.2, is also included for comparison. The output of the OFDMA demodulator in case of PIC implementation for the uth user at the ith iteration

is given by:

$$\vec{\mathbf{Z}}_{u,i}^{\text{SI-MUIC,PIC}} = \mathbf{A}_u \Bigg(\vec{\mathbf{Y}}_u + \sum_{u_1=0;u_1\neq u}^{U-1} \mathbf{C}_{(\epsilon f_{u_1-u}^{\text{mFFT}})} \vec{\mathbf{I}}_{u_1,i-1}^{\text{SI-MUIC,PIC}}$$

$$+ \mathbf{C}_{(-\epsilon f_u)} \vec{\mathbf{V}} \Bigg) \tag{5.22}$$

$$\vec{\mathbf{I}}_{u,i}^{\text{SI-MUIC,PIC}} = \begin{cases} \vec{\mathbf{Y}}_u & i = 0 \\ \vec{\mathbf{Y}}_u - \mathbf{A}_u \vec{\mathbf{Z}}_{u,i}^{\text{SI-MUIC,PIC}} & i > 0 \end{cases} \tag{5.23}$$

Firstly, Fig. 5.5 shows that the performance of the SIC implementation is always superior than those of the PIC, for both FD-MUIC and SI-MUIC, even at the iteration $i = 0$. This can be explained by looking at (5.20) and (5.22): PIC only utilizes the estimations from the previous iteration, whereas in SIC the estimation of the uth user is done based on current estimates $\mathbf{A}_{u_1} \vec{\mathbf{Z}}_{u_1,i}^{\text{SI-MUIC}}$ of the u_1^{th} users ($u_1 < u$). Since these new estimates are with less interference, the performance of SIC is always superior compared to PIC. Nevertheless, the SIC is penalized with a longer delay than PIC, since the last user can only be processed when all the others have been demodulated. Secondly, as more iterations are performed, the FD-MUIC schemes quickly come to an irreducible noise floor, due to the fact that the power loss and the self-interference term remain unchanged, compared to the CLJL scheme. The SI-MUIC scheme does not have such an irreducible noise floor. The CFO-free performance can be achieved after 4 iterations. The performance of the CTYH scheme is also plotted in Fig. 5.5 for comparison.

It is worth noting that the SI-MUIC scheme does not require the Channel State Information (CSI), all it needs to know is the CFO value of each user. The residual noise and interference term in SI-MUIC can be further removed, which is the aim of the CA-MUIC explained in the next section.

5.4.2 The CA-MUIC scheme

The main different between CA-MUIC and SI-MUIC scheme is that, instead of the output of the OFDMA demodulator $\vec{\mathbf{Z}}_{u,i}^{\text{SI-MUIC}}$, the estimation $\hat{\mathbf{Y}}_{u,i}$ is used to calculate the feedback.

CA-MUIC's SIC Algorithm

Initialization: Set $i = 0$

$$\hat{\mathbf{r}}_{u,i}^{\text{CA-MUIC}} = 0 \text{ for } u = 0, 1, \ldots U - 1 \tag{5.24}$$

Loop A: $i = i + 1$ *and* $u = 0$
  Loop B:

$$\vec{\mathbf{Z}}_{u,i}^{\text{CA}-\text{MUIC}} = \mathbf{A}_u \mathbf{F}_N \mathbf{c}_{(\epsilon f_u)} \times$$
$$\left(\vec{\mathbf{r}} - \sum_{u_1=0}^{u-1} \hat{\mathbf{r}}_{u_1,i}^{\text{CA}-\text{MUIC}} - \sum_{u_2=u+1}^{U-1} \hat{\mathbf{r}}_{u_2,i-1}^{\text{CA}-\text{MUIC}} \right) \qquad (5.25)$$

Estimate $\hat{\mathbf{Y}}_{u,i}$ from $\vec{\mathbf{Z}}_{u,i}^{\text{CA}-\text{MUIC}}$, and calculate the feedback:

$$\hat{\mathbf{r}}_{u,i}^{\text{CA}-\text{MUIC}} = \mathbf{c}_{(-\epsilon f_u)} \mathbf{F}_N^H \hat{\mathbf{Y}}_{u,i} \qquad (5.26)$$

$u = u + 1$
  Go to Loop B until $u > U - 1$
  Go to Loop A until $i > N_{loop}$
Fig 5.4 shows the demodulation block for CA-MUIC scheme. Similar to the SI-MUIC scheme, (5.25) can be re-written as:

$$\vec{\mathbf{Z}}_{u,i}^{\text{CA}-\text{MUIC}} = \mathbf{A}_u \left(\vec{\mathbf{Y}}_u + \sum_{u_1=0}^{u-1} \mathbf{C}_{(\epsilon f_{u_1-u}^{\text{mFFT}})} \vec{\mathbf{I}}_{u_1,i}^{\text{CA}-\text{MUIC}} \right.$$
$$\left. + \sum_{u_2=u+1}^{U-1} \mathbf{C}_{(\epsilon f_{u_2-u}^{\text{mFFT}})} \vec{\mathbf{I}}_{u_2,i-1}^{\text{CA}-\text{MUIC}} + \mathbf{C}_{(-\epsilon f_u)} \vec{\mathbf{V}} \right) \qquad (5.27)$$

$$\vec{\mathbf{I}}_{u,i}^{\text{CA}-\text{MUIC}} = \begin{cases} \vec{\mathbf{Y}}_u & i = 0 \\ \vec{\mathbf{Y}}_u - \mathbf{A}_u \hat{\mathbf{Y}}_{u,i} & i > 0 \end{cases} \qquad (5.28)$$

And the output of the CA-MUIC demodulator in case of the PIC implementation is given by:

$$\vec{\mathbf{Z}}_{u,i}^{\text{CA}-\text{MUIC,PIC}} = \mathbf{A}_u \left(\vec{\mathbf{Y}}_u + \sum_{u_1=0; u_1 \neq u}^{U-1} \mathbf{C}_{(\epsilon f_{u_1-u}^{\text{mFFT}})} \vec{\mathbf{I}}_{u_1,i-1}^{\text{CA}-\text{MUIC,PIC}} \right.$$
$$\left. + \mathbf{C}_{(-\epsilon f_u)} \vec{\mathbf{V}} \right) \qquad (5.29)$$

$$\vec{\mathbf{I}}_{u,i}^{\text{CA}-\text{MUIC,PIC}} = \begin{cases} \vec{\mathbf{Y}}_u & i = 0 \\ \vec{\mathbf{Y}}_u - \mathbf{A}_u \hat{\mathbf{Y}}_{u,i}^{\text{PIC}} & i > 0 \end{cases} \qquad (5.30)$$

where $\hat{\mathbf{Y}}_{u,i}^{\text{PIC}}$ is estimated from $\vec{\mathbf{Z}}_{u,i}^{\text{CA}-\text{MUIC,PIC}}$. It is important to note that the task of estimating $\hat{\mathbf{Y}}_{u,i}$ and $\hat{\mathbf{Y}}_{u,i}^{\text{PIC}}$ in the CA-MUIC algorithm is actually

boiled down to estimating the CTF, $\hat{H}_{u,i}[k]$, and the transmitted data symbol, $\hat{X}_{u,i}[k]$, for the uth user. If such estimations are correct, the second term in (5.27) will go to zero, leaving no cross-interference at the output of the uth user's OFDMA demodulator. In order to achieve correct estimation of the data symbols, channel coding is applied in the CA-MUIC scheme, hence it is referred to as code-aided TD-MUIC scheme.

5.4.3 Computational complexity

The SI-MUIC scheme requires two FFT operations for each user in each iteration, one for demodulation and another for regenerating the corresponding time-domain signal. Therefore, the computation complexity of the SI-MUIC scheme is $\text{O}(2UN_{loop}N\log_2 N)$, where $\text{O}(.)$ and N_{loop} denote the order of complexity and number of iterations, respectively. Note that the SIC and PIC implementations are equivalent on complexity, as they require the same number of FFT operations per user per loop. The complexity of CA-MUIC scheme is larger than SI-MUIC, as decoding/coding, symbol demapping/mapping and channel insertion are involved. CA-MUIC's complexity is not accounted for in this work, as it is considered only as an enhancement to SI-MUIC.

The FD-MUIC needs only one FFT operation at the beginning, but it requires U circular convolutions for each user in each iteration. The complexity of circular convolution can be reduced by considering only $P-1$ out of $N-1$ most dominant interfering subcarriers, at the cost of performance degradation [66]. The computation complexity of the FD-MUIC scheme in that case is $\text{O}(UN_{loop}NP)$ [34], without considering the complexity of constructing the CFO correction matrices $\mathbf{C}_{(-\epsilon f_u)}$. Constructing CFO correction matrices requires computation of periodic sinc-function $\tilde{\mathcal{C}}(\phi)$, which can be costly and subjected to fixed-point precision problem. The CTYH scheme does not depend on the number of users and the number of iterations, but in principle it cost $\text{O}(N^3)$ due to matrix inversion [34]. The complexity of the CTYH scheme can also be reduced by considering only $P-1$ most dominant interfering subcarriers, but the trade-off is performance degradation. Table 5.1 shows the number of arithmetic operations required for SI-MUIC, FD-MUIC and CTYH for different number of FFT size, where $U = 10$ and $N_{loop} = 5$. The complexity of the SI-MUIC is comparable to that of the FD-MUIC with $P = 25$, while its performance exceeds that of the FD-MUIC with $P = N$.

Table 5.1: Number of arithmetic operations (in thousand)

Scheme	N=1024	N=2048	N=4096
SI-MUIC	1.024	2.253	4.915
FD-MUIC (P=5)	256	512	1.024
FD-MUIC (P=15)	768	1.536	3.072
FD-MUIC (P=25)	1.028	2.560	5.120
FD-MUIC (P=N)	52.429	209.715	838.861
CTYH	1.073.742	8.589.935	68.719.477

5.5 Numerical Evaluation

5.5.1 CFO estimation

In the previous section, the performance of the proposed schemes has been analyzed under assumption of perfect CFO knowledge. In this section, we demonstrate the feasibility of the proposed schemes by using a realistic CFO estimation technique.

To assist CFO estimation during data transmission, pilot subcarriers are inserted repeatedly in the first two OFDMA symbols by all active users. Let Δ_u^p denote the indexes of pilot subcarriers for the uth user, and $Z_{u,1} = \{z_{u,1,p}, p \in \Delta_u^p\}$ and $Z_{u,2} = \{z_{u,2,p}, p \in \Delta_u^p\}$ are the sets of pilot subcarriers transmitted at the first and the second symbol, respectively. The maximum likelihood (ML) estimate of the CFO $\hat{\epsilon f}_u$, given the observations $Z_{u,1}$ and $Z_{u,2}$, is the value of $\hat{\epsilon f}_u$ that maximizes the conditional joint density function of the observations:

$$\hat{\epsilon f}_u = \max_{\hat{\epsilon f}_u}[f(Z_{u,1}, Z_{u,2}|\hat{\epsilon f}_u)] \tag{5.31}$$

The result of this estimate is given by [46]

$$\hat{\epsilon f}_u = \frac{1}{2\pi} \tan^{-1} \frac{\sum_{p \in \Delta_u^p} \text{Im}(z_{u,2,p} z_{u,1,p}^*)}{\sum_{p \in \Delta_u^p} \text{Re}(z_{u,2,p} z_{u,1,p}^*)} \tag{5.32}$$

where $\tan^{-1}$ is the arctangent function, and $\text{Im}(.)$ and $\text{Re}(.)$ are imaginary and real part of the complex value, respectively. The limit of this estimator is half of the subcarrier spacing. Therefore, prior to uplink data transmission, a coarse frequency synchronization must be performed, for example using estimation techniques described in [47, 46] or via the initial or periodic ranging procedures stated in IEEE 802.16 standard [74], to bring the CFO down to tolerable value.

Table 5.2: System parameters

Parameter	Value
System bandwidth	40MHz
Number of subcarriers	1024
CP length	400 samples
Subcarrier allocation scheme	Block and Interleaved
Modulation	QPSK
Channel coding/decoding	1/2 convolution code with Viterbi decoder [77]
Channel model	7-tap exponential decay Rayleigh fading channel [43]
Channel rms delay spread	1us
CNR	40dB
Number of users	5
Number of subcarriers per user	200
Number of iterations (N_{loop})	5

5.5.2 Simulation results

Unless otherwise stated, the basic simulation parameters are taken from Table 5.2. Thanks to a coarse synchronization stage, the TOs of all users are well within the CP and the CFOs are less than the maximum torelable value of the system, ϵf_{max}. We assume the received powers of all active users are equal and the CTF is perfectly estimated. Note that the CTF information is only required for CA-MUIC, not SI-MUIC. There are 5 users in the system, and at each transmission they experiences a CFO between $[-\epsilon f_{max}, +\epsilon f_{max}]$. Both block and interleaved subcarrier allocation schemes are used for evaluation, and there is no guardband between users in frequency domain. Only SIC implementation is evaluated for the sake of simplicity.

Fig. 5.6 shows the uncoded bit error rate (BER) performance of the proposed schemes with different maximum CFO values. While the performance of the single-FFT receiver drops dramatically with the increase of the maximum CFO value, both the SI-MUIC and CA-MUIC schemes can tolerate up to 10% of subcarrier spacing with little degradation. Especially in block allocation setting, the CA-MUIC scheme can achieve offset-free performance with up to 40% of subcarrier spacing.

For a fair comparison, the performance of FD-MUIC is only compared to that of the SI-MUIC, which also does not utilize channel coding. In general, the SI-MUIC extends the maximum torelable CFO by about 5% of subcarrier spacing, compared to the FD-MUIC. This is due to the fact that the SI-MUIC
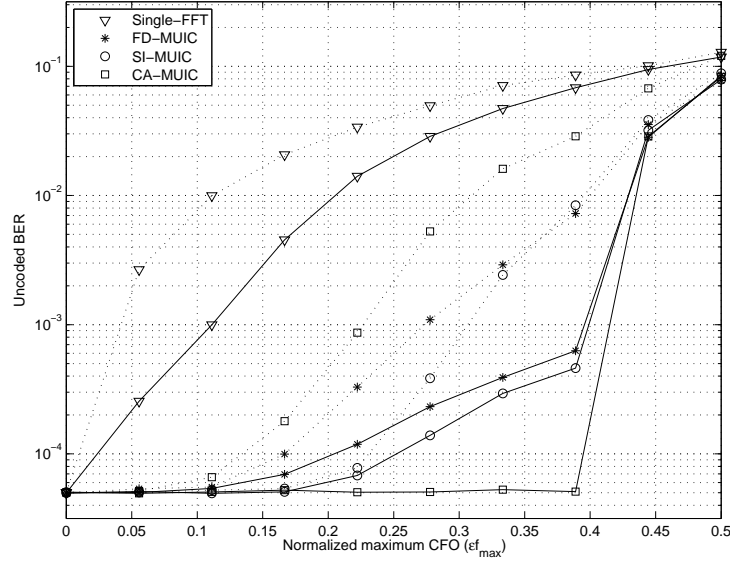
Figure 5.6: Comparison of uncoded BER performances with different maximum CFO values. Solid line indicates block allocation, and dotted line represents interleaved allocation.
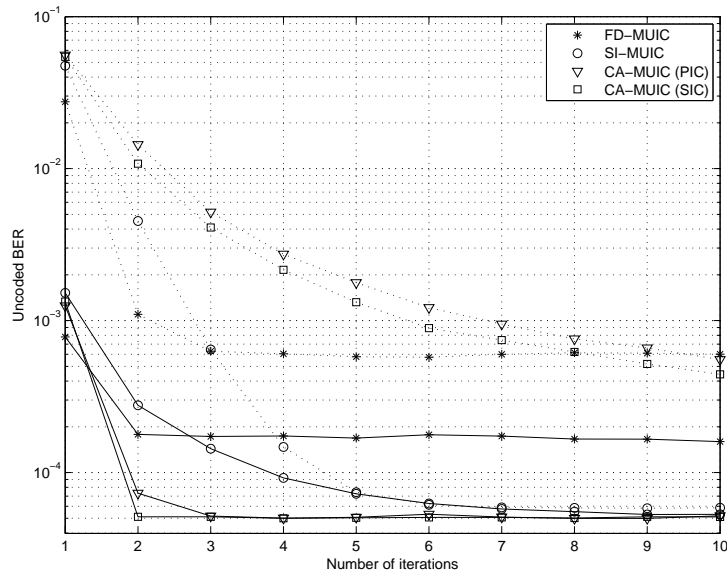

Figure 5.7: Uncoded BER performances versus number of iterations. Solid line indicates block allocation, and dotted line represents interleaved allocation.
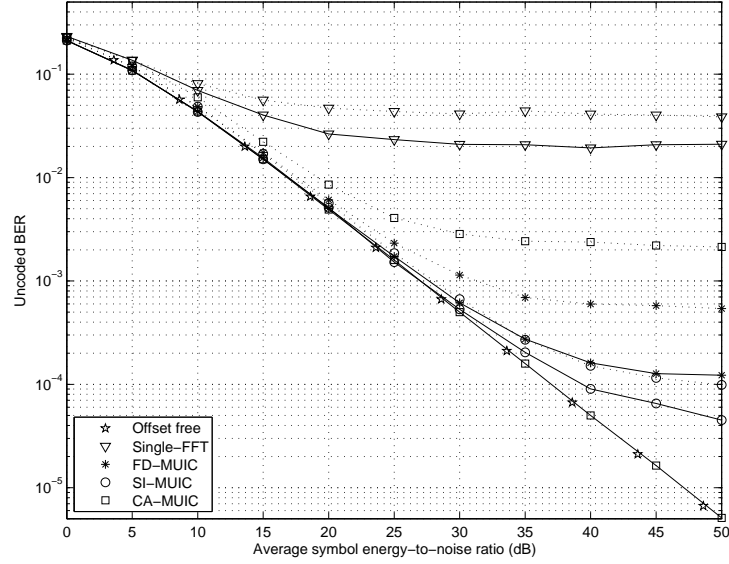
Figure 5.8: Uncoded BER performances with different CNR values. Solid line indicates block allocation, and dotted line represents interleaved allocation.
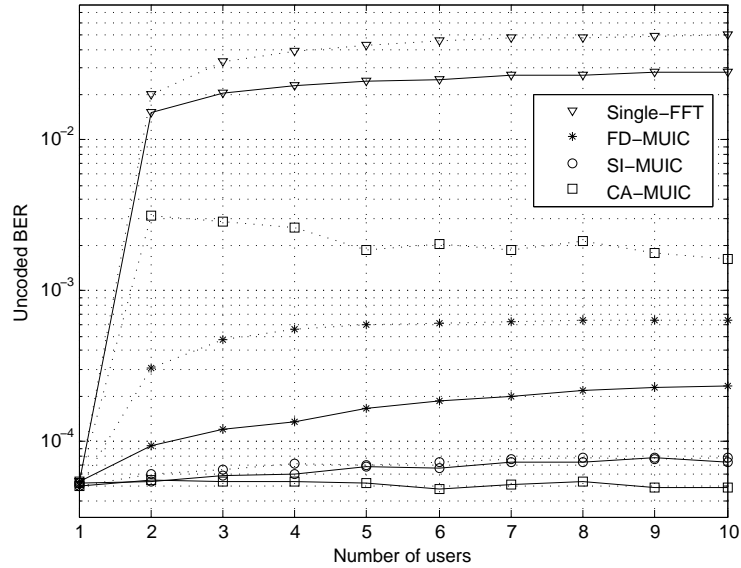

Figure 5.9: Uncoded BER performance versus number of users. Solid line indicates block allocation, and dotted line represents interleaved allocation.

can avoid the power loss and the self-interference problems occurring in the FD-MUIC scheme. Negligible performance degradation is observed for most of the discussed IC schemes when $\epsilon f_{max} = 0.25$, therefore we will hereafter use this value.

Fig. 5.7 shows the convergence properties of the CA-MUIC scheme, plotted along with the SIC implementation of FD-MUIC and SI-MUIC. In case of block allocation, the CA-MUIC converges faster than SI-MUIC, achieving the CFO-free performance in only two iterations. In interleaved allocation setting, it converges much slower than the SI-MUIC scheme. The main source of performance degradation in this case is the error propagation phenomenon: the applied convolutional code is not strong enough to overcome large MUI from neighboring users, thus produce bit errors in detection, and those errors propagate from one iteration to the others. A stronger code is required to achieve better performance in interleaved subcarrier allocation scenario, or alternatively, the SI-MUIC can be applied in the first few iterations to clean up the received signal to a level which the the CA-MUIC scheme can work effectively. Similar to SI-MUIC, the PIC implementation of the CA-MUIC scheme performs worse than its SIC version.

The uncoded BER performance versus CNR is shown in the Fig. 5.8. In the single-FFT receiver, the self- and cross-interference causes an irreducible error floor, which cannot be overcome by increasing the transmit power. This error floor is brought down by applying IC schemes, such as FD-MUIC, SI-MUIC or CA-MUIC. The SI-MUIC scheme shows considerable performance gain compared to the FD-MUIC, in both block and interleaved subcarrier allocation scenarios. And CFO-free performance can be achieved with CA-MUIC in block subcarrier allocation scenario.

Fig. 5.9 illustrates the uncoded BER performance for different numbers of users. All available subcarriers are divided equally among users using both block and interleaved allocation schemes. The number of iterations is kept constant with the increase of the number of users (i.e. $N_{loop} = 5$). We observe that the single-FFT receiver works well when there is only one user, while the IC schemes can accommodate more users, each of which experiences an independent CFO value. Again, the SI-MUIC shows much better performance than the FD-MUIC: the uncoded BER deteriorates much slower with the increase of the system load. Unlike in the Code Division Multiple Access (CDMA) technique, the MUI in OFDMA does not increase linearly with the number of users, since the MUI caused by one subcarrier to another subcarrier decreases quickly as the distance between these two subcarriers increases [42]. Therefore, the performance of the SI-MUIC scheme is expected to change insignificantly when the number of users becomes greater than 10. In the block subcarrier allocation, the CA-MUIC achieves CFO-free perfor-

mance even at 10 users. On the contrary, the CA-MUIC performs poorly in interleaved subcarrier allocation scheme, especially when there are only two users. This is due to the fact that all MUI to a subcarrrier of the first user are coming from the second user, and vice versa. If the relative CFO between them is large, the system performance will experience great impact due to the error propagation phenomena. When the number of users increases, the MUI to a subcarrier of a user comes from several adjacent users, and the probability that all relative CFOs are simultaneously large is small, therefore we can observe some performance gain.

Due to the limited space of the chapter, we consider that each user is allocated the same number of subcarriers. However, the SI-MUIC scheme works well in any subcarrier allocation schemes, provided that the CFO estimates of users are available. The number of subcarriers dictates the coding length and the coding diversity for the CA-MUIC scheme, therefore too few subcarriers allocated to a user can cause its performance to degrade. It is also worth noting that the interleaved subcarrier allocation scheme analyzed in this chapter is considered as the worst case scenario for all the other allocation schemes.

5.6 Conclusions

This chapter has proposed novel MUI cancellation schemes, which are very effective against the effects of multiple CFOs scenario in the uplink of the OFDMA-based system. Analytical and numerical evaluation has shown that the schemes outperform the performance of the conventional OFDMA receiver and the FD-MUIC scheme, for both block and interleaved subcarrier allocations. The proposed schemes are especially useful in scenarios where BS cannot instruct users to adjust their CFO or implementation of such instruction is expensive (e.g. there is no feedback channel or low cost terminal does not have ability to adjust its frequency base accurately). They are compatible with current standard for MS using OFDMA technique, for example IEEE 802.16, since all changes are transparent for MS. The proposed schemes introduce additional complexity, which can be justified by the fact that the complexity is added only to BS and the lower cost and faster operation of FFT processing chip. It worth noting that the complexity of the proposed schemes is comparable or lower than the existing frequency-domain MUI cancellation techniques in literature. The schemes show good performance under practical CFO estimator, and the performance converge after several iterations.

Chapter 6

Conclusions and futures

Technology advancement has changed the way we communicate, cooperate and entertaining ourselves. The goal of the next generation wireless systems is to provide high-quality information and services to people ubiquitously, i.e. having reliable and high-speed connections on anytime and anywhere basis. Orthogonal Frequency Division Multiplexing (OFDM) has proven to be the key modulation technique for realizing the broadband wireless communications. It is capable of simplifying the equalization task at the receiver in a frequency-selective fading environment, increasing the robustness to narrowband interference and offering high spectra efficiency. A multiuser version of the OFDM technique is Orthogonal Frequency Division Multiple Access (OFDMA), which combines the advantages of Frequency Division Multiple Access (FDMA) technique with those of OFDM. By letting users share available subcarriers simultaneously, OFDMA offers an increment in the level of bit-granularity and also the possibility to achieve multiuser diversity by applying dynamic subcarrier allocation scheme.

A major problem with OFDMA is that it inherits from OFDM the sensitivity to Carrier Frequency Offset (CFO) and phase noise, especially in the uplink. In Chapter 2, we have shown that the frequency misalignment destroys the orthogonality between subcarriers, which causes Inter-Carrier Interference (ICI) and consequently produces Multi-User Interference (MUI) among users. While the CFO can be estimated and corrected relatively easily in the downlink using traditional methods designed for OFDM technique, these tasks become more challenging in the uplink. In uplink scenario, each user experiences an independent Timing Offset (TO) and Carrier Frequency Offset (CFO), and the received signal is the sum of multiple signals coming from different users. These multiple CFOs must be corrected, otherwise the system performance degrades severely. Numerical evaluation indicates that, for any subcarrier allocation scheme, the performance of the OFDMA

uplink is more sensitive to carrier frequency misalignment than that of the OFDM or OFDMA downlink. Due to the fact that correction to one user's CFO might cause even larger misalignments of the others, new techniques must be introduced to alleviate this problem. The aim of this thesis is to provide practical solutions to the synchronization problems occurring in the uplink of the OFDMA-based wireless systems. It is worth to note that no special assumptions about the input of the OFDMA's subcarriers were made in our analysis, and therefore it is possible to apply the works in this thesis to linearly-precoded OFDMA systems, such as the hot and attractive SC-FDMA scheme.

In Chapter 3, our focus is the synchronization procedure for MSs entering the OFDMA-based wireless network for the first time or after a signal loss. The initial ranging scenario defined in the IEEE 802.16e-2005 standard is used as illustrative model, but the techniques discussed in the chapter can be applied for any OFDMA-based system in general. To allow first-time users to overlap on the ranging channel, CDMA principle is used. Two code detection and TO estimation techniques is analyzed in the chapter, namely Direct Time-Domain Ranging (DTDR) and Indirect Time-Domain Ranging (ITDR). While DTDR utilizes a bank of correlators for code detection and TO estimation, the ITDR employs FFT blocks to perform the required correlations. Due to the fact that the delays in initial ranging scenario are often large, the DTDR is more computational demanding than the ITDR. In addition, thanking to the nature of the FFT-based circular correlation, ITDR technique has complete N-point correlation output vectors, which facilitates the implementation of more advanced detection and estimation algorithms. Simulation shows that ITDR performs slightly better than DTDR, due to the fact that more information is available for ITDR-based schemes. As a result, we conclude that the ITDR is a preferred method for code detection and TO estimation in the initial ranging scenario.

Our main contribution in Chapter 3 is the CFO estimation scheme that can work on both DTDR and ITDR techniques. The scheme estimates the CFOs of ranging users using ML criterion from the phase difference between two sets of auto-correlation peaks at N-sample apart. Numerical results have shown that our proposed CFO estimator can achieve very high probability, up to 97%, that the CFO estimation error is less than 2% of the subcarrier spacing, which is a requirement in the IEEE 802.16e standard. The accuracy of the estimate depends on the threshold used in selecting the auto-correlation peaks. If it is equal to the threshold for code detection, then the choice of the threshold is a trade-off between the success detection rate and accurate TO and CFO estimation. If there exists a strict requirement on the accuracy of TO and CFO estimates, then a high and fixed threshold should be used to

guarantee such a requirement, at the cost of lower successful detection rate.

Chapter 4 proposes two CFO estimation techniques for the OFDMA uplink during data transmission phase, where each MS has been allocated a unique resource for communication with the BS. The first estimator, Moose-based Shortened Observation Distance (MSOD), is a generalized version of the Moose's CFO estimator, where the observation distance between two FFT windows can be selected arbitrary and less than the length of the OFDMA symbol. The second one, CSOD, is based on time-domain correlation technique, which has been proposed in the previous chapter for initial ranging scenario, but modified to allow for shorter distance between observation vectors. Both schemes aim at shortening the length of the preamble required for synchronization in the OFDMA uplink, thus reducing the overhead in packet-based wireless communications. The MSOD scheme is less complex, but also more prone to excessive interference than the CSOD one. Our contribution also includes the Iterative Estimation and Adjustment (IEA) algorithm, which improves the performance of the above-mentioned estimators in scenarios where self-interference is the dominant source of estimation error. In particular scenario, the proposed algorithm can achieve MSE of 10^{-4} with the observation distance only one fourth of the length of the OFDMA symbol.

Once the multiple CFO are estimated, the BS can instruct the MSs, via downlink control channel, to adjust their carrier frequency. However, if the downlink control channel does not exists, or the low-cost terminals do not have the capability to adjust its frequency base accurately, the BS must resort to alternative strategies. In Chapter 5, we propose novel MUI cancellation schemes, which can alleviate the negative effects of multiple CFOs in the OFDMA uplink. The proposed schemes have two stages: Prior to the uplink transmission, the MS performs a coarse synchronization with BS, probably via downlink broadcast, so that the CFO is within a tolerable range. In the second stage, novel signal processing techniques are employed at the BS's side to estimate and correct the residual CFOs, and to remove the ICI. The ICI compensation is performed in time-domain, using one of two different algorithms, namely Simple Time-Domain Multi-User Interference Cancellation Scheme (SI-MUIC) or CA-MUIC. No further adjustment at the MS's side is required, and therefore no additional signalling overhead is necessary, and low complexity terminal can be used. The additional complexity added to the BS is more FFT blocks, which can be justified by the lower and lower cost of fast FFT processing chips. It is worth noting that the complexity of the proposed schemes is comparable or even lower than the existing frequency-domain MUI cancellation techniques in the literature. The proposed schemes work with both block and interleaved subcarrier allocation schemes, and show

good performance under practical CFO estimator and converge after few iterations. Under particular scenario, CFO-free performance can be achieved with CFO values as high as 38% of subcarrier spacing.

Throughout the thesis, we assume equal received powers from all active users in the system. In the future, it could be an interesting topic to relax this assumption, and consider the impact of near-far effect on CFO estimation and ICI compensation algorithms. Investigating the problem of received power measurement and channel estimation in the OFDMA uplink with the present of excessive multiple CFOs is also an attractive direction for the future works.

Bibliography

[1] E. U. I. Project, "Imagining the Internet: History and Forecast," http://www.elon.edu/e-web/predictions/150/1960.xhtml.

[2] G. V. Online, "Internet Growth Statistics," http://www.internetworldstats.com/emarketing.htm.

[3] Wikipedia, "Digital Subscriber Line," http://en.wikipedia.org/wiki/Digital_Subscriber_Line.

[4] ——, "Mobile Phone," http://en.wikipedia.org/wiki/Mobile_phone.

[5] M. Shafi, A. Hashimoto, M. Umehira, S. Ogose, and T. Murase, "Wireless Communications in the Twenty-First Century: A Perspective," *The Proceedings of the IEEE*, vol. 85, no. 10, pp. 1622 – 1638, October 1997.

[6] J. Mikkonen, C. Corrado, C. Evci, and M. Progler, "Emerging Wireless Broadband Networks," *IEEE Communications Magazine*, vol. 36, no. 2, pp. 112–117, February 1998.

[7] S. Hartwig, M. Luck, J. Aaltonen, R. Serafat, and W. Theimer, "Mobile Multimedia - Challenges and Opportunities," *IEEE Transactions on Consumer Electronics*, vol. 46, no. 4, November 2000.

[8] T. Otsu, I. Okajima, N. Umeda, and Y. Yamao, "Network Architecture for Mobile Communications Systems Beyond ITM-2000," *IEEE Personal Communications*, October 2001.

[9] M. Frodigh, S. Parkvall, C. Roobol, P. Johansson, and peter Larsson, "Future-Generation Wireless Networks," *IEEE Personal Communications*, October 2001.

[10] T. Zahariadis, "Trends in the path to 4G," *IEEE Communications Engineer*, February 2003.

[11] P. Mahonen, J. Riihijarvi, M. Petrova, and Z. Selby, "Hop-by-Hop Toward Future Mobile Broadband IP," *IEEE Communications Magazine*, March 2004.

[12] M. Steer, "Beyond 3G," *IEEE Microwave Magazine*, February 2007.

[13] Y. K. Kim and R. Prasad, *4G Roadmap and Emerging Communication Technologies (Universal Personal Communications)*. Artech House: McGraw Hill Publications, January 2006.

[14] A. Jamalipour, T. Wada, and T. Yamazato, "A Tutorial on Multiple Access Technologies for Beyond 3G Mobile Networks," *IEEE Communications Magazine*, February 2005.

[15] W. C. J. Jr., *Microwave Mobile Communications*. New York: Wiley, May 1994.

[16] T. S. Rappaport, *Wireless Communications Principles and Practice*. Prentice-Hall, January 1996.

[17] G. L. Stuber, *Principles of Mobile Communications*. Kluwer Academic Publisher, January 1996.

[18] J. G. Proakis, *Digital Communications*, 4th ed. McGraw-Hill, August 2000.

[19] J. D. Parsons, *The Mobile Radio Propagation Channel, 2nd Edition*, 2nd ed. Wiley Europe, November 2000.

[20] R. van Nee and R. Prasad, *OFDM Wireless Multimedia Communications*. Artech House Publishers, December 1999.

[21] R. Mosier and R. Clabaugh, "Kineplex, a bandwidth-efficient binary transmission system," *AIEE Transaction*, vol. 76, pp. 723–728, January 1958.

[22] R. Chang, "Synthesis of band-limited orthogonal signals for multichannel data transmission," *Bell System Technology Journal*, vol. 45, pp. 1775–1796, December 1966.

[23] B. Saltzberg, "Performance of an efficient parallel data transmission system," *IEEE Trans. Comm. Technol.*, vol. COM-15, December 1967.

[24] "Orthogonal frequency division multiplexing," *U.S. Patent 3,488,445, filed Nov. 14, 1966, issued Jan. 6, 1970.*

[25] S. Weinstein and P. Eber, "Data transmission by frequency division multiplexing using the discrete Fourier transform," *IEEE Trans. Comm. Technology*, vol. COM-19, no. 15, October 1971.

[26] S. J. Vaughan-Nichols, "OFDM: Back to the Wireless Future," *Computer*, vol. 35, no. 12, pp. 19–21, December 2002.

[27] H. G. Myung, J. Lim, and D. J. Goodman, "Single Carrier FDMA for Uplink Wireless Transmission," *IEEE Vehicular Technology Magazine*, vol. 1, no. 3, pp. 30–38, September 2006.

[28] T. Pollet, M. van Bladel, and M. Moeneclaey, "BER sensitivity of OFDM systems to carrier frequency offset and Wiener phase noise," *IEEE Trans. Comm.*, vol. 43, no. 2/3/4, Feb/Mar/Apr 1995.

[29] R. Prasad and S. Hara, "An Overview of Multi-Carrier CDMA," in *IEEE ISSSTA*, September 1996, pp. 107–114.

[30] S. Hara and R. Prasad, "Overview of Multicarrier CDMA," *IEEE Communications Magazine*, pp. 126–133, December 1997.

[31] A. McCormick and E. Al-Susa, "Multicarrier CDMA for future generation mobile communication," *IEEE Electronics and Communication Engineering Journal*, vol. 12, pp. 52–60, April 2002.

[32] V. Chakravarthy, A. S. Nuez, J. P. Stephens, A. K. Shaw, and M. A. Temple, "TDCS, OFDM and MC-CDMA: A brief tutorial," *IEEE Radio Communications*, September 2005.

[33] H. Sari and G. Karam, "Orthogonal frequency-division multiple access and its applications to CATV networks," *Eur. Trans. Telecommun.*, December 1998.

[34] M. Morelli, C.-C. J. Kuo, and M.-O. Pun, "Synchronization Techniques for Orthogonal Frequency Division Multiple Access (OFDMA): A Tutorial Review," *Proceedings of the IEEE*, vol. 95, no. 7, pp. 1394–1427, July 2007.

[35] M. Speth, S. Fechtel, G. Fock, and H. Meyr, "Optimum receiver design for wireless broadband systems using OFDM - Part I," *IEEE Transactions on Communications*, vol. 47, no. 11, November 1999.

[36] J.-J. van de Beek, P. O. Borjesson, M.-L. Boucheret, D. Landstrom, J. M. Arenas, P. Odling, C. Osterberg, M. Wahlqvist, and S. K. Wilson,

"A time and frequenc synchronization scheme for multiuser OFDM," *IEEE Journal on Selected Areas in Communications*, vol. 17, no. 11, November 1999.

[37] D. Galda, H. Rohling, and E. Costa, "On the effects of user mobility on the uplink an OFDMA system," in *IEEE VTC*, vol. 2, April 2003, pp. 1433–1437.

[38] R. V. Nee and R. Prasad, *OFDM for Wireless Multimedia Communications*. Artech House Publishers, January 2000.

[39] J. Heiskala and J. Terry, *OFDM Wireless LANs: A Theoretical and Practical Guide*, 2nd ed. Sams Publishing, July 2001.

[40] M. Morelli, "Timing and frequency synchronization for the uplink of and OFDMA system," *IEEE Transactions on Communications*, vol. 52, no. 2, February 2004.

[41] H. Tang, K. Y. Lau, and R. W. Brodersen, "Synchronization schemes for packet OFDM system," *IEEE International Conference on Communications (ICC'03)*, May 2003.

[42] Z. Cao, U. Tureli, Y.-D. Yao, and P. Honan, "Frequency Synchronization for Generalized OFDMA Uplink," in *IEEE Globecom*, November 2004.

[43] R. Vaughan and J. B. Andersen, *Channels propagation and antennas for mobile communications*. IEE Electromagnetic Waves Series 50, 2003, no. ISBN 0-85296084-0.

[44] IEEE LAN/MAN Standards Committee, "Part 16: Air interface for fixed and mobile broadband wireless access systems - Amendment 2: Physical and Medium Access Control Layers for combined fixed and mobile operation in licensed bands," *IEEE*, 2005.

[45] "Wimax forum website," http://www.wimaxforum.org.

[46] P. H. Moose, "A technique for orthogonal frequency division multiplexing frequency offset correction," *IEEE Trans. Comm.*, vol. 42, pp. 2908–2914, October 1994.

[47] T. M. Schmidl and D. C. Cox, "Robust frequency and timing synchronization for OFDM," *IEEE Trans. Comm.*, December 1997.

[48] M. Morelli and U. Mengali, "An improved frequency offset estimator for OFDM applications," *IEEE Communications Letter*, vol. 3, no. 3, pp. 75–77, February 1999.

[49] H. Minn, V. K. Bhargava, and K. B. Letaief, "A robust timing and frequency synchronization for OFDM systems," *IEEE Trans. Wireless Comm.*, July 2003.

[50] Z. Cao, U. Tureli, and Y.-D. Yao, "Deterministic multiuser carrier-frequency offset estimation for interleaved OFDMA uplink," *IEEE Transaction on Communications*, vol. 52, no. 9, September 2004.

[51] X. Fu, Y. Li, and H. Minn, "A new ranging method for OFDMA systems," *IEEE Transactions on Wireless Communications*, vol. 6, no. 2, February 2007.

[52] Itzik Kitroser and Yossi Segal and Zion Hadad, "Bandwidth Request Using CDMA Codes in OFDMA (OFDM) Base PHY," IEEE 802.16 Broadband Wireless Access Working Group, Technical Contribution IEEE 802.16.3c-01/55, April 2001.

[53] J. Krinock, M. Singh, M. Paff, Vincent, A. Lonkar, L. Fung, and C.-C. Lee, "Comments on OFDMA Ranging Scheme described in IEEE 802.16ab-01/01r1," IEEE 802.16 Broadband Wireless Access Working Group, Tech. Rep. Document IEEE 802.16abc-01/24, August 2001.

[54] K.-N. Kim, S.-C. Kim, J.-H. Kim, and S.-J. Cho, "The Scheme to Improve the Performance of Initial Ranging Symbol Detection with Common Ranging Code for OFDMA Systems," *The International Conference on Advanced Communication Technology (ICACT)*, vol. 1, Febuary 2006.

[55] J.-K. Koo, Y.-K. Cho, C.-Y. Oh, S.-R. Jeong, T.-Y. Kim, D.-S. Park, J.-Y. Jung, J.-Y. Choi, E.-T. Lim, C.-H. Suh, and J.-H. Jang, "Apparatus and method for performing ranging in a communication system," *European Patent Application, Application No. 06018466.0*, September 2006.

[56] X. J. Zhuang, K. Baum, V. Nangia, and M. Cudak, "Ranging Enhancement for 802.16e OFDMA PHY," IEEE 802.16 Broadband Wireless Access Working Group, Tech. Rep. Document IEEE C802.16e-04/143, June 2004.

[57] X. Fu and H. Minn, "Initial Uplink Synchronization and Power Control (Ranging Process) for OFDMA Systems," in *IEEE Globecom*, vol. 6, Nov-Dec 2004, pp. 3999–4003.

[58] J.-K. Koo, S.-H. Yoon, C.-H. Suh, J.-M. Ro, D.-S. Park, and Y.-K. Cho, "Apparatus and method for estimating uplink frequency offset in an orthogonal frequency division multiplexing communication system," *Samsung Patent Application, Pub. No. 20060083160*, August 2006.

[59] A. Oppenheim and R. Schafer, *Digital Signal Processing*. Prentice-Hall, Inc., 1975.

[60] A. D. Poularikas, *The transforms and applications handbook*. CRC Press LLC, 2000.

[61] Yue Zhou and Zhaoyang Zhang and Xiangwei Zhou, "OFDMA Initial Ranging for IEEE 802.16e based on time-domain and frequency-domain approaches," in *International Conference on Communication Technologies (ICCT)*, November 2006.

[62] H. C. Nguyen, E. de Carvalho, and R. Prasad, "Multi-user Interference Cancellation Scheme(s) for Multiple Carrier Frequency Offset Compensation in Uplink OFDMA," in *IEEE PIMRC*, Helsinki, Finland, September 2006.

[63] S. Barbarossa, M. Pompili, and G. B. Giannakis, "Channel-Independent Synchronization of Orthogonal Frequency Division Multiple Access Systems," *IEEE Journal on Selected Areas in Communications*, vol. 20, no. 2, February 2002.

[64] M.-O. Pun, M. Morelli, and C.-C. J. Kuo, "Maximum-Likelihood Synchronization and Channel Estimation for OFDMA Uplink Transmissions," *IEEE Transactions on Communications*, vol. 54, no. 4, April 2006.

[65] J. Choi, C. Lee, H. W. Jung, and Y. H. Lee, "Carrier frequency offset compensation for uplink of ofdm-fdma systems," *IEEE Communications Letters*, vol. 4, pp. 414–416, December 2000.

[66] D. Huang and K. B. Letaief, "An Interference-Cancellation Scheme for Carrier Frequency Offsets Correction in OFDMA Systems," *IEEE Transactions on Communications*, vol. 53, no. 7, July 2005.

[67] S. M. Kay, *Fundamentals of Statistics Signal Processing: Estimation Theory.* USA: Prentice Hall PTR, 1993.

[68] K. S. Shanmugan and A. Breipohl, *Random Signals: Detection, Estimation and Data Analysis.* USA: John Wiley & Sons, 1988.

[69] M. Gudmundson and P.-O. Anderson, "Adjacent channel interference in an OFDM system," in *Vehicular Technology Conference, IEEE*, April 1996.

[70] C. Muschallik, "Improving an OFDM reception using an adaptive Nyquist windowing," *IEEE Transactions on Consumer Electronics*, vol. 42, August 1996.

[71] J. Armstrong, "Analysis of new and existing methods of reducing intercarrier interference due to carrier frequency offset in OFDM," *IEEE Transactions on Communications*, vol. 47, March 1999.

[72] Y. Zhao and S.-G. Haggman, "Intercarrier Interference Self-Cancellation Scheme for OFDM Mobile Communication Systems," *IEEE Transactions on Communications*, vol. 49, July 2001.

[73] Z. Cao, U. Tureli, and Y.-D. Yao, "User Separation and Frequency-Time Synchronization for the Uplink of Interleaved OFDMA," in *IEEE Signals, Systems and Computers*, Pacific Grove, USA, November 2002.

[74] IEEE LAN/MAN Standards Committee, "Part 16: Air interface for fixed broadband wireless access systems," *IEEE*, 2004.

[75] J. M. Cioffi, G. P. Dudevoir, M. V. Eyuboglu, and G. D. Forney, "MMSE Decision-Feedback Equalisers and Coding - Part I: Equalization Results," *IEEE Transactions on Communications*, vol. 43, no. 10, pp. 2582–2594, October 1995.

[76] D. Tse and P. Viswanath, *Fundamentals of Wireless Communications.* Cambridge Press, May 2005.

[77] IEEE LAN/MAN Standards Committee, "Part 11: Wireless LAN Medium Access Control (MAC) and Physical Layer (PHY) specifications: High-speed Physical Layer in the 5 GHz Band," *IEEE*, 1999.